

EXPERIMENTAL MODELING AND LABORATORY  
MEASUREMENTS OF DRAG EMBEDMENT ANCHORS SUBJECTED  
TO IN-PLANE AND OUT-OF-PLANE LOADING

A Thesis

by

AARON C. DRAKE

Submitted to the Office of Graduate Studies of  
Texas A&M University  
in partial fulfillment of the requirements for the degree of

MASTER OF SCIENCE

August 2011

Major Subject: Ocean Engineering

Experimental Modeling and Laboratory Measurements of Drag Embedment Anchors

Subjected to In-Plane and Out-Of-Plane Loading

Copyright 2011 Aaron C. Drake

EXPERIMENTAL MODELING AND LABORATORY  
MEASUREMENTS OF DRAG EMBEDMENT ANCHORS SUBJECTED  
TO IN-PLANE AND OUT-OF-PLANE LOADING

A Thesis

by

AARON C. DRAKE

Submitted to the Office of Graduate Studies of  
Texas A&M University  
in partial fulfillment of the requirements for the degree of

MASTER OF SCIENCE

Approved by:

Co-Chairs of Committee,	Robert E. Randall
	Charles P. Aubeny
Committee Member,	Douglas C. Biggs
Head of Department,	John Niedzwecki

August 2011

Major Subject: Ocean Engineering

## ABSTRACT

Experimental Modeling and Laboratory Measurements of Drag Embedment Anchors  
Subjected to In-Plane and Out-Of-Plane Loading. (August 2011)

Aaron C. Drake, B.S, Texas A&M University

Co-Chairs of Advisory Committee, Dr. Robert E. Randall

Dr. Charles P. Aubeny

Extreme hurricane events of the past decade are responsible for several drag embedment anchor (DEA) mooring failures of mobile offshore drilling platforms stationed within the Gulf of Mexico. A proposed failure mechanism is caused by out-of-plane loading. The current status of DEA holding capacity is based on empirical design charts and does not include the effects of out-of-plane loading. Experimental modeling using a 1:10 scale generic DEA was performed at the Haynes Coastal Engineering Laboratory at Texas A&M University to examine the effects of out-of-plane load conditions. Instrumentation and specialized devices were constructed to measure the anchor's trajectory through a representative sample of Gulf of Mexico clay with average un-drained shear strength of 0.764 kPa (16 psf). The sediment basin allowed for drag distances of 4.87 m (16 ft) and an embedment depth of 1.37 m (4.5 ft).

The measurements included pitch and roll of the anchor and line tension measured at the shank pad-eye. The variables modeled were fluke angle settings of 22°, 36° and 50°. The initial towline angle was varied from a minimum of 5° to upwards of 20°. Surface out-of-plane angles of 45° and 90° and embedment loading of 15°, 30° and 45° were examined. Curves of the ultimate holding capacity with respect to the out-of-plane towline angle and ultimate embedment depth were developed as functions of out-of-plane loading angles. Analysis of the rate effect indicates that a 46% increase in towing velocity causes an average 3% increase of holding capacity. The 50° fluke angle



embeds an average of 0.7 fluke lengths deeper and has a holding capacity of 0.73 units greater than the 36° setting. The surface out-of-plane tests have a 5.1% reduction in holding capacity as the out-of-plane load angle increases from 45° to 90°. For all one fluke length initial towing distance tests, the ultimate holding capacity increases and the ultimate embedment depth decreases as the out-of-plane towing angle increases from 15° to 45°. The three fluke length initial towing distance tests indicate a contrasting trend, in that as the out-of-plane tow angle increases, both the ultimate holding capacity and ultimate embedment depth decrease.

## ACKNOWLEDGEMENTS

I would like to thank my committee chair, Dr. Robert Randall, and committee members, Dr. Charles Aubeny and Dr. Douglas Biggs, for their guidance and advice over the course of this research. I would also like to recognize the outstanding efforts and help provided by Mr. John Reed, Dr. Po Yeh, Mr. Ryan Beemer, Mr. William Cenac and Mr. Rusty Permenter. Thank you Mr. Evan Zimmerman and Delmar Systems Inc., for providing the anchor model and additional industry support and guidance.

Thanks also go to my friends and colleagues and the department faculty and staff of the Ocean Engineering program for making my time at Texas A&M University a great experience. Finally, thanks to my family for their encouragement and to my wife for her patience and love.

## TABLE OF CONTENTS

	Page
ABSTRACT .....	iii
ACKNOWLEDGEMENTS .....	v
TABLE OF CONTENTS .....	vi
LIST OF FIGURES.....	ix
LIST OF TABLES .....	xii
1. INTRODUCTION.....	1
1.1 Overview of Drag Embedment Anchors .....	1
1.2 Research Objectives.....	3
2. BACKGROUND AND LITERATURE REVIEW .....	4
2.1 Overview.....	4
2.2 Previous Model Testing and Parameter Identification .....	4
3. EXPERIMENTAL ARRANGEMENTS.....	8
3.1 Facilities and Equipment .....	8
3.2 Sediment Basin and Soil Properties.....	9
3.2.1 Sediment Mixing Device.....	12
3.2.2 Sediment Strength Testing.....	15
3.3 General Test Arrangements .....	17
3.3.1 Main Support Structure.....	17
3.3.2 Chaser Line Principle and Design.....	19
3.3.3 Anchor Towline Angle Measuring Device .....	22
3.3.4 Carriage Force Transducer.....	24
3.4 Instrumentation Installed on the Anchor .....	24
3.4.1 Pressure Transducer .....	25
3.4.2 Inclinator .....	26
3.4.3 Anchor Force Transducer.....	27

	Page
3.5 Breakout Testing Devices.....	27
3.6 Anchor and Towline Properties.....	29
3.7 Data Collection and Instrumentation Notes.....	32
 4. PROCEDURES.....	 33
4.1 In-Plane Testing.....	33
4.2 Initial Surface and Sub-surface Out-of-Plane Tests (Case 1).....	34
4.3 Main Tow Line Out-of-Plane Tests (Case 2).....	35
4.4 Continuous Degree Change Out-of-Plane Tests (Case 3).....	38
4.5 Breakout Test Procedures.....	39
 5. RESULTS AND DISCUSSION.....	 41
5.1 Sediment Strength Testing.....	41
5.2 In-Plane Results.....	42
5.2.1 In-Plane Initial Tow Angle Results.....	46
5.2.2 In-Plane Velocity Comparison.....	48
5.2.3 In-Plane Roll Comparison.....	49
5.3 Out-of-Plane Initial Surface and Sub-surface (Case 1).....	51
5.3.1 Velocity Comparison.....	52
5.3.2 Fluke Angle Comparison.....	53
5.3.3 Roll Comparison.....	55
5.4 Out-of-Plane Main Tow Line (Case 2).....	58
5.4.1 Initial Tow Distance Comparison.....	60
5.4.2 Fluke Angle Comparison.....	62
5.4.3 Analysis of Extrapolated Data.....	63
5.4.4 Roll Comparison.....	66
5.5 Out-of-Plane Continuous Degree Change (Case 3).....	69
5.6 Breakout Tests Results.....	72
5.7 Pressure Depth and Carriage Force.....	75
 6. CONCLUSIONS AND RECOMMENDATIONS.....	 79
6.1 Conclusions.....	79
6.1.1 Overview and In-Plane.....	79
6.1.2 Out-of-Plane (Case 1).....	80
6.1.3 Out-of-Plane (Case 2).....	80
6.1.4 Out-of-Plane (Case 3).....	81
6.1.5 Breakout Tests.....	82

	Page
6.2 Recommendations and Future Work .....	82
REFERENCES .....	84
APPENDIX A .....	86
VITA .....	104

## LIST OF FIGURES

	Page
Fig. 1-1. Anchor Definitions .....	2
Fig. 1-2. Eight Point MODU Mooring Configuration .....	3
Fig. 2-1. The Effect of Fluke Length on Prototype Anchor Weight .....	6
Fig. 3-1. Haynes Coastal Engineering Laboratory Towing Tank .....	9
Fig. 3-2. Sediment Basin Global Coordinates.....	10
Fig. 3-3. Side Profile of Sediment Basin.....	10
Fig. 3-4. Sediment Mixing Device .....	13
Fig. 3-5. Sediment Mixing Device at Work.....	13
Fig. 3-6. Sediment Surface after Mixing.....	14
Fig. 3-7. T-bar Sediment Strength Testing Device .....	16
Fig. 3-8. Sediment Strength Testing Locations.....	17
Fig. 3-9. Main Support Structure and General Layout.....	18
Fig. 3-10. Side View of Support Structure.....	19
Fig. 3-11. Chaser Line Displacement Sensor .....	20
Fig. 3-12. Chaser Line Angle Measuring Device.....	21
Fig. 3-13. Anchor Line Angle Measuring Device.....	23
Fig. 3-14. Anchor and Chaser Line Angle Convention and Definitions.....	23
Fig. 3-15. Anchor Mounted Instrument Positions.....	25
Fig. 3-16. Anchor Pitch and Roll Sign Convention .....	26
Fig. 3-17. Transverse Breakout Testing Device.....	28
Fig. 3-18. Rotational Breakout Device (left), in Operation (right) .....	29

	Page
Fig. 3-19. Fluke Centroid Location (left), Fluke Plate Dimensions (right) .....	30
Fig. 3-20. Anchor Fluke Angle Settings .....	30
Fig. 3-21. Anchor Coordinates .....	31
Fig. 3-22. Anchor Used in Experiment .....	32
Fig. 4-1. Anchor Surface Position Detail (left), In-Plane Line Position (right) .....	34
Fig. 4-2. Surface Out-of-Plane (Case 1) .....	35
Fig. 4-3. Towline Paths for 15° (Case 2) .....	37
Fig. 4-4. Towline Paths for 30° and 45° Tests (Case 2) .....	37
Fig. 4-5. Carriage Ladder Towing Path (Case 3) .....	39
Fig. 5-1. Sediment Strength Profile from March 25, 2010 .....	41
Fig. 5-2. Spherical Coordinates for Trajectory Calculations .....	43
Fig. 5-3. 36° In-Plane 5° Tow Angle $N_{eq}$ and Pitch vs. Depth .....	44
Fig. 5-4. 36° In-Plane Velocity Comparison, 5° Tow Angle .....	45
Fig. 5-5. 50° In-Plane Initial Tow Angle Comparison: $N_{eq}$ and Pitch vs. Depth .....	47
Fig. 5-6. In-Plane Tow Angle and Velocity Comparison .....	48
Fig. 5-7. In-Plane Tow Angle and Velocity Regression .....	49
Fig. 5-8. 36° In-Plane Roll vs. Depth .....	50
Fig. 5-9. 50° In-Plane Roll vs. Depth .....	50
Fig. 5-10. Surface Out-of-Plane Angle Comparison .....	52
Fig. 5-11. Surface Out-of-Plane Tow Angle Velocity Comparison .....	53
Fig. 5-12. Out-of-Plane Surface Angle $N_{eq}$ and Pitch vs. Depth (Case 1) .....	54
Fig. 5-13. 36° Surface Out-of-Plane 45° Roll Comparison .....	56

	Page
Fig. 5-14. 50° Surface Out-of-Plane 45° Roll Comparison.....	56
Fig. 5-15. 36° Surface Out-of-Plane 90° Roll Comparison.....	57
Fig. 5-16. 50° Surface Out-of-Plane 90° Roll Comparison.....	58
Fig. 5-17. Out-of-Plane Tow Angle Comparison (Case 2) .....	59
Fig. 5-18. 1 Fluke Length Comparison (Case 2).....	61
Fig. 5-19. 3 Fluke Length Comparison (Case 2).....	62
Fig. 5-20. Extrapolated Out-of-Plane Ultimate $N_{eq}$ .....	64
Fig. 5-21. Extrapolated Ultimate Embedment Depth.....	65
Fig. 5-22. 36° 1 Fluke Length Roll Comparison (Case 2) .....	67
Fig. 5-23. 50° 1 Fluke Length Roll Comparison (Case 2) .....	67
Fig. 5-24. 36° 3 Fluke Length Roll Comparison (Case 2) .....	68
Fig. 5-25. 50° 3 Fluke Length Roll Comparison (Case 2) .....	68
Fig. 5-26. Out-of-Plane $N_{eq}$ and Pitch vs. Depth (Case 3) .....	70
Fig. 5-27. Roll Comparison (Case 3) .....	71
Fig. 5-28. Y-Trajectory (Case 3) .....	72
Fig. 5-29. Normal Breakout Tests .....	73
Fig. 5-30. 36° Fluke Angle FWR Transverse Breakout Tests .....	74
Fig. 5-31. Transverse Breakout Tests Center of Pressure and Moment Arm .....	75
Fig. 5-32. Pressure Depth Data (Case 2).....	76
Fig. 5-33. Pressure Depth Data for In-Plane Example.....	77
Fig. 5-34. Anchor and Carriage Load Cell Example.....	78



## LIST OF TABLES

	Page
Table 3-1. Sediment Composition.....	11
Table 5-1. Max Embedment and $N_{eq}$ by Fluke Angle (Case 1).....	55
Table 5-2. Embedment Depth and Holding Capacity (Case 2).....	63
Table 5-3. Equations of Fit (Case 2).....	66
Table 6-1. Equations of $N_u$ and $Z_u$ for Out-of-Plane Loading.....	81

# 1. INTRODUCTION

## 1.1 Overview of Drag Embedment Anchors

Drag embedment anchors (DEA) are commonly utilized for mooring floating mobile offshore drilling units (MODU) in the Gulf of Mexico (GOM). MODU are often considered temporary installations, and may only remain in a given site for a period of weeks to months before relocating. DEA have the capability of being retrieved and installed using anchor handling vessels. The costs for handling DEA are considerably lower than alternatives such as suction caisson anchors. For this reason DEA will continually be employed in mooring configurations. As offshore energy companies continue to expand into deeper water depths, anchoring technology must evolve to handle the new design constraints. Recent hurricane activity in the GOM has caused several failures in MODU mooring systems resulting in the rigs being set adrift. Hurricanes Ivan (2004), Katrina (2006), and Rita (2006), were responsible for 17 MODU that lost their ability to maintain position Det Norske Veritas (2007). The pipeline damage survey performed by Det Norske Veritas (2007) suggested that the anchors from the drifting rigs were responsible for a large portion of the observed pipeline damage. In many of the cases, the rigs traveled for several kilometers (miles), damaging much of the subsea infrastructure located along their paths. In order to prevent future environmental and economic losses, a complete understanding of the failure mechanisms is required.

Anchoring and maritime terminology is in a class of its own. The basic terminology and anchor components discussed herein, such as the fluke, shank, shackle pad-eye and fluke angle are illustrated below in Fig. 1-1. The common eight point mooring configuration used on MODU is depicted in Fig. 1-2. Eight mooring lines connecting to anchors are grouped in pairs and connect to the quadrants of the MODU.

---

This thesis follows the style of *Journal of Waterway, Port, Coastal and Ocean Engineering*.

This figure also defines out-of-plane loading. The dashed lines in Fig. 1-2 indicate the MODU original position and corresponding direction of the mooring legs. As the rig begins to drift from the original position, the angle between the original anchor line position and the current position increases; therefore, the degree of angle change is related to the mooring line position and drift direction. The lateral lines with respect to drift direction, as indicated by the pair's numbered two and three, are subjected to the largest degree of out-of-plane loading. Position one sees the least change, and position four does not provide any holding capacity until the rig passes one mooring line length beyond the location of the anchors in the seabed.

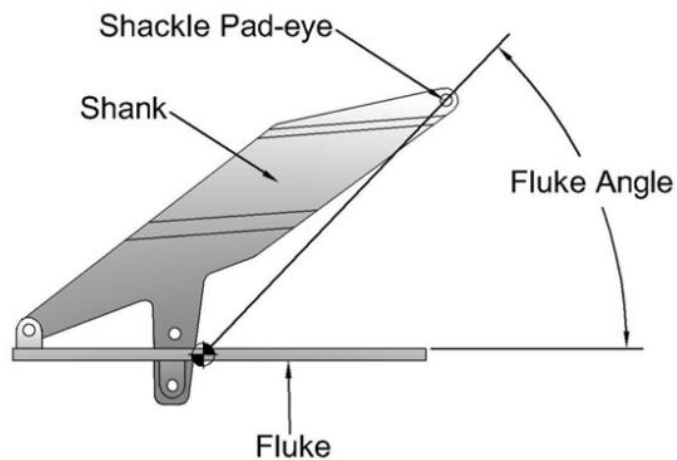


**Fig. 1-1.** Anchor Definitions

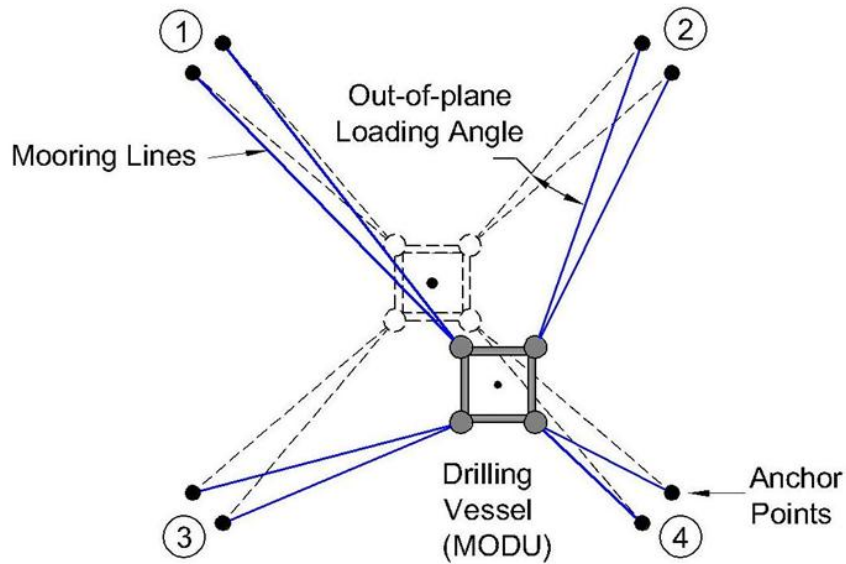


**Fig. 1-2.** Eight Point MODU Mooring Configuration

## 1.2 Research Objectives

The primary objective of the research presented in this thesis is to analyze the performance of drag embedment anchors and to identify any relationships present due to in-plane and out-of-plane loading. Experimental methods were designed and specialized equipment was installed at the Haynes Coastal Engineering Laboratory at Texas A&M University to assist in this research. A generic 1:10 scale drag embedment anchor was constructed and provided by Delmar Systems Inc. This anchor has a simplified geometry and the ability to adjust the fluke angle settings. The testing included in-plane loading for examining the effects of the fluke angle setting, rate dependencies and is used as a baseline to compare with the out-of-plane results. The out-of-plane loading conditions included surface angles of  $45^\circ$  and  $90^\circ$  in addition to examining embedded cases where the angle range was  $15^\circ$ ,  $30^\circ$ , and  $45^\circ$ . The depth dependency was also examined by towing the anchor an initial distance of one fluke length and three fluke lengths.

## 2. BACKGROUND AND LITERATURE REVIEW

### 2.1 Overview

Drag embedment anchors (DEA) function with their greatest holding capacity in the horizontal direction, with little ability to resist vertical loadings. The typical size and weight of deep water DEA range from 1.7-6.5 m (5.6-21.3 ft) and 1.5-65 mT (1.65-71.6 T). The ultimate holding capacity is based primarily on anchor weight, properties of soil contained in the failure wedge, friction between the anchor and soil, and bearing capacity of the shank and mooring line Vryhof (2010). Prediction of holding capacity for mooring designs is based heavily on empirical charts, such as those developed by the Naval Civil Engineering Laboratory (NCEL), (1987). Moreover, the American Petroleum Institute (API), (2005) has adopted much of the data from NCEL (1987) for use in recommended practices and currently applies a reduction of safety only for towline to mud-line angles. Unfortunately, the behavior and mechanics of anchors subjected to out-of-plane loading are currently beyond the capabilities of the traditional design charts. Critical research is currently aimed at refining design guidelines for DEA through the use of analytical models capable of predicting the trajectory and ultimate holding capacity for given conditions, such as the work performed by (Stewart 1992; Neubecker and Randolph 1995, 1996; Dahlberg 1998), in addition to the finite element studies performed by O'Neill et al. (2003), and the examination of out-of-plane loading by Aubeny and Chi (2010A).

### 2.2 Previous Model Testing and Parameter Identification

Comprehensive model testing is the basis for most empirical design charts. Large-scale field tests such as (Vryhof 2005; and Omega Marine Services International 1990) are prohibitively costly in nature. Centrifugal model testing on a much smaller scale such as Dunnivant and Kwan (1993) has proven useful for relating the ultimate embedment

depth and capacities as a function of the anchor fluke properties and the portion of the mooring line embedded within the soil. In most of their tests, the anchor embedded an average of 5-6 fluke lengths. However, out-of-plane loading conditions were outside the scope of study for these experiments. The general practice for identifying an anchor's ultimate embedment depth is to examine the pitch angle of the fluke plate with respect to the sediment surface.

Previous research has shown that ultimate depth has been reached when the anchor's fluke is in a nearly horizontal position Stewart (1992). Aubeny and Chi (2010B) expanded on these principles in a theoretical study relating trajectory predictions to the rate of change of the anchor topline angle with respect to depth. Their work has provided the basis for identification of the key parameters to be measured over the course of our experiments.

In this research, the anchor properties to be measured are the pitch and roll motions of the fluke plate, anchor line tension at the connection point to the shank pad eye and the overall weight. Regarding anchor weight as a function of size and corresponding scale effects, Fig. 2-1 was developed from a range of prototype anchor data provided by Vryhof (2010). The weight of the model anchor ( $W_m$ ) is related to the prototype ( $W_p$ ) by:

$$W_m = W_p^{1/3} \quad (1)$$

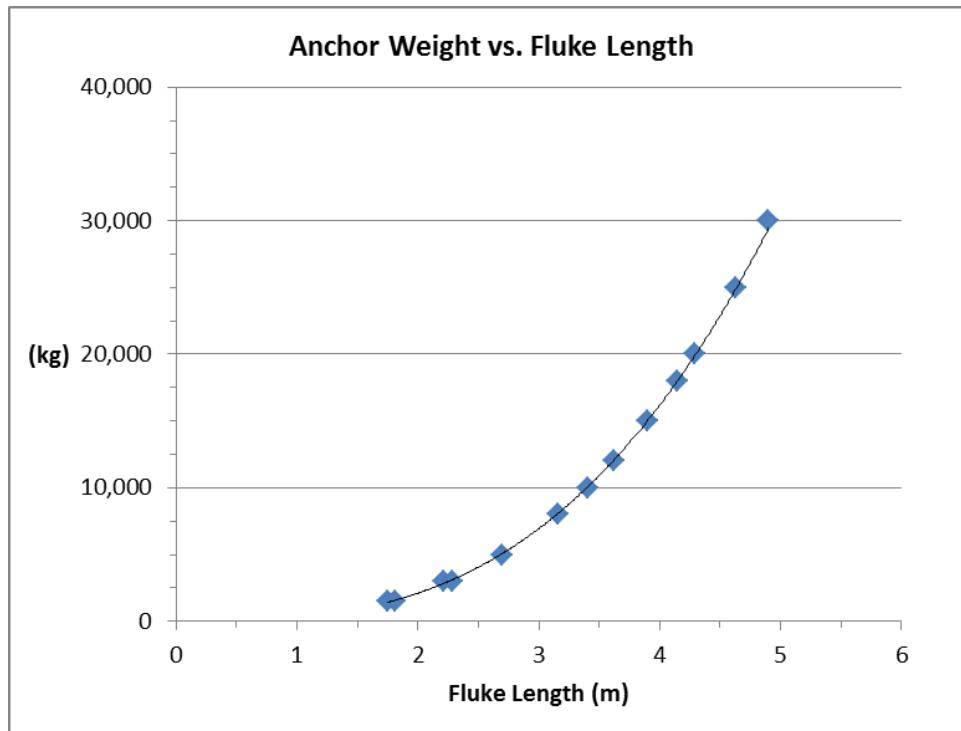


**Fig. 2-1.** The Effect of Fluke Length on Prototype Anchor Weight

A general function of anchor weight is determined to be a power law equation as listed below where ( $W_p$ ) is the weight in kg and ( $L_p$ ) is the fluke length in meters.

$$W_p = 275(L_p)^{2.94} \quad (2)$$

Rate effect on holding capacity is examined by using two towing velocities of 0.13 m/s (0.42 ft/s) that correspond to a prototype equivalent speed of 2 fluke lengths/min and 0.19 m/s (0.62 ft/s) the equivalent of 3 fluke lengths/min. These values are compared to the previous work by Aubeny and Shi (2007) that examined the rate dependency of a cylinder penetrating into soft clay. They established that a factor of 10 increase in rate corresponds to an approximate 11-12% increase of holding capacity.

Different methods for determining the trajectory of the anchor within the sediment have been employed in previous research. Vryhoff (2005) field data used acoustic monitoring equipment; Dunnivant and Kwan (1993) defined procedures using

lead powder slurry injected into the anchors trench, while the University of Texas group Aubeny and Gilbert et al. (2011) used a magnetometer for tracking the anchors position. Carchedi et al. (1984) used thin nylon lines connected to precision potentiometers to monitor anchor trajectory. The three lines were offset and in fixed known positions so that the displacement measured by the potentiometers could be used to triangulate the position of the anchor. The technique employed in this research involved using a small diameter wire as a chaser line similar in principle to the Carchedi et al. (1984) techniques. The angles and displacement of the chaser line were used to triangulate the position of the anchor within the sediment.



### 3. EXPERIMENTAL ARRANGEMENTS

#### 3.1 Facilities and Equipment

Model testing of the drag embedment anchors was conducted in the towing tank at the Haynes Coastal Engineering Laboratory at Texas A&M University. The towing tank dimensions are 45.6 m (149.5 ft) long, 3.66 m (12 ft) wide, with a maximum depth of 3.05 m (10 ft); the overall layout is depicted in Fig. 3-1. The dredge towing carriage provided the power and motion simulating the movement of a MODU. The carriage is equipped with two electric traction motors capable of propelling the carriage to velocities of up to 2 m/s (6.56 ft/s). The torque provided by the motors allows for a very short ramp-up distance estimated at less than 10 cm (3.93 in) before a constant velocity is obtained. The carriage is controlled via a computer for both position and velocity. A laser-positioning sensor provides feedback for the East to West direction of motion allowing for precise displacements and velocities to be achieved.

Attached to the towing carriage is a dredging ladder. The ladder extends downward from the main carriage and is capable of controlled motion in both the  $z$  and  $y$  directions (Fig. 3-2). Attached to the ladder is an articulating arm equipped with a powered driveshaft propelling a dredge cutter head. The original cutter head was removed and re-purposed with an attachment for mixing the sediment, which will be discussed in detail in section 3.2.1. The carriage motion was programmed using Lookout Direct software. This program was critical in maintaining repeatability and consistency throughout every testing stage. It was also responsible for setting the locations of start and finish in addition to the velocities of each test.

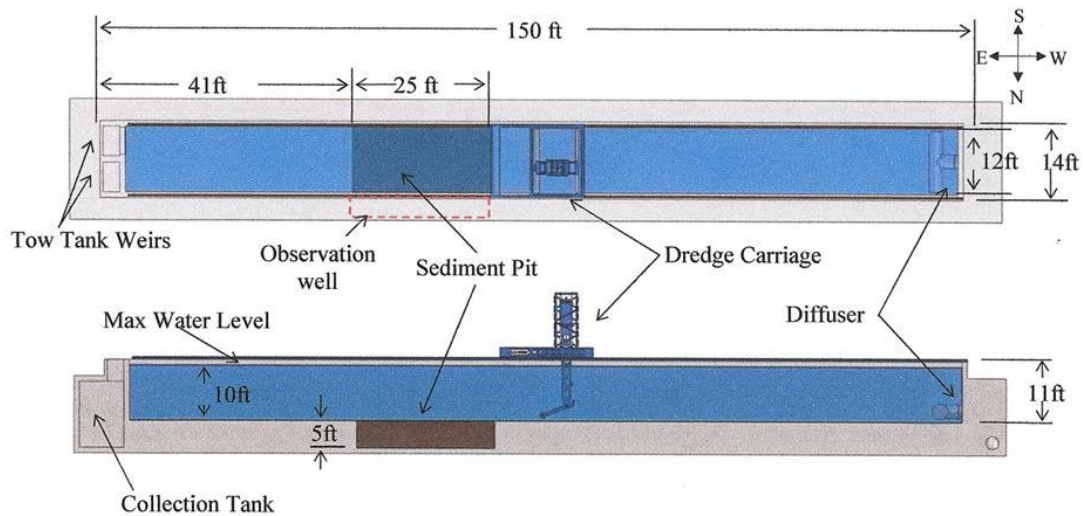


**Fig. 3-1.** Haynes Coastal Engineering Laboratory Towing Tank [courtesy of Young (2009)]

### 3.2 Sediment Basin and Soil Properties

Within the towing tank is a water-tight dredging sediment basin that is 7.6 m (25 ft) long, 3.7 m (12 ft) wide, and 1.5 m (5 ft) that was used to contain the representative sample of deep water Gulf of Mexico soft clay. Approximately  $42.5 \text{ m}^3$  ( $1500 \text{ ft}^3$ ) of sediment was used in the basin for testing. Details of the sediment basin and global coordinates are shown in Fig. 3-2 and Fig. 3-3. Prior to placing the soft clay in the basin, a six-inch layer of fine sand was placed in the bottom of the basin. The sand layer was used as a safety depth gauge. It was predicted that as the anchor transitioned into the sand layer from the soft clay, the force transducers measuring the anchor line tension would spike; indicating to the operators to shut down the system, thus preventing damage to the anchor, the instrumentation and basin floor.

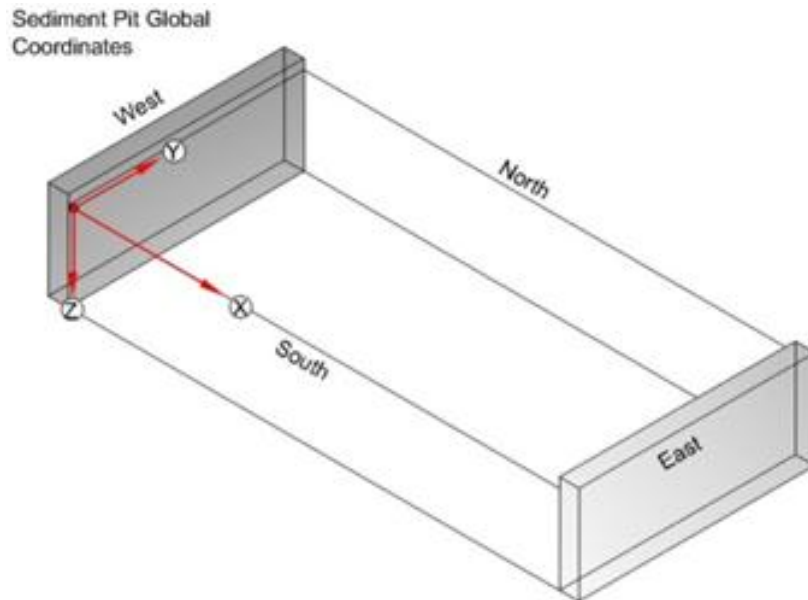


**Fig. 3-2.** Sediment Basin Global Coordinates

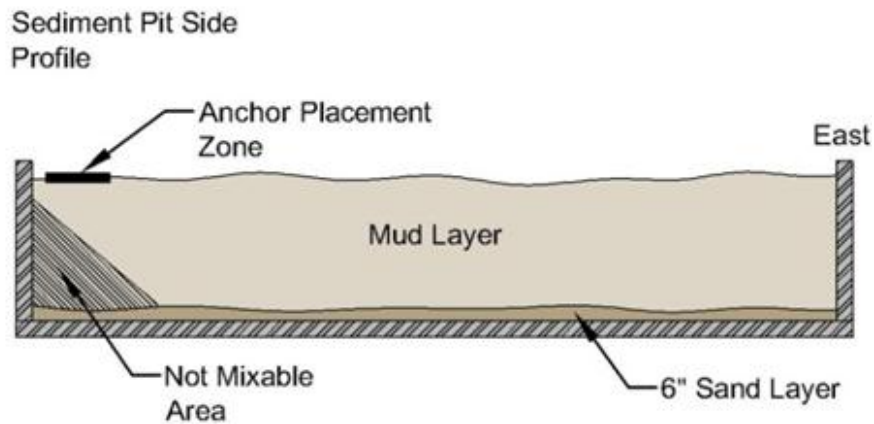


**Fig. 3-3.** Side Profile of Sediment Basin

The composition of the sediment was created from a precise mixture of dry granular bentonite clay and clean fine-grained sand. The granular bentonite clay was chosen over Kaolinite, for reduced airborne dust contamination and costs. These clays are predictable and relatively constant in their properties. Additionally, bentonite has the

characteristic of holding onto water molecules, therefore not easily changing pore pressure or water composition. The mixture was made on site using a motorized cement mixer and standard 18.92 L (5 gal.) buckets to measure by volume the desired amounts of sand, bentonite and water. The desired sediment mixture was 50% sand, 50% bentonite, and 125% water that resulted in a volumetric equivalent of 2.2 buckets of sand, 2.5 buckets of bentonite, and 7.7 buckets of water. The 0.57 m<sup>3</sup> (0.75 cubic yards) dump bucket was transported with the overhead crane in order to place the mud mixture into the sediment pit until it reached a depth of 15.24 cm (6 in) below the tow tank floor-to-basin opening transition line.

Samples of the sediment were taken periodically throughout the testing stage and analyzed for composition and bulk density. The results are provided in Table 3-1, which contains the composition by percent weight, bulk density, date and location of sample. As shown from the Table 3-1 over the course of the three months of testing, the overall composition of the sediment changed very little and was relatively uniform in distribution across the sediment basin.

**Table 3-1.** Sediment Composition

<b>Date</b>	<b>% Sand</b>	<b>% Bentonite</b>	<b>% Water</b>	<b>Bulk density kg/m<sup>3</sup> (lb/ft<sup>3</sup>)</b>
March 10, 2010 East End of Pit	48.4	51.6	128.2	1380.3 (86.17)
March 10, 2010 West End of Pit	50.2	49.8	120.7	1398.4 (87.30)
May 27, 2010	51.6	48.4	112.7	1410.8 (88.07)

An event occurred just prior to testing where water from an adjacent holding tank had leaked through and flooded over the top of the mixed sediment. The excess water was pumped off the sediment and large fans were used over the course of a few days to reduce the presence of surface water. After consulting with geotechnical engineering

experts, it was concluded that the flooding event would have little effect on the overall composition of the sediment. This conclusion is supported by the data obtained on May 27, 2010 that shows the percent water equal to 112.7, which is slightly less than the target goal of 125%. Otherwise, no additional water was added, therefore maintaining the composition over the course of the testing.

### *3.2.1 Sediment Mixing Device*

Preparing the sediment prior to and during testing required developing and constructing a mixing device. The mixing device was used extensively to mix the sediment matrix by breaking up clumps and distributing any pockets of water. For a period of approximately one week after initially placing the sediment into the basin, daily mixing occurred. The mixing device is powered by the dredge carriage cutter driveshaft. The device resembles a modified helix and was constructed out of 1.27 cm (0.5 in) diameter stainless steel solid round rod affixed to a 2.54 cm (1 in) diameter shaft leading outwards to an approximately 0.6 m (2 ft) diameter retaining ring as shown in Fig. 3-4. The device was approximately 1.52 m (5 ft) in length and was lowered vertically into the soft clay to a depth of 1.22 m (4 ft) and inclined approximately 40° to the horizontal for mixing the sediment.

This configuration was necessary due to the limitations of motion of the articulating arm and resulted in the shadow zone as shown in Fig. 3-3, where mixing did not occur over the testing phase. However, this area was expected and therefore used as the anchor initial placement site, which being on the surface, should have little effect on the tests. Fig. 3-5 shows the condition of the surface of the sediment just after being placed into the basin. The mixer successfully acted as a bed leveler, turning the initial lumpy and uneven surface into a smooth testing bed, which exhibited only minor peaks and valleys due to the mixer's path, and is shown in Fig. 3-6.



**Fig. 3-4.** Sediment Mixing Device



**Fig. 3-5.** Sediment Mixing Device at Work



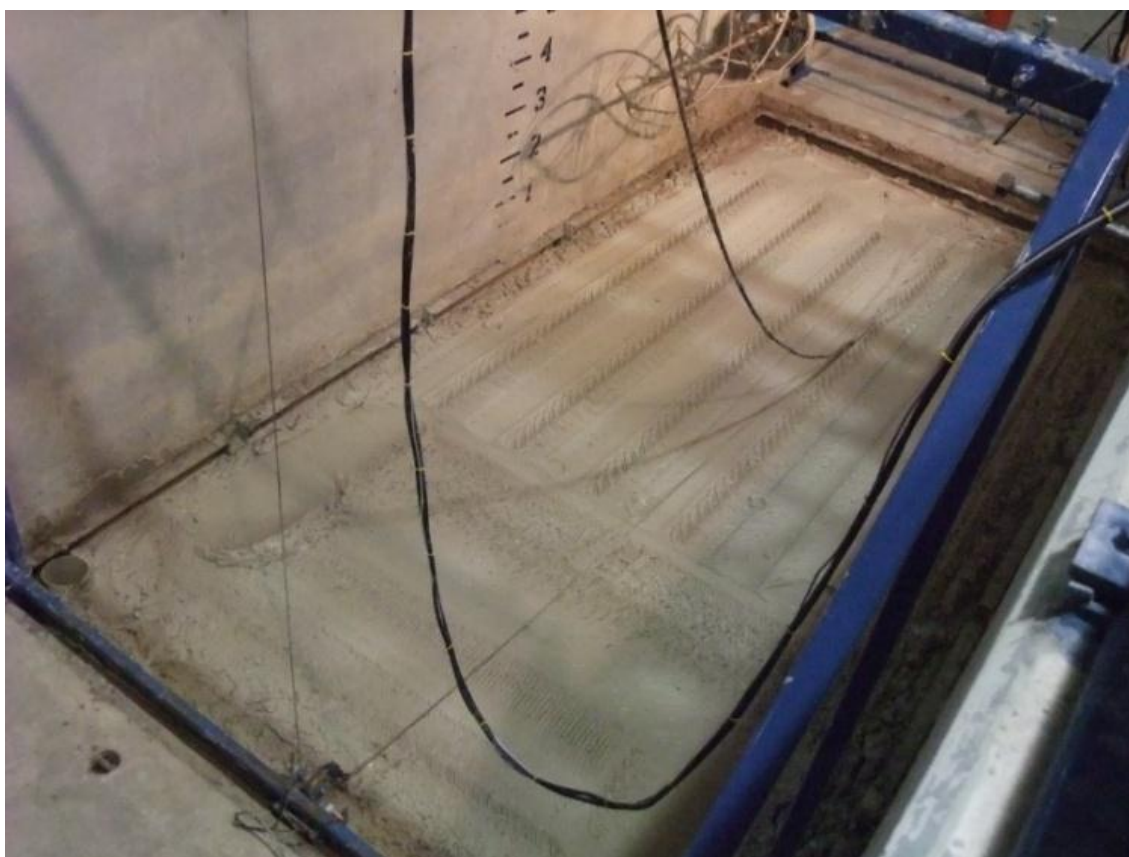


**Fig. 3-6.** Sediment Surface after Mixing

Mixing of the sediment was necessary after a series of tests contaminated the basin sediment with the tracks of the anchor. Removal of the tracks was performed in a semi-automated mixing procedure that involved overlapping paths of the mixing device. Removal of the tracks was important because the anchor chain and cable created a large trough in the sediment in addition to sheer paths from the anchor's movement through the soil, which would affect the trajectory and load results of an anchor whose path coincided with a previous track. It was necessary to uniformly disturb the sediment after the basin was completely contaminated with previous anchor tracks in order to maintain repeatability for subsequent tests.

### 3.2.2 Sediment Strength Testing

To determine the sediment strength, a testing device aptly named the T-bar was built and is shown in Fig. 3-7. The device used a cylindrical steel head that is 8.89 cm (3.5 in) in diameter and 30.48 cm (12 in) in length, giving a total projected area of 0.271 m<sup>2</sup> (0.292 ft<sup>2</sup>). The dimensions follow Stewart and Randolph (1994) for a length to width ratio greater than or equal to four. The 3.81 cm (1.5 in) square steel tube that connected the head to a load cell was polished and fitted to a slip joint. This prevented binding and rotational movement of the head and insured consistent measurement as the device was lowered into the sediment by the automated carriage ladder. The load cells used were Omega Engineering Inc. (2010), LCCD series. Initially, a 222.4 N (50 lb) rated cell was used but was replaced with a 444.8 N (100 lb) unit due to an overload condition. The sensors have a linearity of 0.03% Full Scale Output, (FSO) or 0.066 N (0.015 lb) and 0.133 N (0.03 lb), respectively. Each was calibrated in both tension and compression using a dead weight method. The strength profile was recorded to a depth of 0.91 m (3 ft) at a travel rate of 0.76 cm/s (0.3 in/s). A remolded profile was also recorded as the T-bar was lifted out after reaching the final depth. The un-drained shear strength is given by:

$$S_u = \frac{F}{N A_t} \quad (3)$$

where  $F$  is the measured force from the load cell in kN or lb,  $N$  is the constant bearing factor with a value of 10, and  $A_t$  is the constant projected area of the T-bar head 0.271 m<sup>2</sup> (0.292 ft<sup>2</sup>).





**Fig. 3-7.** T-bar Sediment Strength Testing Device

Before anchor drag tests were performed, the strength profile was tested at nine locations across the sediment pit for a measure of uniformity. The locations are illustrated in Fig. 3-8. Throughout the test schedule, two strength profiles were taken each day of testing from locations five and six, to measure consistency.



pressure pads work by compressing a rubber layer mounted to a steel plate that is attached to three-quarter inch diameter steel screw affixed to the support structure. This method was chosen in order to maintain the watertight integrity of the towing tank.

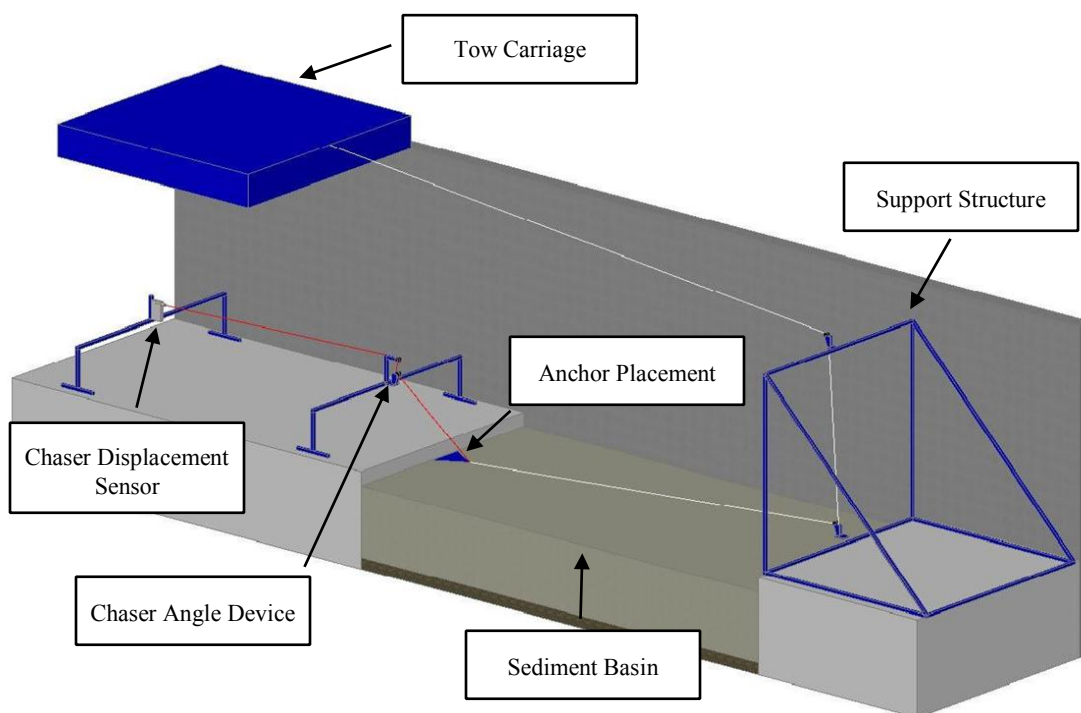


**Fig. 3-9.** Main Support Structure and General Layout

Additional design features of the support structure include the ability to slide the adjustable anchor towline device and top pulley across the width of the tank on the structure. This design feature was required to allow for multiple testing lanes across the width of the tank during in-plane experiments and to achieve the necessary out-of-plane pull angles. The second key design feature of the main support structure is to allow for an adjustable range of initial towline angles. This function is performed by moving the lower support crossbar vertically on welded tracks and locking it into position with jam bolts. The principle is illustrated in Fig. 3-10. This function was used for in-plane testing only. The black lines represent the main towline and angles formed with respect to the

sediment surface. Two additional support structures were constructed for the chaser line displacement sensor and chaser line angle measuring device represented by the blue T shaped crossbars in Fig. 3-9. The structures also used compression pads to prevent inadvertent movement and allowed the supported devices to be adjusted across the width of the tank to be in line with the main towline pulleys.

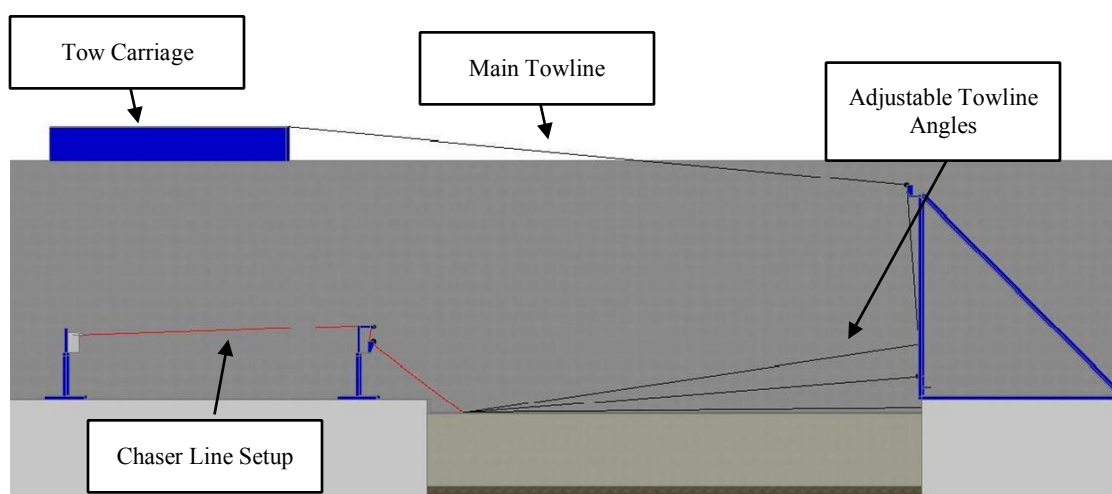


**Fig. 3-10.** Side View of Support Structure (Adjustable Tow Angle Range)

### 3.3.2 Chaser Line Principle and Design

The chaser line and associated devices are used to track the anchors path through the sediment. It works on the assumption that the small diameter wire line 0.53 mm (0.021 in) that connects to the anchors shank remains as a straight segment as it is pulled behind the anchor during testing. The cable was sized accordingly to impart minimal resistance and was pre-stretched to reduce elongation. The displacement of the chaser line was measured using an Automation, Sensors and Measurements (2010), (ASM) model WS17KT position sensor as shown in Fig. 3-11.



**Fig. 3-11.** Chaser Line Displacement Sensor

This device functions similar to a retractable tape measure: a cable wound around the sheave connects to a potentiometer that sends an analog voltage signal out representing the displacement. The device has a maximum measuring range of 14.69 m (48.2 ft) a linearity of  $\pm 0.10\%$  FSO or 1.49 cm (0.59 in). Calibration was obtained by using a tape measure and extending the sensor cable to fixed points and recording the voltage readings. The sheave was spring-loaded and imparted a measured constant 19.57 N (4.4 lb) of tension on the chaser line.

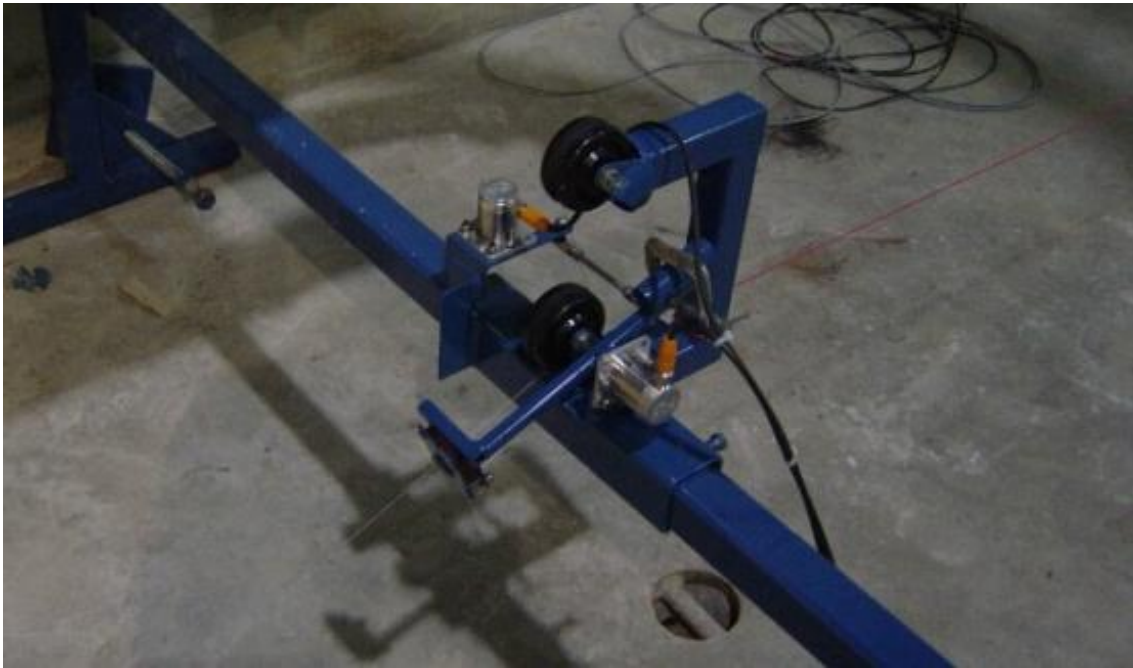


**Fig. 3-12.** Chaser Line Angle Measuring Device

Working in conjunction with the displacement device is a custom fabricated chaser line angle sensor. The device is shown in Fig. 3-12. The principle of this device is to measure the horizontal and vertical angle of the chaser line leading to the anchor. It functions by routing the chaser line through two grooved bearing mounted pulleys. The top pulley is fixed in position and is used solely as a guide. The bottom pulley has additional bearings that allow it to rotate freely in the horizontal plane. A follower arm that extends outwards and through which the chaser line exits, controls the direction of the pulley. This pulley is connected by linkage to a magnetic angular displacement sensor for measuring the horizontal angle of the cable.

An additional magnetic angular displacement sensor that acts as the pivot point for the follower arm measures the vertical angle of the cable. Due to the relatively low tension in the chaser line, the follower arm was precisely counterbalanced to prevent distortion of the line and subsequent vertical angle measurements. At the point on the follower arm through which the chaser line exited, two rubber grommets were placed with a hole sized according to the cable diameter. This served two functions, the first

was to remove excess accumulation of sediment from the line as it retracted, and the second was to allow for precise adjustments of the follower arm to the tangential point where the cable left the lower pulley. The type of sensor used is an ASM (2010), model POSIROT/PRAS analog magnetic angle sensor. These sensors impart minimal rotational resistance and allow for a full 360° range of motion, with a resolution of 0.03% FSO or 0.10° and a linearity of  $\pm 0.3\%$  FSO or 1.08°. The sensors were calibrated using a digital level. The vertical angle sensors were zeroed in-situ so that the 0° position was aligned with the horizontal plane. The horizontal sensors were aligned perpendicular to the support bar so that the 0° position ran parallel to the sediment basin's  $x$ -axis.

### *3.3.3 Anchor Towline Angle Measuring Device*

A second device was constructed to measure the horizontal and vertical angles of the main towline with respect to the sediment surface. It functions in the same manner as the chaser line device; however, it uses a single cast-iron grooved pulley with a load rating of 4 kN (900 lb). It employs two additional magnetic angle displacement sensors attached by linkage and the follower arm to measure the anchor line angles. The follower arm consists of the same rubber grommet principle for the exit point, but was not counterbalanced due to the greater tension within the anchor towline. The device was calibrated in the same manner as the chaser line and is viewed in Fig. 3-13. The convention used for defining the angle measurements for both the chaser line and the anchor line is illustrated in Fig. 3-14.



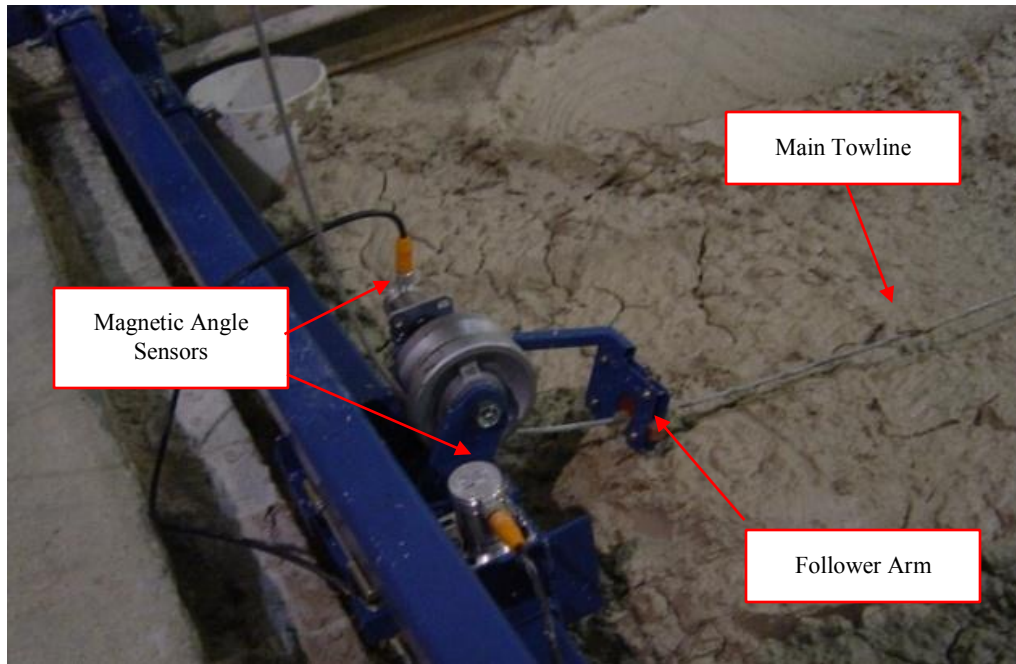


**Fig. 3-13.** Anchor Line Angle Measuring Device

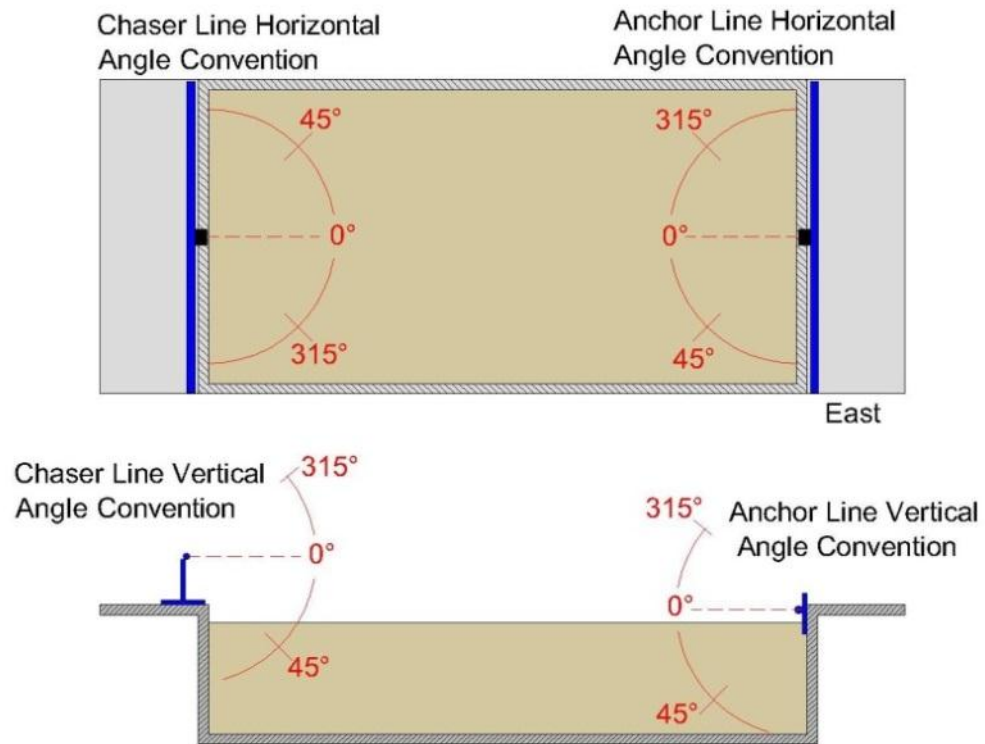


**Fig. 3-14.** Anchor and Chaser Line Angle Convention and Definitions



### *3.3.4 Carriage Force Transducer*

An Omega LCCD 2.2 kN (500 lb) rated load cell with a linearity of 0.03% FSO or 0.66 N (0.15 lb) was used as a redundant instrument for measuring the anchor's force. It was placed at the last link between the tow carriage and the main towline. It was predicted to show a higher force due to the added resistance of the towline in the sediment as well as the frictional resistance from the pulleys. Hemispherical ball joints were used to prevent torsion from acting on the sensor due to the inherent twisting found in wire rope cable. Prior to installation, the load cell was calibrated in tension and compression using a dead weight method.

### **3.4 Instrumentation Installed on the Anchor**

Three sensors were mounted to the anchor, including a pressure depth transducer, a two-axis inclinometer, and a force transducer for measuring the load at the anchor shank. Care was taken regarding the placement of the sensors in order to minimize any alteration of the anchors natural behavior and trajectory. The pressure transducer and inclinometer were mounted to the base of the fluke and positioned directly in line with the  $x$ -axis of the anchor. The data cables connecting to the sensors were bundled together and routed out from the back of the anchor and over the top where they were secured to the anchor chain. The locations of the sensors are illustrated in Fig. 3-15. Details regarding the specifics of each sensor and calibration methods are discussed in the following subsections.

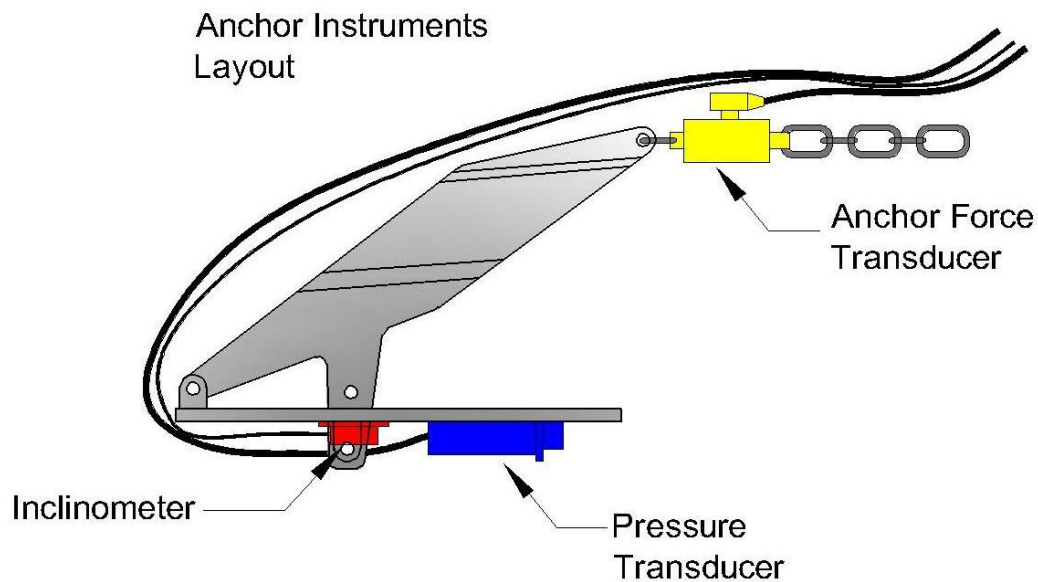


**Fig. 3-15.** Anchor Mounted Instrument Positions

#### 3.4.1 Pressure Transducer

The pressure transducer used for additional depth measurements was a Stellar Technology Inc. (STI) (2010), FT-2900 analog internally amplified, submersible open diaphragm 0-1034 kPa (0-150 psig) transducer. The transducer has an accuracy of 0.25% FSO or 2.58 kPa (0.375 psig). The pressure face was positioned to prevent shielding and reduce exposure to recently disturbed sediment due to the chain and shank's path. The transducer was calibrated by mounting it vertically to a pole that an operator lowered into the sediment basin in measured increments from the surface to a depth of 1.21 m (4 ft). Further calibration involved lowering the transducer into a fresh water basin to a depth of 4.87 m (16 ft) and converting the values from meters of water to meters of sediment by using the specific weight (bulk density) of  $1361.5 \text{ kg/m}^3$  ( $85 \text{ lb/ft}^3$ ) for the sediment. The weight of the transducer in air is 0.6 kg (1.33 lbs).

### 3.4.2 Inclinometer

The ASM POSITILT/PTAM 2-axis analog inclination angle sensor is used to measure the anchor's pitch and roll. The measurement range is  $\pm 60^\circ$  from the horizontal with the resolution of  $0.05^\circ$  and linearity of  $0.5^\circ$ . It was placed directly behind the pressure transducer on the bottom side of the fluke. The weight of the sensor in air is 0.095 kg (0.21 lb). The calibration process consisted of careful alignment of the sensor axis to the anchor axis. After which a digital level and shims were used to vary the inclination along an isolated axis. The digital level's value and the sensor's voltage were recorded and this process was repeated for the second axis. The output angle sign convention is illustrated below in Fig. 3-16. The angle between the fluke with respect to the horizontal "surface" plane is defined as the pitch angle and should not be confused with the fluke angle setting that is defined as the fixed angle between the fluke and the shank.

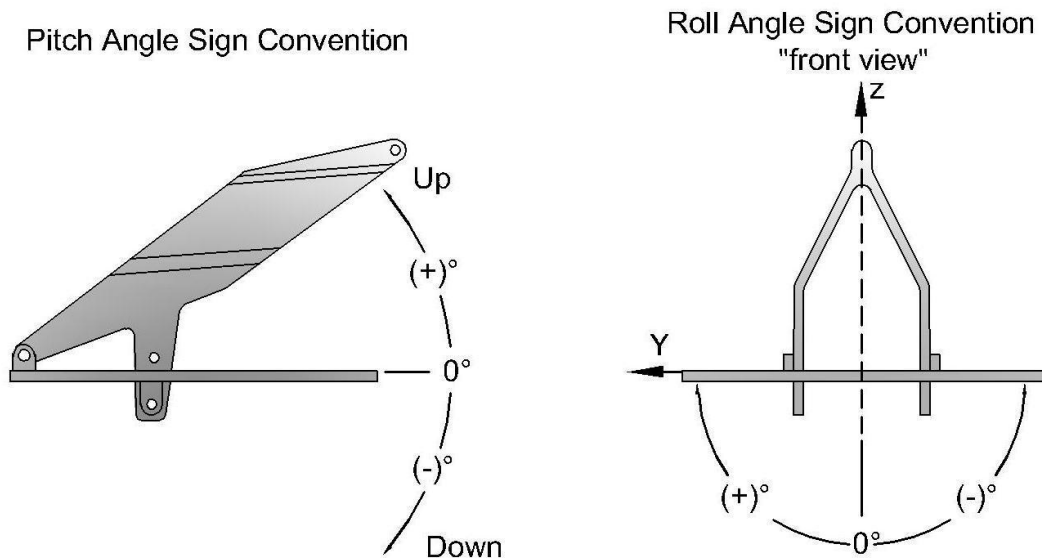


**Fig. 3-16.** Anchor Pitch and Roll Sign Convention

### 3.4.3 Anchor Force Transducer

A tension only, 0-2.22 kN (0-500 lb) analog, internally amplified, submersible Stellar Technology Inc. (STI) (2010), model RDE900-500LBTL-141 force transducer was mounted as the last link between the anchor and the chain as shown in Fig. 3-15. The transducer has a static accuracy of 0.022% FSO or 0.489 N (0.11 lb) and a repeatability of 0.011% FSO or 0.244 N (0.055 lb). The data cable was placed behind the anchor chain and cable ties were used to secure it. The sensor weighs 0.535 kg (1.18 lb) in air. The calibration method used precisely measured lead weights incrementally placed into a bucket connected to the force transducer that was suspended from the overhead crane.

## 3.5 Breakout Testing Devices

The breakout tests required two additional devices to be constructed in order to isolate the anchors breakout strength in the respective directions. A modified version of the T-bar was used to perform the normal breakout tests. The device isolated the anchor movement to pure normal i.e. perpendicular to the fluke. The original 444.82 N (100 lb) load cell was replaced with a 2.22 kN (500 lb) version that is the same one used for the carriage load cell, because the estimated load exceeds the original capacity. The cylindrical head of the T-bar was unbolted and new mounts were welded to the anchor fluke centroid.

In order to isolate the pure transverse breakout strength of the anchor, a moment arm device was built as shown in Fig. 3-17. The device is attached to the carriage ladder. A 2.22 kN (500 lb) cell is used in a compression only connection. The connection to the anchor is made again through the fluke plate centroid and measures the forward and after rotating the anchor 90° the lateral transverse breakout strength. Due to the moment arm geometry, a 6.52 amplification ratio is applied to the load cell and was back calculated to provide the moment at the fluke base.

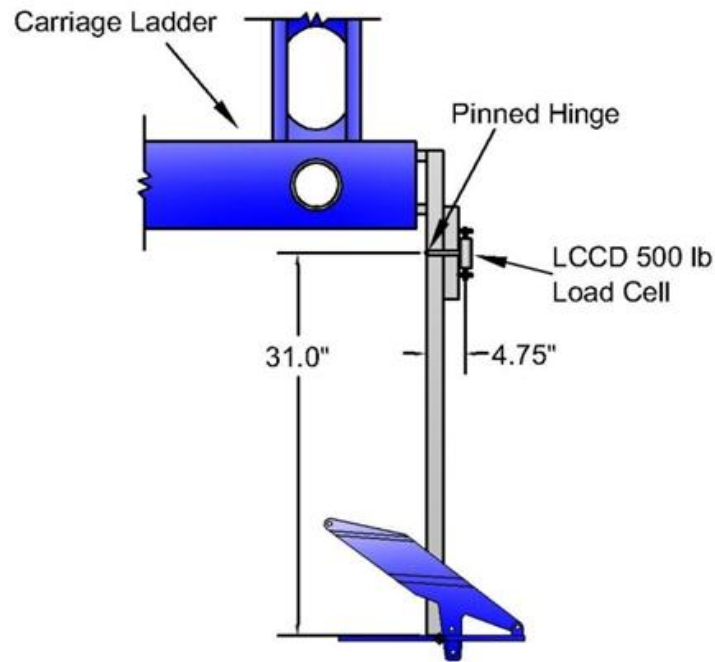


**Fig. 3-17.** Transverse Breakout Testing Device

In order to measure the rotational breakout strength, a device was constructed to measure the breakout moment around anchors  $x$ ,  $y$  and  $z$ -axis through the fluke centroid. A bearing mounted shaft was fixed to the carriage ladder with an adjustable moment arm connection using the 444.82 N (100 lb) load cell from the T-bar testing device. The anchor fluke base is directly welded to the shaft at points coincident with the respective axis of rotation about the fluke plate's centroid an example is shown in Fig. 3-18 (left). The device features an adjustable moment connection used to optimize the force applied to the load cell with a midpoint of approximately 222.4 N (50 lb) as a target. Trial runs were performed for each axis of rotation to determine the final moment arm connection distance per respective axis. An example of the testing in operation is provided in Fig. 3-18 (right). These values were applied to the raw data to produce the moment around the fluke plate.

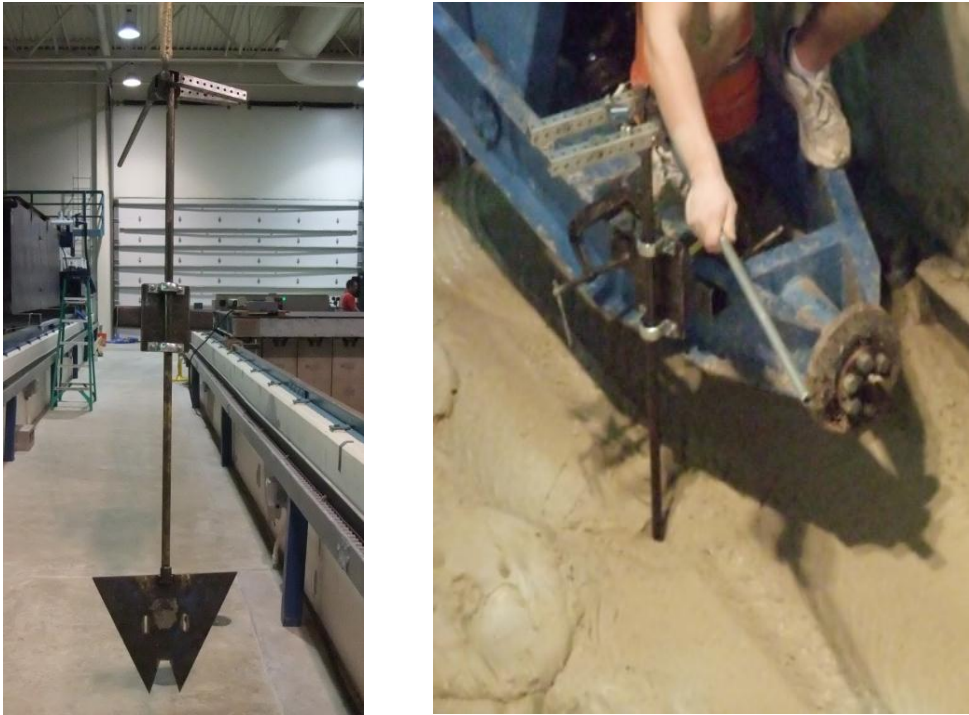


**Fig. 3-18.** Rotational Breakout Device (left), in Operation (right)

### 3.6 Anchor and Towline Properties

The 1:10 length scale generic anchor was fabricated by Delmar Systems Inc. The anchor was built from 0.635 cm (0.25 in.) thick mild steel designed to have adjustable fluke angle settings. The fluke length is 0.45 m (1.48 ft). The raw weight of the anchor in air is 7.16 kg (15.8 lb), and with the addition of the aforementioned sensors, the total weight is 7.86 kg (17.34 lb). Comparison to the typical prototype weight and fluke length for a 4.5 m (14.7 ft) using Fig. 2-1 indicates a weight of 22,891.0 kg (50,466.0 lb). Scaled accordingly would give a model weight of 28.4 kg (62.6 lb), a factor of 3.61 greater than the tested model; therefore a distorted weight scale was used.

The centroid location was calculated based on the fluke plate dimensions as shown in Fig. 3-19. The centroid location was used to determine the three adjustable fluke to shank angle settings that are 22°, 36° and 50° and the associated heights from

the fluke plate to the shank pad-eye as illustrated in Fig. 3-20. Definitions regarding the anchor coordinate and motions are illustrated in Fig. 3-21.

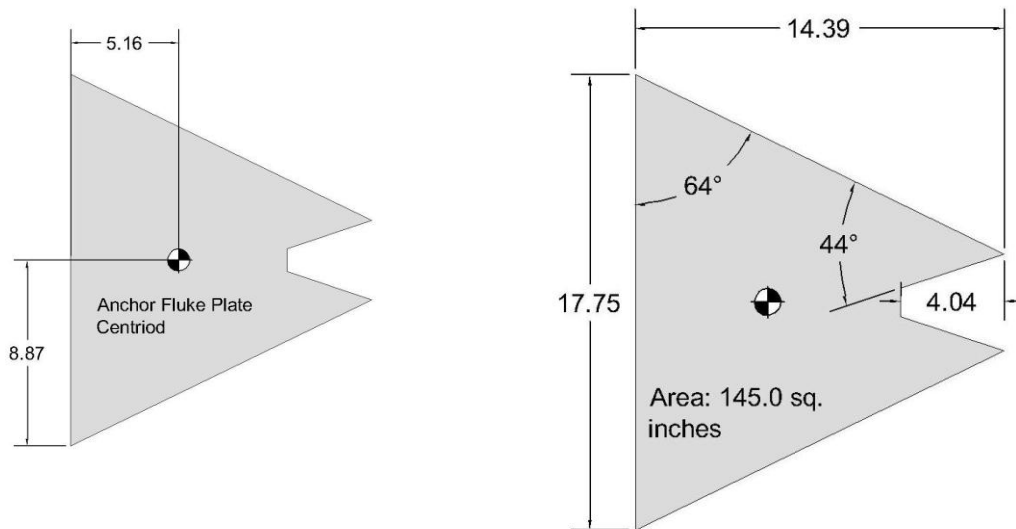


**Fig. 3-19.** Fluke Centroid Location (left), Fluke Plate Dimensions (right), (units listed in inches)

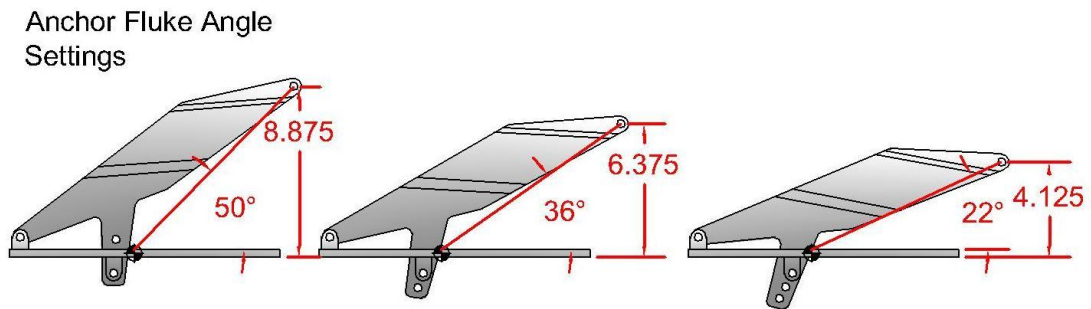


**Fig. 3-20.** Anchor Fluke Angle Settings. (Units in degrees and inches as measured to the fluke plate centroid)

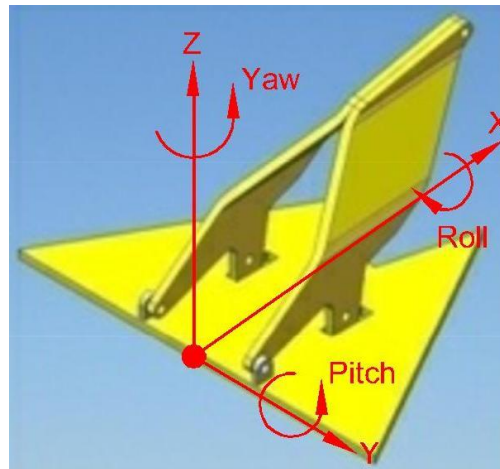


**Fig. 3-21.** Anchor Coordinates

The primary towline was created from 4.76 mm (3/16 in) diameter galvanized wire rope. The connection to the anchor was made through a series of swivels and shackles to a 0.86 m (2.83 ft) length of 4.76 mm (3/16 in) open link chain with a projected cross sectional area of  $0.0483 \text{ cm}^2$  ( $0.75 \text{ in}^2$ ). The unit weight of the chain per foot is 0.048 kg/m (0.348 lb/ft), combined with the unit weight of the three data cables for the anchor mounted sensors of 0.012 kg/m (0.09 lb/ft) gives a total of 0.0729 kg/m (0.528 lb/ft). The actual anchor used for the experiment with the bundled data cables, shackle force transducer and chain is shown below in Fig. 3-22.





**Fig. 3-22.** Anchor Used in Experiment

### **3.7 Data Collection and Instrumentation Notes**

Ten individual sensors were used during the experiment. The calibration of each sensor was used to transform the voltage outputs into the associated physical parameter. The physical equations were programmed into LabVIEW to record the data at a rate of 25 Hz. Due to the scale of the model testing and the physical size of the towing tank, each sensor required a very long run of shielded data cable. The long distances also required that the sensors have internal amplification that gave an output voltage range of 0 to 28 V. The ASM sensors were unique by having a nonzero start position. The minimum voltage reading was 0.5 V and was used to gauge whether or not the instrument was online and working properly.

## 4. PROCEDURES

### 4.1 In-Plane Testing

The goal of in-plane testing has two main functions. The first is to validate the accuracy and repeatability of the testing protocol prior to testing the out-of-plane. The second is to determine the effects of velocity, fluke angle and towline angle. The in-plane tow tests start by aligning the main towline and the chaser angle devices. An operator places the anchor on the surface of the sediment and embeds the anchor until the shank parallel to the mud line at the sediment surface. The slack is removed from the main towline by moving the carriage until the lines are slightly tensioned. The overhead crane lifts the data cables leading to the anchor in order to reduce any influences of the cables on the anchor trajectory. The anchor is pulled a minimum of 4.87m (16 ft) horizontally in the  $x$ -direction for each test. Thirty-six tests were performed, two tests per variable to validate repeatability. The width of the sediment basin allowed for an average of six in-plane tests to be performed before mixing was required. The variables analyzed are the fluke angle settings of  $22^\circ$ ,  $36^\circ$  and  $50^\circ$ . Two tow velocities of 0.13 m/s (0.42 ft/s) that corresponds to a prototype equivalent speed of 2 fluke lengths/min and 0.19 m/s (0.62 ft/s) the equivalent of 3 fluke lengths/min. In addition, the initial towing angle was varied at approximately  $5^\circ$ ,  $10^\circ$ , and  $20^\circ$  with respect to the sediment surface. Examples of the initial placement of the anchor and setup are shown below in Fig. 4-1.



**Fig. 4-1.** Anchor Surface Position Detail (left), In-Plane Line Position (right)

#### **4.2 Initial Surface and Sub-surface Out-of-Plane Tests (Case 1)**

This test was developed to determine the reaction of the anchor during the initial phase of embedment. It simulates the condition of an anchor resting on the seabed prior to drag in and is used to determine if initial out-of-plane towing affects the holding capacity or embedment depth. The anchor's heading was aligned on the surface to an angle of  $45^\circ$  or  $90^\circ$  to the direction of the main pull line as illustrated in Fig. 4-2. The anchor chain and data cable were then routed at the corresponding angle outwards from the anchor for a total distance of the chain length of 0.85 m (2.8 ft). The rest of the anchor towline was aligned parallel with the sediment basin's  $x$ -axis leading back through the anchor towline angle device. The anchor was then towed approximately 4.87 m (16 ft) in the  $x$  direction. Each fluke angle setting was tested four times, two per speed setting and initial degree heading of  $45^\circ$  and  $90^\circ$ . The uplift pull angle remained at the lowest setting of  $5^\circ$  for all tests in this case. The sub-surface tests repeated the above parameters; however, the anchor and chain were manually embedded to an approximate depth of 0.35m (14 in.) to the pad eye at  $45^\circ$  and  $90^\circ$  to the main pull line direction. The anchors were pulled approximately 4.87m (16 ft) and the data cables leading to the

anchor were supported by the crane as described for the in-plane tests. A total of 40 tests were performed including repeats.

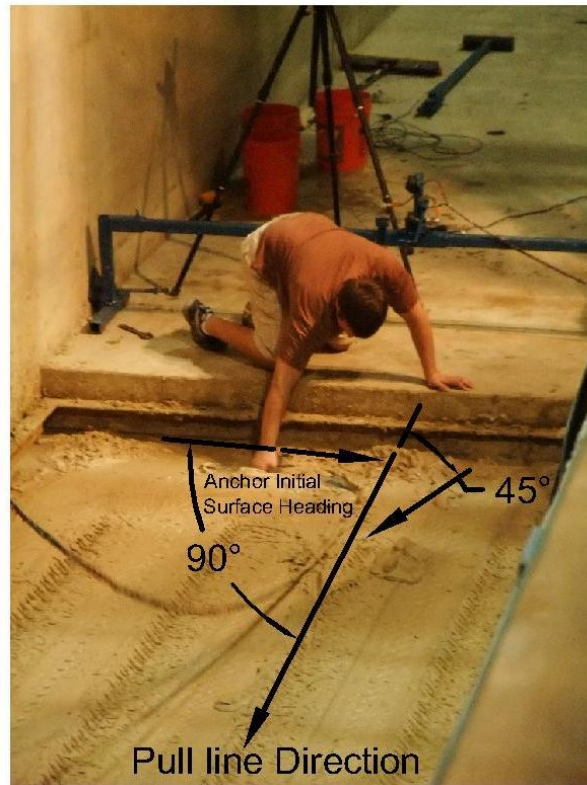


**Fig. 4-2.** Surface Out-of-Plane (Case 1)

### **4.3 Main Tow Line Out-of-Plane Tests (Case 2)**

The purpose behind this procedure is to simulate the conditions of a MODU drifting from the original installed position. The preset anchors are subjected to a rapid out-of-plane angle load. The degree range simulates the angle possibilities applied to individual anchors of an eight-point mooring as initial drift occurs. These out-of-plane tests involved placing the anchor on the surface, similar to the in-plane tests, pre-tensioning the main cable and pulling for a short preset distance of either 0.457 m (18

in.) or 1.01 m (40 in.), which represents an approximation of one and three fluke lengths respectively.

The anchor angle measuring apparatus with the main pull line is re-positioned by sliding the device across the support bar to pre-determined positions after which it is locked into place. The cable is pre-tensioned before completing the pull to a final distance along the new main pull line heading. The change in headings are designed to produce three different out-of-plane pull angles of  $15^\circ$ ,  $30^\circ$  and  $45^\circ$ . Fig. 4-3 shows a  $15^\circ$  test where the dashed line indicates the first pull heading and the solid line indicates the position of the final heading. The motion of the carriage was stopped and reversed to allow for enough slack in the main pull line to reposition the gear without disturbing the anchor. The chaser cable angle measuring apparatus remains in position, and data collection is continuously running.

In order to obtain the  $30^\circ$  pull angle, it is necessary to install one of the 1.52 m (5 ft) wide floor plates over the western edge of the basin and reposition the chaser devices to the edge of the floor plate. The  $45^\circ$  angle requires the installation of two floor plates to achieve the desired heading. Since adding the floor plates shortened the overall distance of the sediment basin, the  $30^\circ$  and  $45^\circ$  tests were not pulled the same distance as the in-plane tests. Examples of the pull paths are shown in Fig. 4-4. The total pull distance was varied by the initial heading length of one or three fluke lengths and by the out-of-plane angle. Each fluke angle setting was pulled twice per initial displacement per out-of-plane angle for a total of 24 tests. The velocity was fixed at 0.13 m/s (0.42 ft/s) as well as the anchor vertical initial pull angle at  $5^\circ$ .

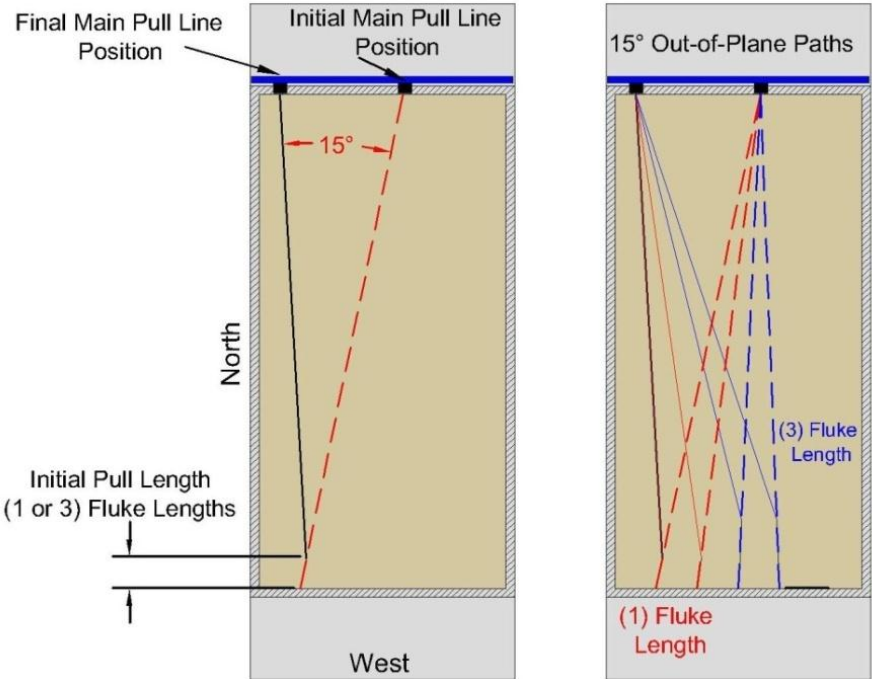


Fig. 4-3. Towline Paths for 15° (Case 2)

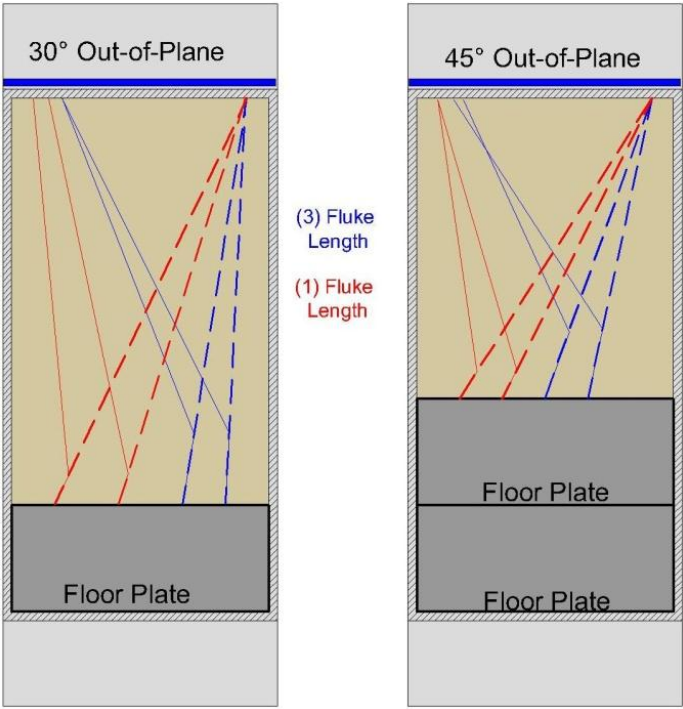


Fig. 4-4. Towline Paths for 30° and 45° Tests (Case 2)

#### 4.4 Continuous Degree Change Out-of-Plane Tests (Case 3)

This test simulates an anchor undergoing a gradual and continuous change of out-of-plane loading that represents a lateral mooring line condition with respect to the drift heading. These out-of-plane tests involve mounting the anchor angle device directly to the lower carriage ladder frame. The vertical anchor angle zero position remains the same, however the horizontal zero position is changed to  $45^\circ$  off the sediment basin's  $x$ -axis directed to the north. This is required to accommodate the potentially large range of angular displacement.

The main pull cable was reduced in length to approximately 0.6 m (2 ft) before connecting to the original chain with a length of 0.863 m (2.83 ft). The chaser angle device was moved to the east end of the basin and functions in the same manner as the previous tests. The anchor is placed on the surface in the same procedure as the in-plane tests but oriented due south and the carriage ladder is in position one as illustrated in Fig. 4-5. The carriage's  $y$ -axis velocity was programmed to 0.13 m/s (0.42 ft/s) to match the  $x$ -axis velocity. The ladder moves south for an initial embedment of one or three fluke lengths depending on the tests schedule. Immediately on reaching position 2, the carriage ladder was moved west at the fixed rate of 0.13 m/s (0.42 ft/s) for a distance of 4.57 m (15 ft). The ladder path is labeled in blue and the black line represents the expected example path of the anchor. Four tests were conducted.



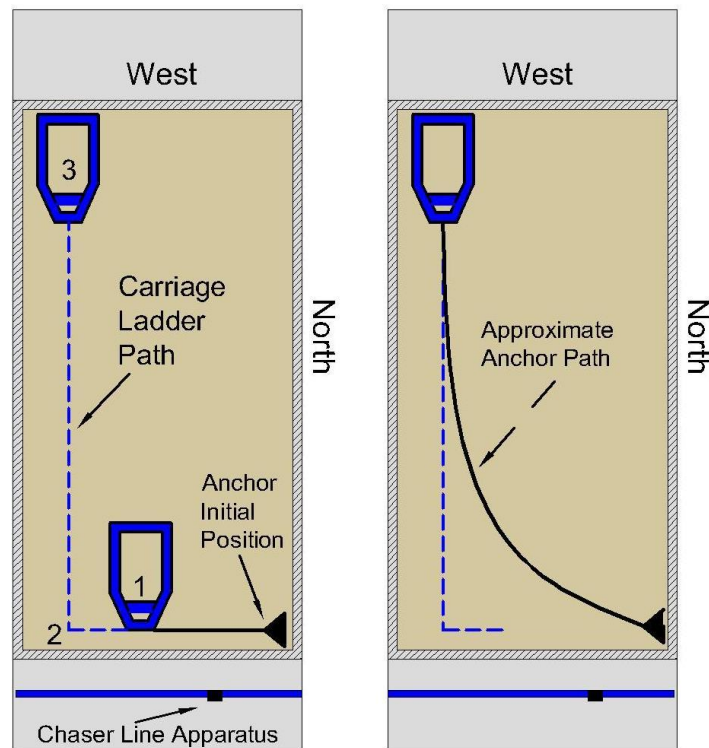


Fig. 4-5. Carriage Ladder Towing Path (Case 3)

#### 4.5 Breakout Test Procedures

For the normal test the anchor is lowered to a depth of 0.81 m (32 in), moved forward two fluke lengths into less disturbed mud and allowed to rest for 5 minutes. The resting phase allows for any internal stresses within the soil to dissipate due to the recent movement of the anchor. The anchor is then raised vertically at a rate of 7.6 cm/s (3 in/s) to the surface while recording the data. Two tests were performed for each fluke angle setting of 22°, 36° and 50° for a total of six tests. The transverse test procedure lowered the anchor to a depth of 0.609 m (2 ft) as measured from the mud surface to the fluke plate. The anchor is moved forward 0.609 m (2 ft) into less disturbed sediment and after a short pause of approximately 10 s the data collection begins and the anchor is moved forward approximately 0.914 m (3 ft) at a rate of 0.13m/s (0.42 ft/s).



Twelve tests were conducted, two tests for each fluke angle setting in x-axis direction of the anchor, and an additional six, two per fluke angle in the y-axis direction requiring the anchor to be unbolted and rotated 90° about its axis. For the rotational tests the anchor is lowered into the mud to a depth of 0.609 m (2 ft) measured from the point of initial mud contact. A waiting period of 5 minutes is applied before the anchor is rotated and data recorded. One single operator was chosen to manually rotate the device for every experiment in this category to support consistency. The operator was directed to maintain a constant rate of rotation through 90° or a quarter of a turn. Two tests were performed for each fluke angle setting about the  $z$  and  $x$ -axis for a total of 12 tests. Rotation about the  $y$ -axis involved four tests per fluke angle, two in down-pitch and two in an up-pitch rotation direction. This was needed because the  $y$ -axis of the anchor is the only one that is asymmetrical.

## 5. RESULTS AND DISCUSSION

### 5.1 Sediment Strength Testing

The data obtained from the sediment strength testing is critical for determining the anchors holding capacity. The results shown from March 25, 2010 in Fig. 5-1 indicate that the variation of the un-drained shear strength of the sediment across tank is fairly uniform with the exception of points eight and nine. These points correspond with the northwestern most section of the sediment basin. Any testing performed in this section will result in higher anchor line tension when compared to areas adjacent to the site.

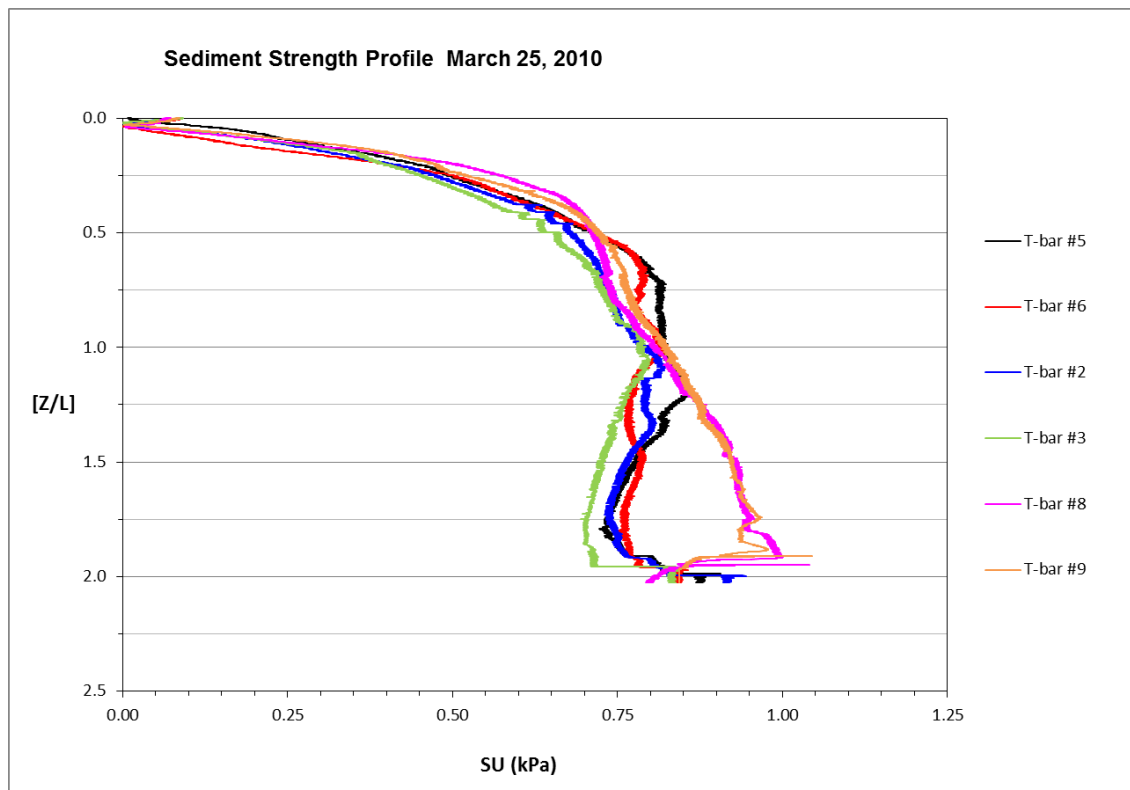


**Fig. 5-1.** Sediment Strength Profile from March 25, 2010

The average value of the un-drained shear strength used for calculating the holding capacity of the anchors is 0.764 kPa (16 psf). The values measured at T-bar location eight and nine are approximately 25% greater in strength with  $S_u$  equal to 0.95 kPa (19.8 psf). Inspection of the sediment strength profiles taken on a daily testing basis for T-bar locations five and six show little variation from the average value of 0.764 kPa (16 psf).

## 5.2 In-Plane Results

A total of 36 tests were conducted for the in-plane testing with the fluke angle at 22°, 36° and 50°, the towing angle at approximately 5°, 10°, and 20°, and the towing speed of 0.13 m/s (0.42 ft/s) that is the prototype equivalent speed of 2 fluke lengths/min and 0.19 m/s (0.62 ft/s) that is the prototype equivalent speed of 3 fluke lengths/min.

The trajectories for all of the experiments were derived from the raw data. The initial origin is taken from the tangential point on the bottom of the lower chaser line angle devices pulley. Measuring from this point down to the surface of the sediment gives a fixed height (distance) equal to 0.82 m (2.7 ft), which is used in conjunction with the vertical chaser line angle to solve for the initial radius  $\rho_o$  indicated by the blue line segment in (Fig. 5-2).  $\Delta x$ ,  $\Delta y$  and  $\Delta z$  are then calculated using spherical coordinates based on the measured initial horizontal and vertical angles.

The origin is then transformed by moving it from the initial origin by the corresponding displacements  $\Delta x$ ,  $\Delta y$  and  $\Delta z$  creating the new origin for the anchor pad-eye. The chaser displacement initial value is then zeroed out and all subsequent displacements and changes in the horizontal and vertical angles are used to determine  $\Delta x$ ,  $\Delta y$  and  $\Delta z$  that trace the anchors path with time. This method for calculating the anchor trajectory was used for each test case.

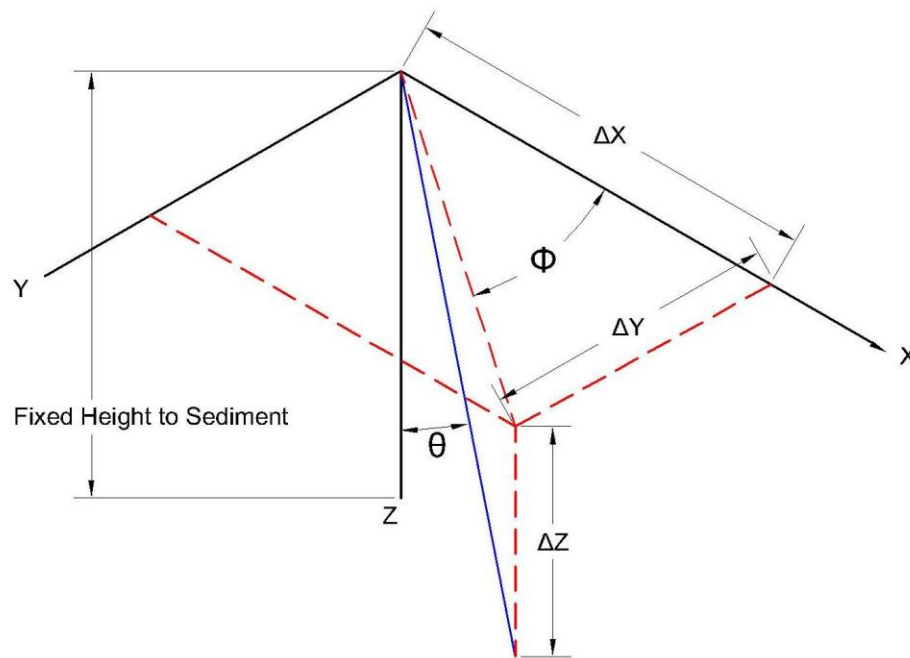


**Fig. 5-2. Spherical Coordinates for Trajectory Calculations**

The data for the in-plane experiments were compiled and analyzed for trends relating the anchors dimensionless holding capacity ( $N_{eq}$ ) to changes in velocity, fluke angle, and tow angle. ( $N_{eq}$ ) is given by:

$$N_{eq} = \frac{F_a}{S_u A_F} \quad (4)$$

where  $F_a$  is the measured anchor shackle force,  $S_u$  is the un-drained shear strength of the sediment determined from the T-bar testing device, and  $A_F$  is the area of the fluke plate. Composite charts such as the one shown in Fig. 5-3 were developed to determine the relationship of  $N_{eq}$  and normalized pitch with respect to normalized depth. Normalizing the pitch is simply a matter of taking the recorded pitch angle data provided by the inclinometer and dividing it by the respective fluke angle, in this case  $36^\circ$ . The normalized depth is achieved by dividing the depth determined from the trajectory calculations by the anchors fluke length.

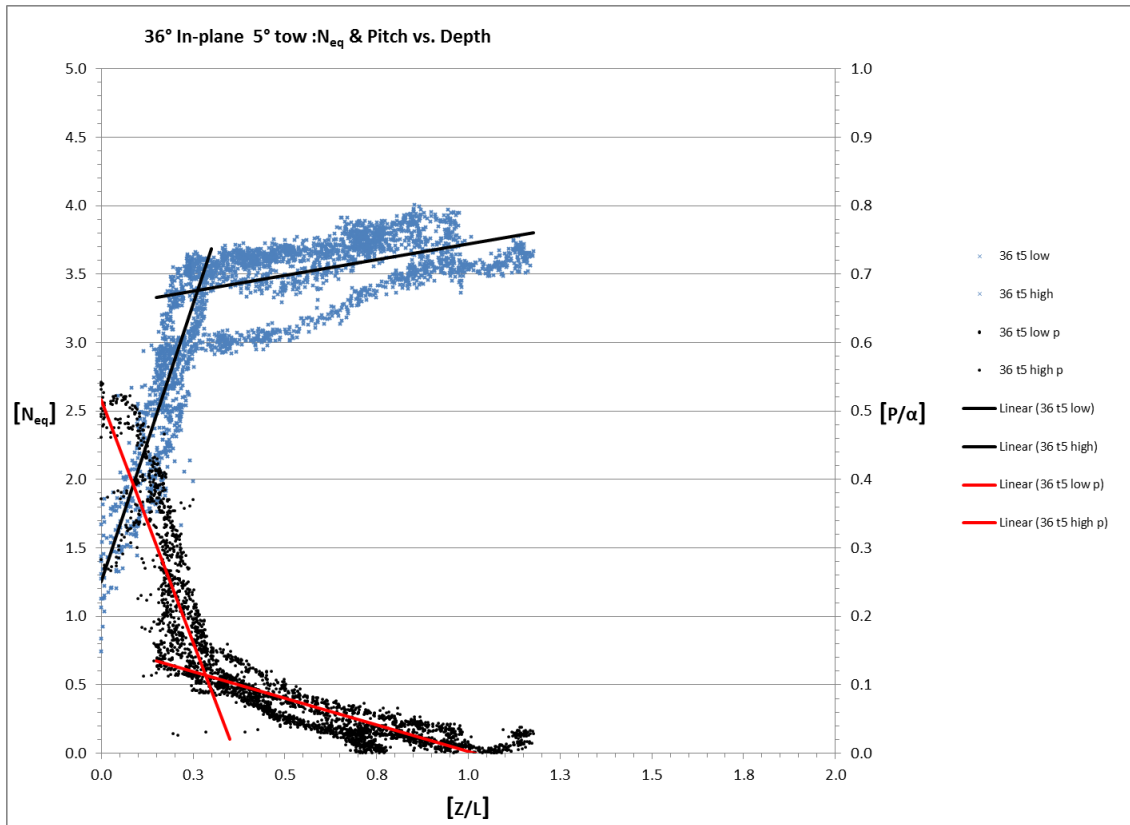


**Fig. 5-3.** 36° In-Plane 5° Tow Angle  $N_{eq}$  and Pitch vs. Depth

Fig. 5-3, above shows the combined data from four in-plane 36°, 5° tow angle, 0.13 m/s (0.42 ft/s) and 0.19 m/s (0.62 ft/s) velocity tests. Trimming of the tail end of the data sets used in developing these plots was required because data was still recording after the carriage stopped moving. The blue data points indicate the non-dimensional holding capacity with respect to normalized depth, the black data points represent the non-dimensional pitch angle with respect to normalized depth plotted on the secondary vertical axis of the chart. The data shows a clear pattern relating holding capacity changes with pitch angle changes.

Linear trend lines were fitted to the data in two stages. In each test there exists a transitional period where the anchor rapidly climbs to a holding capacity as indicated by the first black fitted line before transitioning to a more gradual slope line for the remainder of the embedment. The red lines representing the rate of change of pitch with respect to normalized depth are clearly proportional to the holding capacity. As the pitch angle levels out to a nearly horizontal position with respect to the sediment surface, there is little change to the increase of holding capacity. The data sets were further broken down into velocity pairs for analysis of velocity dependencies as shown in Fig. 5-4.

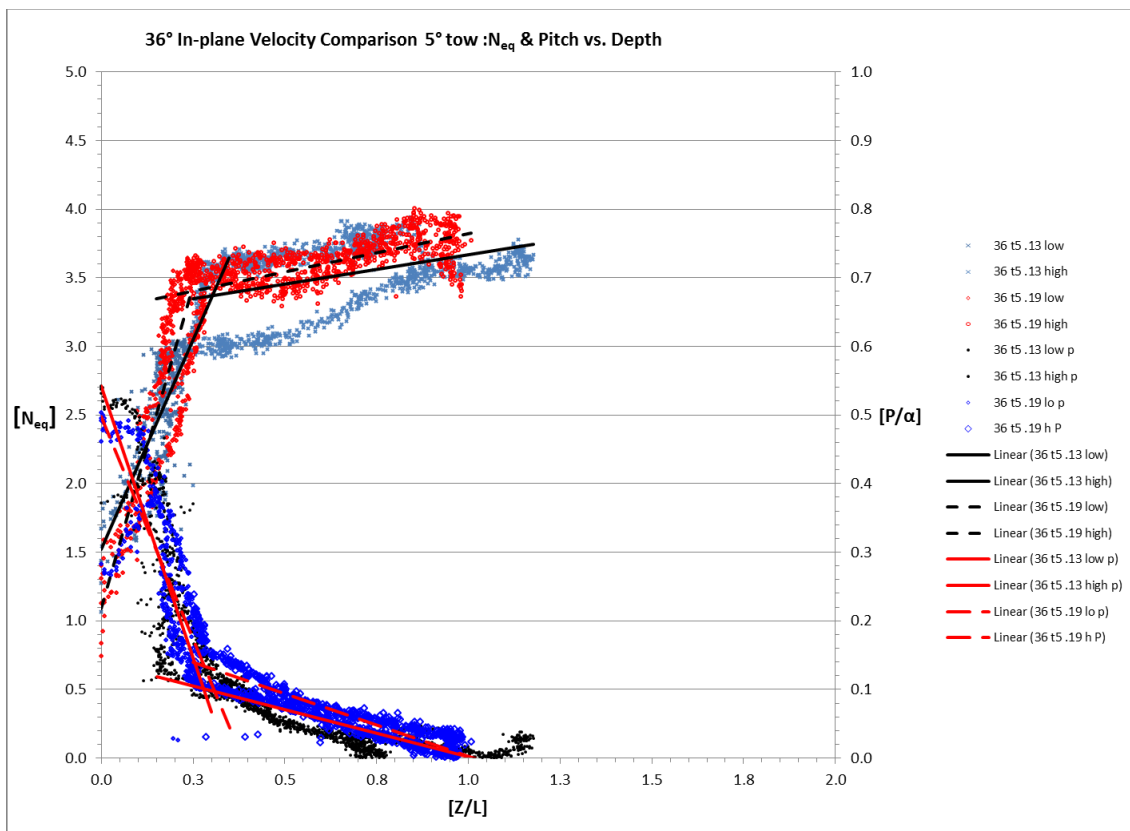


Fig. 5-4. 36° In-Plane Velocity Comparison, 5° Tow Angle

In Fig. 5-4, the data sets are differentiated by velocity. The 0.13 m/s (0.42 ft/s) test are represented by the solid lines and the 0.19 m/s (0.62 ft/s) tests by the dashed

lines. The rate of change of the holding capacity and the pitch both increase with velocity. Composite charts were developed for each test within the experiment and may be referenced in the appendix. The slopes of the holding capacity and pitch lines were extracted from the referenced plots for comparison purposes.

### *5.2.1 In-Plane Initial Tow Angle Results*

The composite charts for the 50° fluke angle tests with combined velocities produced the slopes used for comparison purposes of the second stage (high range) holding capacity and pitch versus depth for the 5°, 10°, and 20° initial towing angles as shown in Fig. 5-5. The chart indicates that as the towing angle increases the rate of change of the holding capacity increases proportionally. However, the rate of change of the pitch with respect to depth does not exhibit the same increase. Each line is nearly parallel with the others.

The angle of the main towline with respect to the sediment surface is not constant in any given test; rather it increases as the anchor moves closer to the main towline pulley. Increasing the initial towline angle intuitively creates a load applied to the anchor that is no longer directly horizontal with the surface of the mud. Vryhoff (2010) suggests that drag embedment anchors have low resistance to vertical loads; however, the data presented here in comparison of the 5° initial towline angle to the 20° initial towline angle shows that capacities are similar. Moreover, the 20° initial towline angle achieved the same holding capacity at a shallower depth than the 5°. The 10° tests support the trend of increasing rate of change of holding capacity with respect to depth by having a slope that is higher than the 5° towline and less than the 20° towline, however the ultimate holding capacity is less. This may be attributed to the variation of soil strength within the sediment basin.

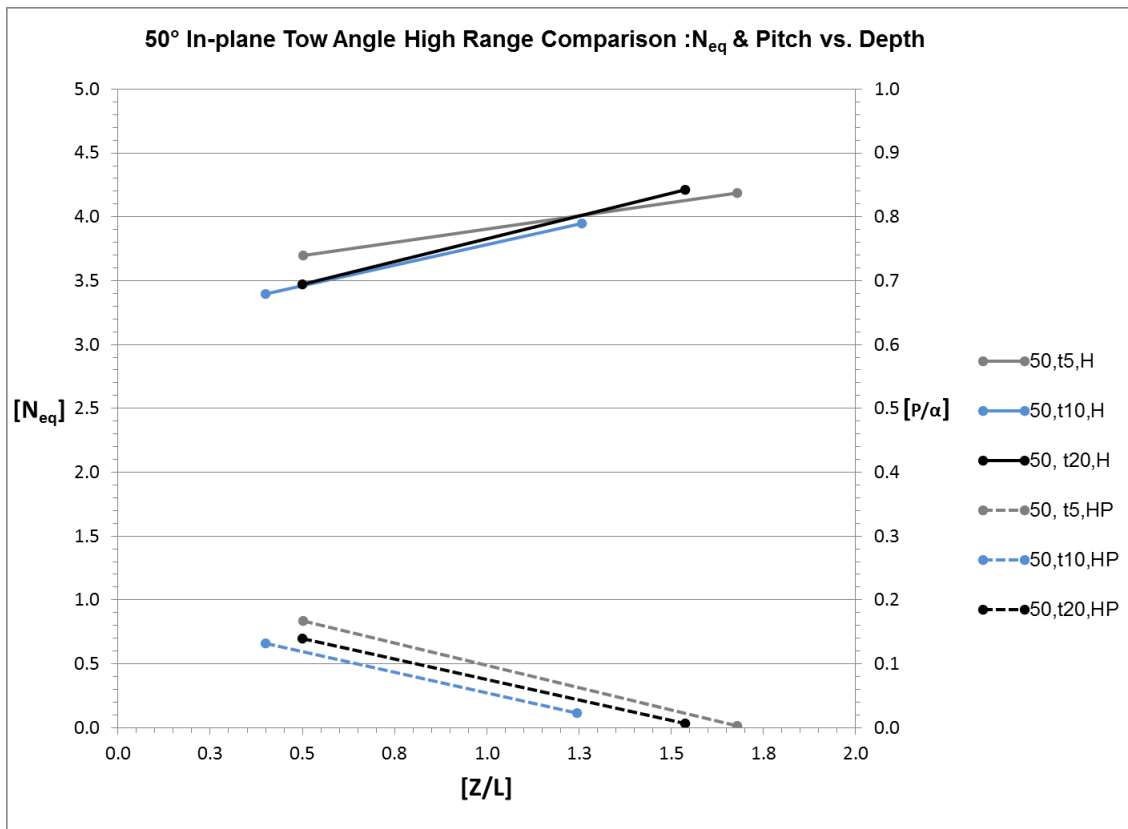


**Fig. 5-5.** 50° In-Plane Initial Tow Angle Comparison:  $N_{eq}$  and Pitch vs. Depth

Satisfactory data for the 36° fluke angle were collected only for the 5° initial tow range. The trajectory data from those tests indicated that the anchor actually rose up out of the sediment surface, which is physically impossible. A possible explanation of this phenomenon is thought to have been related to the timing between mixing of the sediment tank and when testing began. It was observed that a crust formed on the surface of the sediment that prevented the chaser wire from following the anchor in a straight-line path.

The 22° fluke angle was not included for comparison because the anchor was incapable of embedding completely below the surface. This is attributed to the 22° fluke angle being too shallow for the use in soft cohesive clays. Traditional design guidelines do not suggest the use of fluke angles shallower than 32° for this type of sediment.



### 5.2.2 In-Plane Velocity Comparison

Analysis of the in-plane data with respect to velocity indicated that the 46% increase in velocity from 0.13 m/s (0.42 ft/s) to 0.19 m/s (0.62 ft/s) produced an average increase in holding capacity of 3.78%. These values were taken from Fig. 5-6 which was developed from the corresponding composite charts using the individual fitted lines and a constant non-dimensional depth value equal to 1.0. The largest difference in velocity occurred in the 50° fluke angle, 10° tow angle test. Fig. 5-7 clearly shows the corresponding velocity differences with the second order polynomial trend lines.

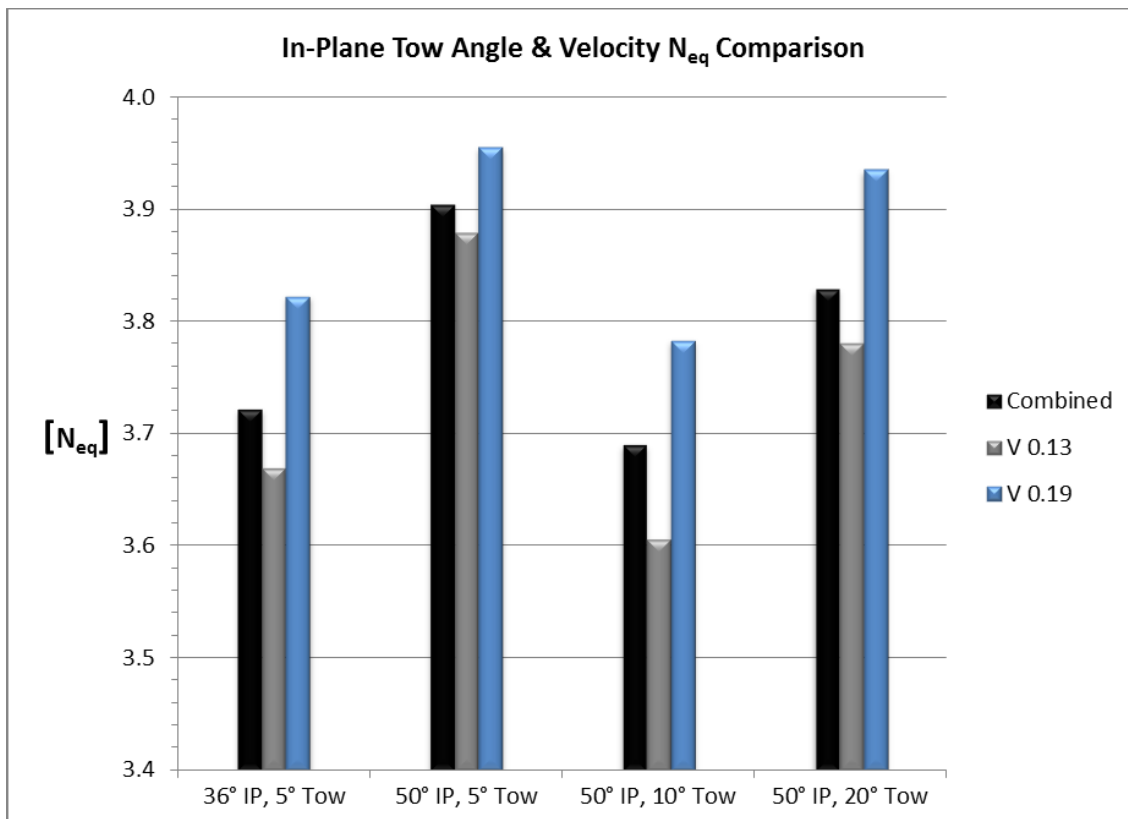


**Fig. 5-6.** In-Plane Tow Angle and Velocity Comparison

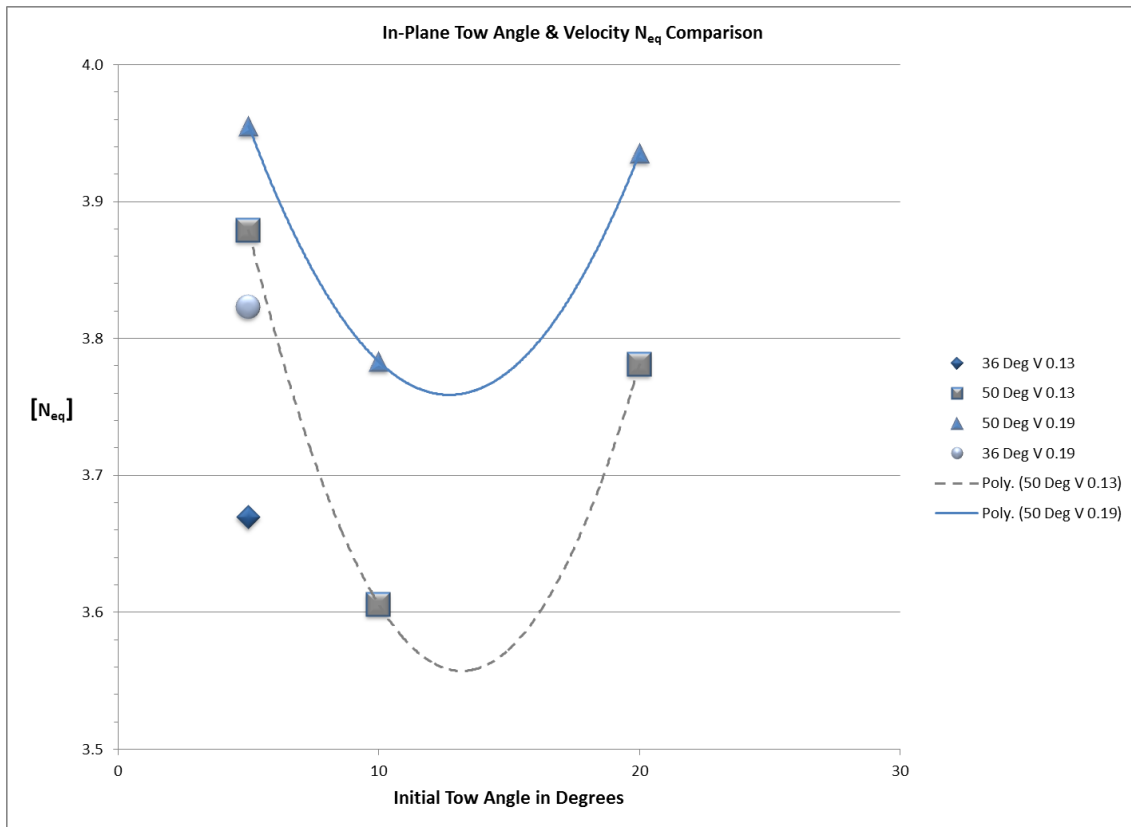


**Fig. 5-7.** In-Plane Tow Angle and Velocity Regression

### 5.2.3 In-Plane Roll Comparison

The in-plane roll effects are important for this experiment because these effects are used as a baseline comparison for the out-of-plane experiment data. Fig. 5-8 and Fig. 5-9 display the non-dimensional roll versus depth for 36° fluke angle and 50° fluke angle respectively. Roll occurred during every test. By inspection, the 50° fluke angle is more susceptible to rolling compared to the 36° fluke angle. The rate of change of roll versus depth for the 36° fluke angle remained fairly constant after the initial transitional phase, and displays marginal recovery, since there is little tendency for the roll angle to return to the 0° position.

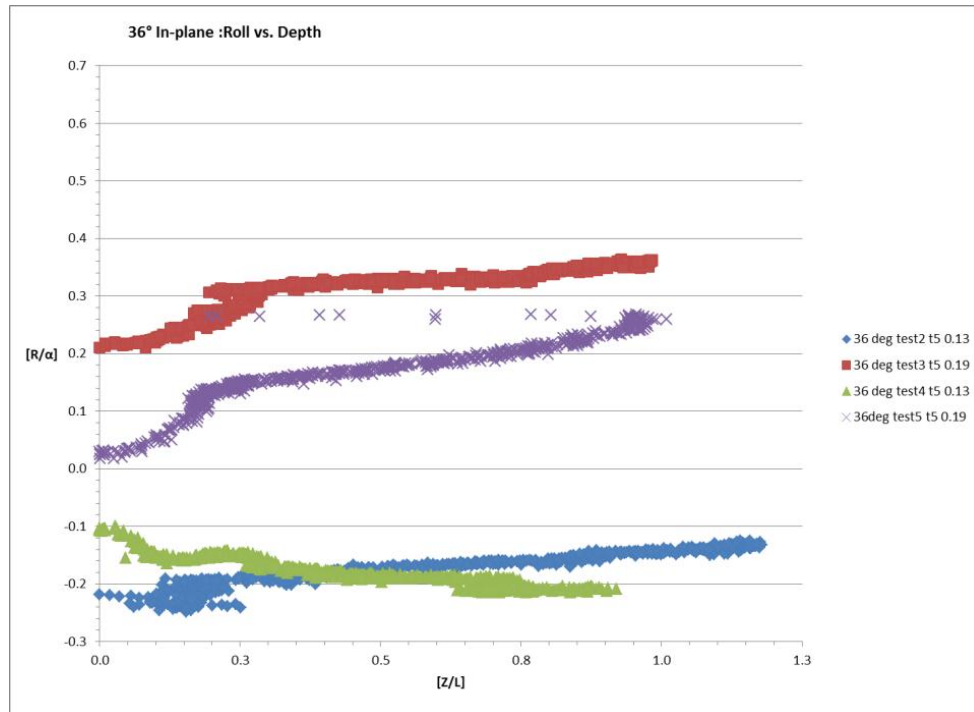


Fig. 5-8. 36° In-Plane Roll vs. Depth

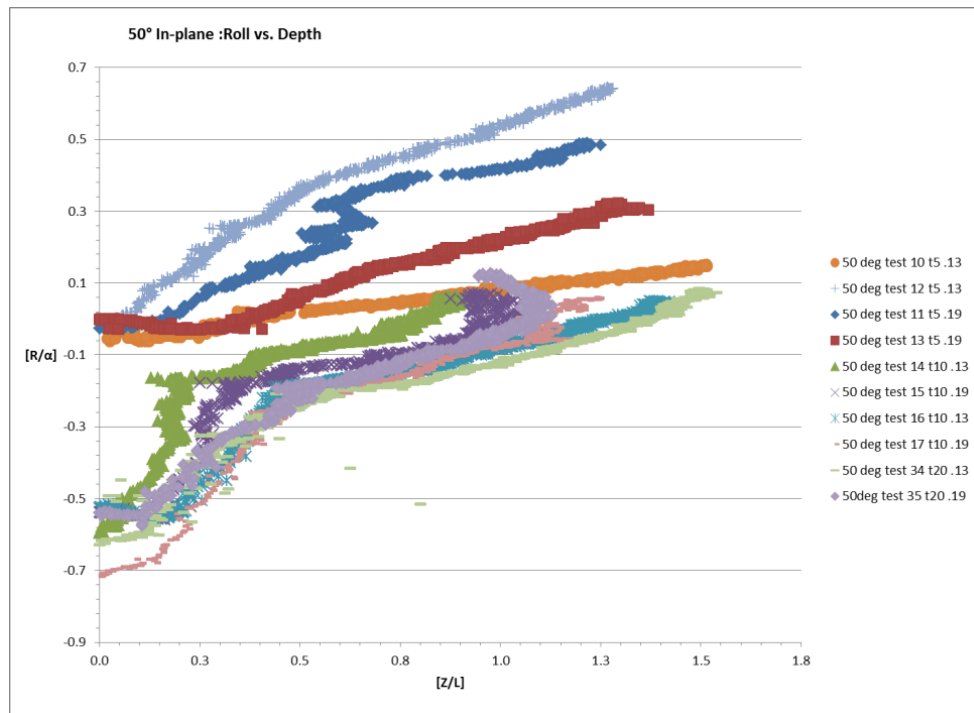


Fig. 5-9. 50° In-Plane Roll vs. Depth

Examining the initial positions and the corresponding roll indicates that the anchor may not have been placed perfectly level on the surface of the sediment and human error may have been the cause. This is displayed in the 50° tests where a majority of the cases start at nearly -0.5. The 50° tests however did not show a leveling off or a strong tendency to recover from initial roll, as indicated by test numbers 12 and 13 in comparison to the 36° tests. Since the in-plane tests were performed early on in the experimentation, the excess of roll may be attributed to twisting caused by the main towline. The swivel that was used in the connection of the towline to the chain was not a sealed unit. Sand from the sediment created friction that prevented the swivel from turning freely.

### **5.3 Out-of-Plane Initial Surface and Sub-surface (Case 1)**

Of the forty tests performed for case one, only 20 provided usable data. It was determined later on that by hand embedding the anchor and chain the vertical angle of the chaser cable exceeded the physical range of measurements, by binding on its support bracket. This altered the trajectory data by providing a false initial position. This problem was identified late in the testing phase and the schedule of testing did not allow for the time to repeat those experiments affected. Only the surface tests were examined for this case.

Composite charts were created for each test case and may be referenced in the appendix. The same procedure for the in-plane composite charts was used for the out-of-plane tests. Fig. 5-10 illustrates the 36° and 50° fluke angle, broken down into velocity components and the out-of-plane surface tow angle of either 45° or 90°. The data sets were fitted using linear regression, and the non-dimensional holding capacity is compared for a constant non-dimensional depth equal to one fluke length. Fig. 5-10 indicates a tendency for the holding capacity to be reduced by approximately 0.5 units of holding capacity as the surface out-of-plane towing angle increases for all cases except the 50°, 0.19 m/s (0.62 ft/s) 90° test.

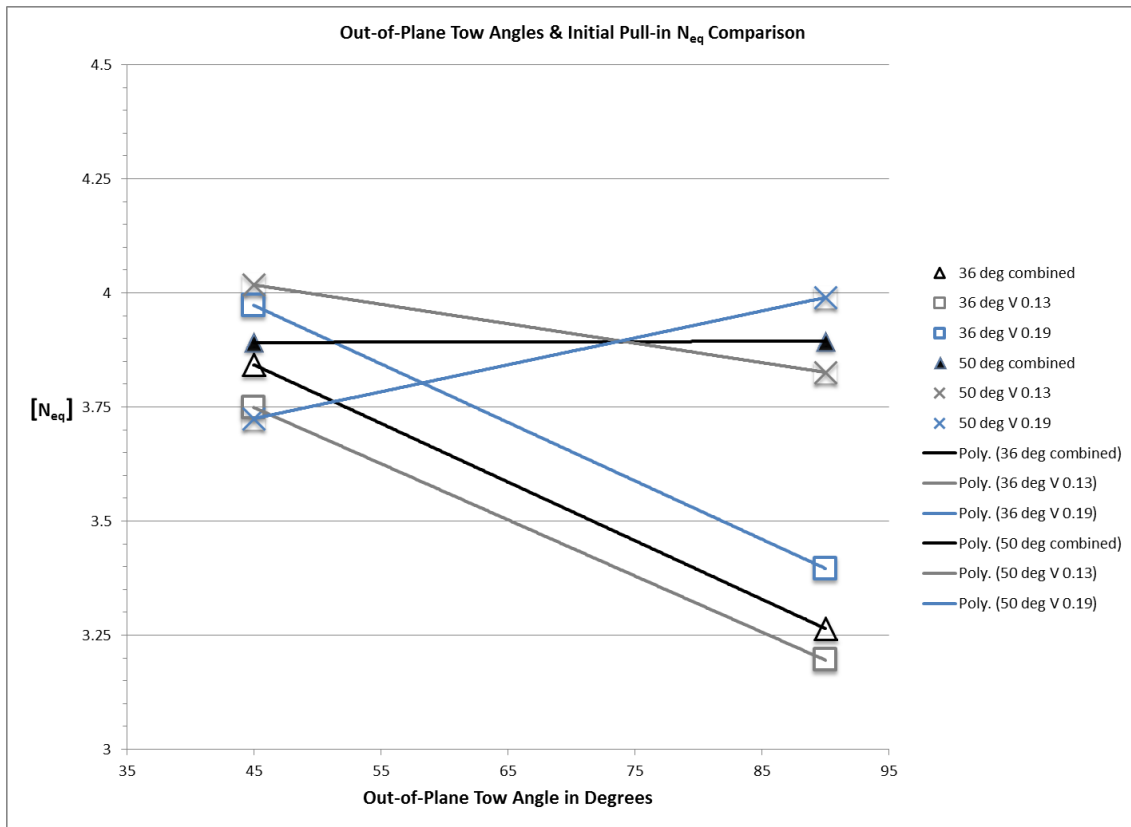


**Fig. 5-10.** Surface Out-of-Plane Angle Comparison

### 5.3.1 Velocity Comparison

Fig. 5-11 is a comparison of the surface out-of-plane towing angles broken down into velocity components and compared to the velocity components of the respective in-plane tests for a fixed depth of one fluke length. This figure indicates an average of 2.31% increase in holding capacity with the 46% increase in velocity and that is less than the average determined from the in-plane results. The reduction could be attributed to the velocity difference between the 50° fluke angle 45° out-of-plane tow angle velocity difference which gave an -7.3% reduction of capacity with increase of velocity. Again, a possible explanation of this may be due to the gradient of the un-drained shear strength of the sediment across the tank. If the aforementioned case is removed, the average

increase in holding capacity is 5.51%, which exceeds the 3.78% increase found in the in-plane tests.

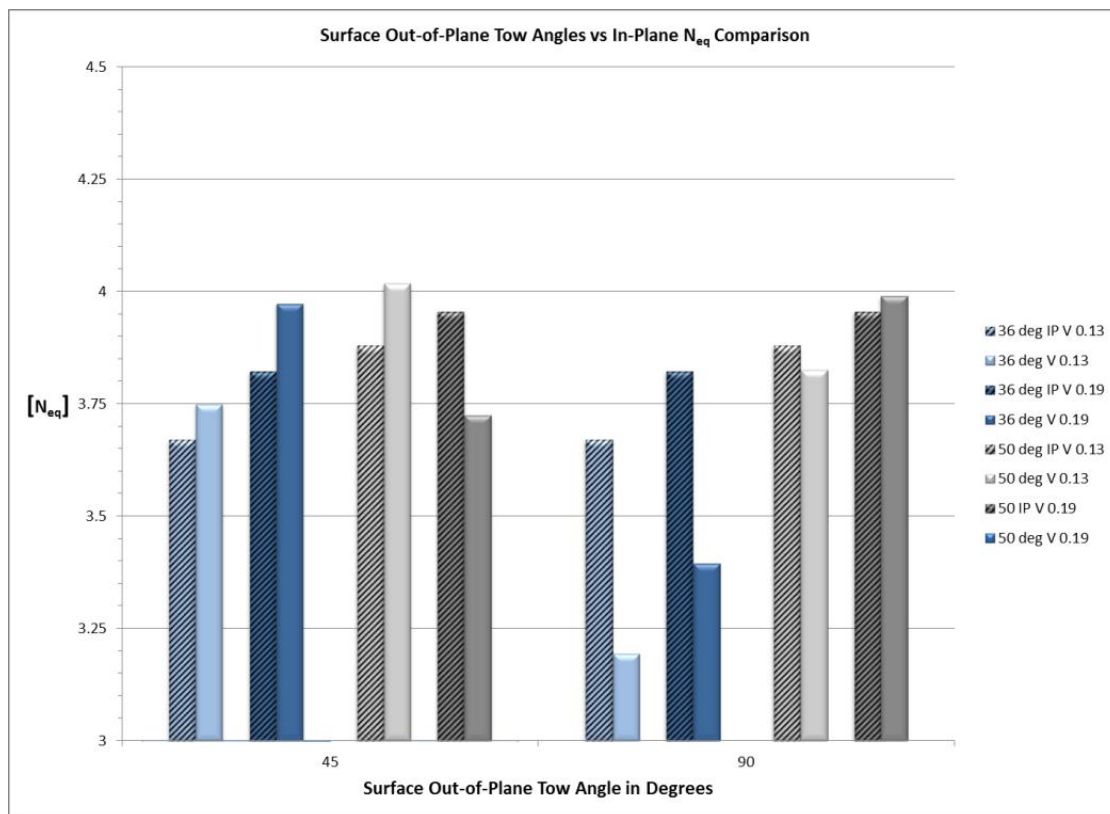


**Fig. 5-11.** Surface Out-of-Plane Tow Angle Velocity Comparison

### 5.3.2 Fluke Angle Comparison

Fig. 5-12 reveals that each test reached its ultimate embedment depth by verifying that the anchor's pitch leveled out to the horizontal position. The ultimate embedment depth and holding capacity as a function of the fluke angle and out-of-plane surface angle is collected from Fig. 5-12 and tabulated in Table 5-1. The 50° fluke angle setting embedded 0.95 fluke lengths deeper on average than the 36° fluke angle setting. The holding capacity for the 50° fluke angle increased by 0.95 units more than 36° fluke

angle. This supports the trend that the 50° fluke angle as a deeper embedment depth and holding capacity than the 36° fluke angle for the given sediment.

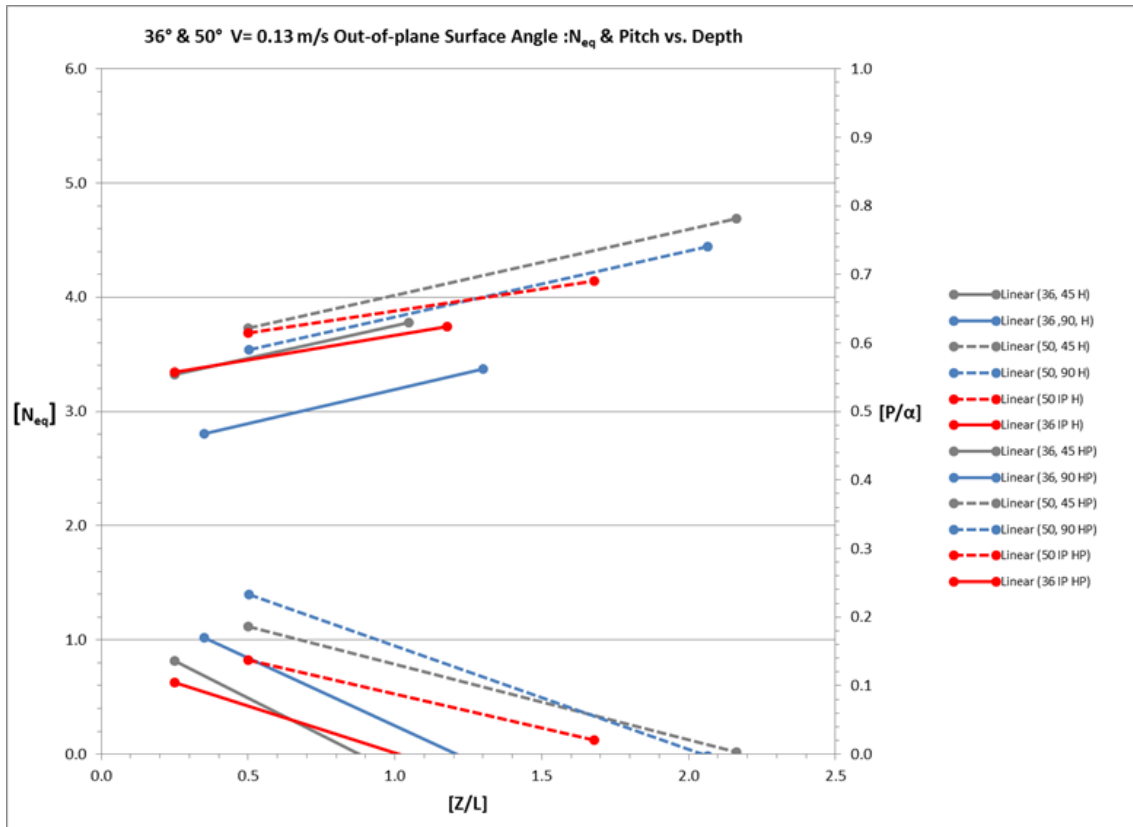


Fig. 5-12. Out-of-Plane Surface Angle  $N_{eq}$  and Pitch vs. Depth (Case 1)

**Table 5-1.** Max Embedment and  $N_{eq}$  by Fluke Angle (Case 1)

Embedment Depth [Z/L]			
Out-of-plane Angle	Fluke Angle		$\Delta$
	50°	36°	
45°	2.2	1.1	1.1
90°	2.1	1.3	0.8
<b>Average=</b>			<b>0.95</b>
$N_{eq}$			
45°	4.6	3.7	0.9
90°	4.4	3.4	1
<b>Average=</b>			<b>0.95</b>

### 5.3.3 Roll Comparison

Analysis of the non-dimensional roll with respect to depth for these cases indicates that out-of-plane pulling does cause an increase of roll; furthermore there exists a distinct pattern between the 45° and the 90° out-of-plane tests as indicated by Fig. 5-13 through Fig. 5-16. The 36°, 45° out-of-plane tests show a tendency of recovery after the initial induced roll with the exception of test number 44. In comparison to the 50° fluke angle, only test number 51 exhibited the same tendency of recovery. The rest of the tests showed little change of roll with the depth. A common feature between the 45° out-of-plane tests was an approximate magnitude of 0.2 units of induced roll.



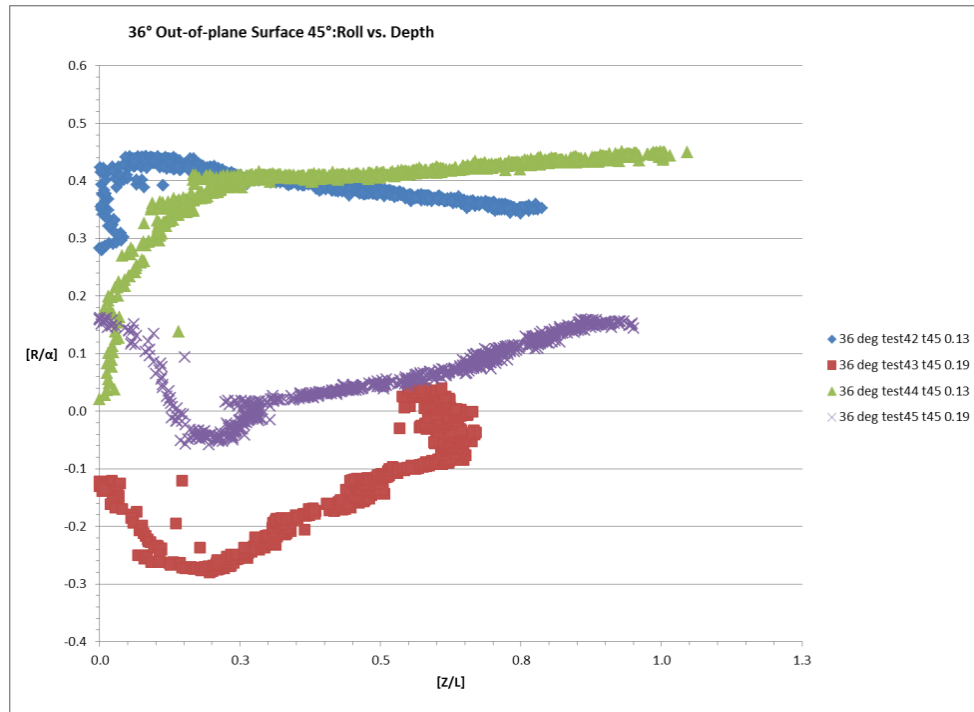


Fig. 5-13. 36° Surface Out-of-Plane 45° Roll Comparison

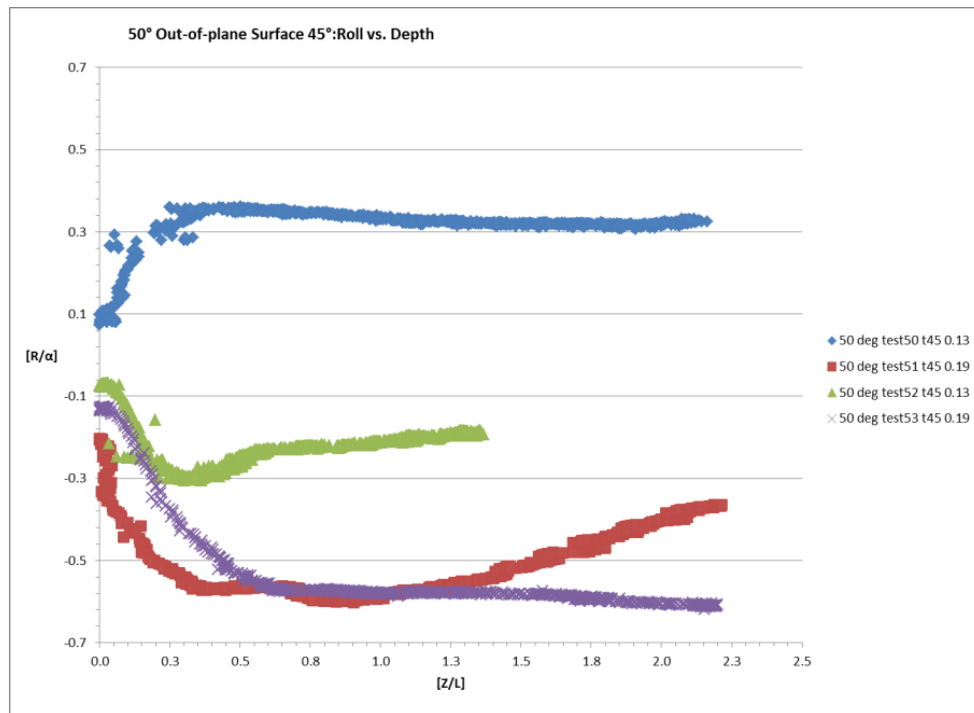
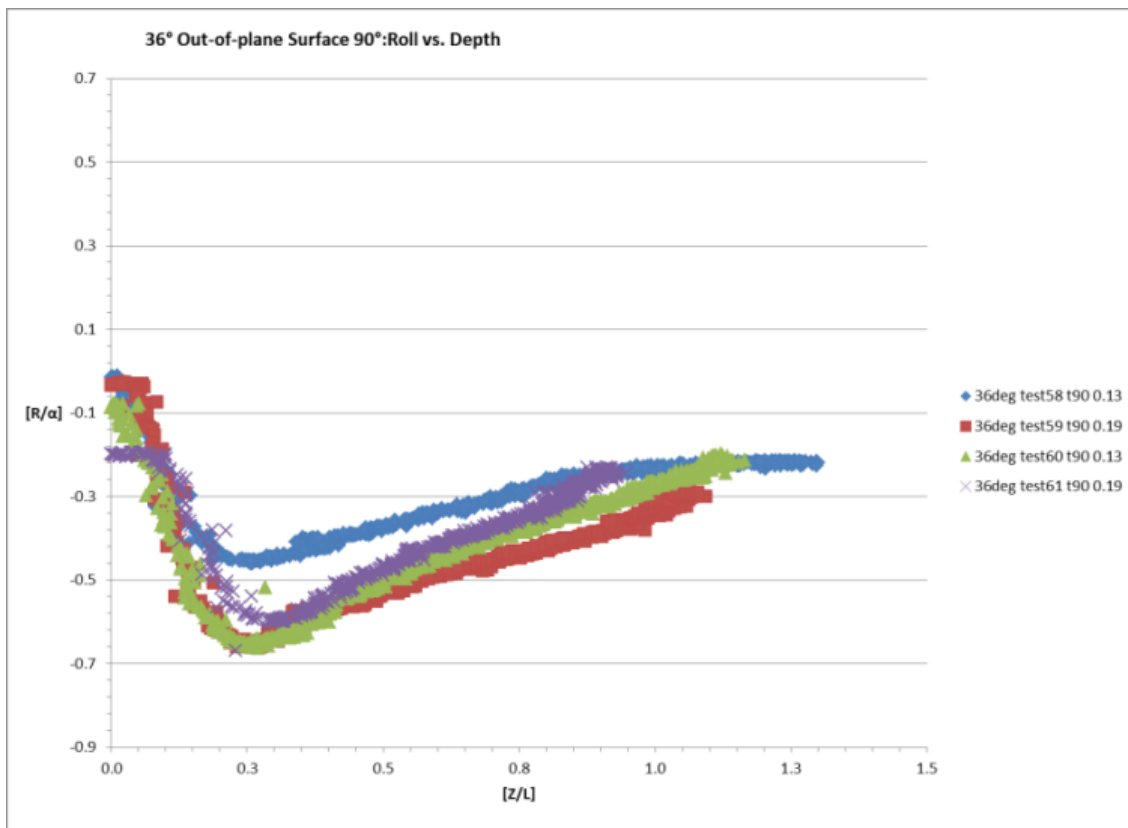
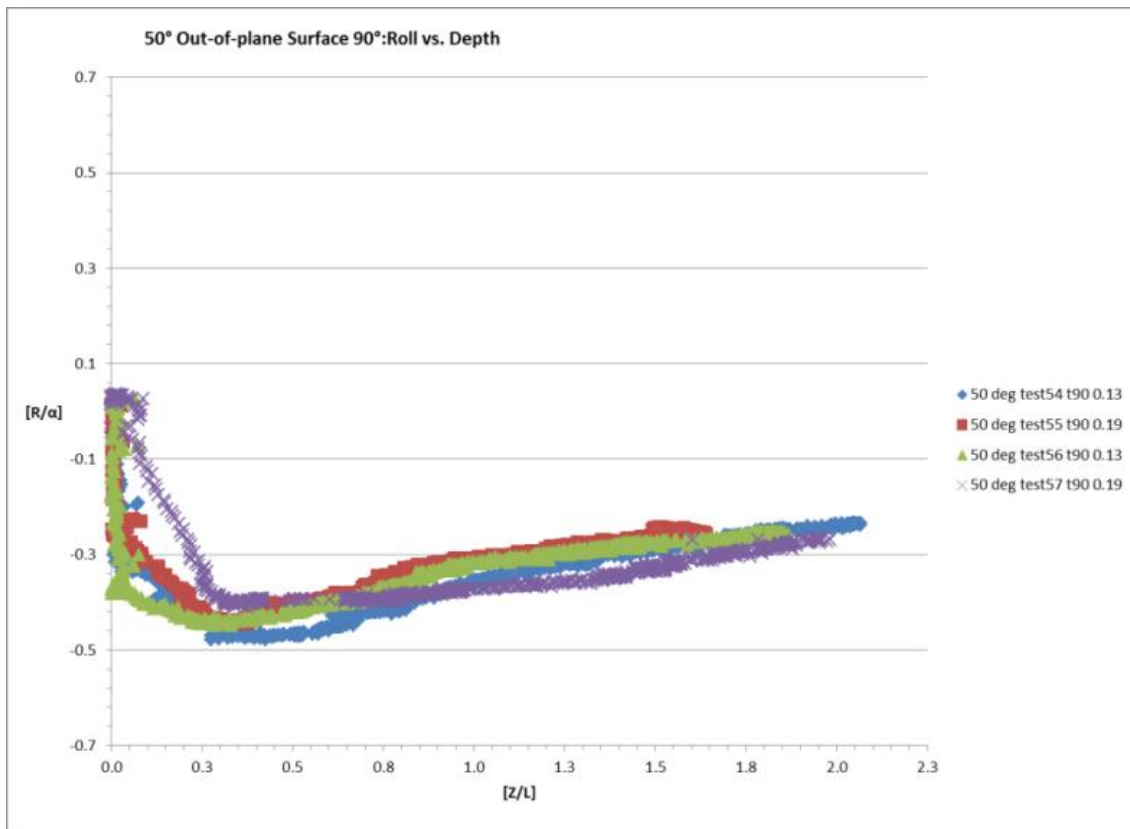


Fig. 5-14. 50° Surface Out-of-Plane 45° Roll Comparison

Inspection of the 90° out-of-plane plots indicate that 36° and 50° cases both exhibit a tendency for recovery. Moreover, the 36° cases recover at a faster rate than the 50°; supporting the observation, that 50° fluke angle is more susceptible to roll with less ability to recover. The magnitude of the induced roll increases as the out-of-plane angle increases. Furthermore, a trend common to both fluke angle and surface out-of-plane pull angle is that the induced roll reaches its maximum magnitude within 0.3 fluke lengths of depth.



**Fig. 5-15.** 36° Surface Out-of-Plane 90° Roll Comparison



**Fig. 5-16.** 50° Surface Out-of-Plane 90° Roll Comparison

#### 5.4 Out-of-Plane Main Tow Line (Case 2)

Composite charts were developed for the out-of-plane case two loading scenarios using the same procedures as the previous cases and may be referenced in the appendix. The difficulty for comparing case two experiments with the in-plane and Case 1 out-of-plane tests is due to the fact that the total pull distance is varied by the out-of-plane pull angle.

The reduction of the total pull distance is caused by the addition of the floor plates needed to achieve the respective out-of-plane pull angle as described in the procedures section. Fig. 5-17 is developed by using the linear regression lines from the composite charts with a constant depth of 0.5 fluke lengths. The plot illustrates the data obtained from the out-of-plane pull angles of 15°, 30°, and 45° and the initial pull distance of one and three fluke lengths. The power fit trend lines indicate that the

holding capacity increases for both the 36° and 50° one fluke length initial pull-in distance.

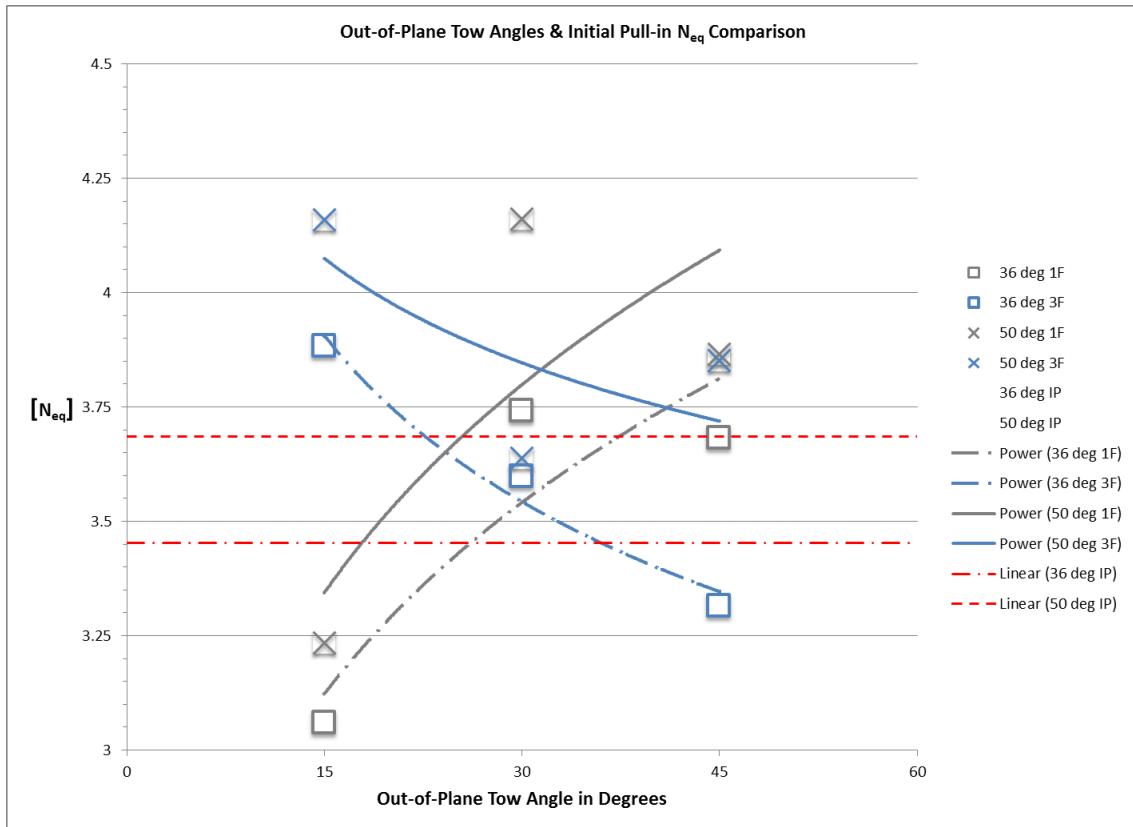


**Fig. 5-17.** Out-of-Plane Tow Angle Comparison (Case 2)

#### *5.4.1 Initial Tow Distance Comparison*

Examinations of the three fluke lengths pull in tests contradict the trend lines present for the one fluke length cases. For both the 36° and 50° fluke angles the trend lines indicate a decrease in holding capacity with the increase of out-of-plane pulling angle. The red dashed line is used as a reference for the 50° in-plane holding capacity, and the red dashed-dot line represents the 36° in-plane capacity.

Since the holding capacity in Fig. 5-17 was determined using a constant 0.5 fluke length of depth, which would be considered relatively shallow embedment, it is important to examine the rate of change of holding capacity with respect to depth, in addition to the ultimate embedment depth and ultimate holding capacity. Fig. 5-18 portrays the 36° and 50° fluke angles for a one fluke length initial pull in distance. The dashed lines represent the 50° fluke angle and the solid lines represent the 30° fluke angle. It is evident that as the out-of-plane towing angle increases, the rate of change of holding capacity increases proportionally.

The rate of change of pitch with depth exhibits the same proportionality as the holding capacity in that as out-of-plane pull angle increases the slope of the pitch increases as well. The red lines indicate the equivalent in-plane tests for comparison. The 15° out-of-plane tests have nearly the same slope as the in-plane tests. The 15° and 30° out-of-plane tests show that the pitch is nearly horizontal for the given pull distance, and that maximum holding capacity was reached. The 45° tests however would need to be pulled further before the pitch value leveled out to the horizontal position equal to zero.

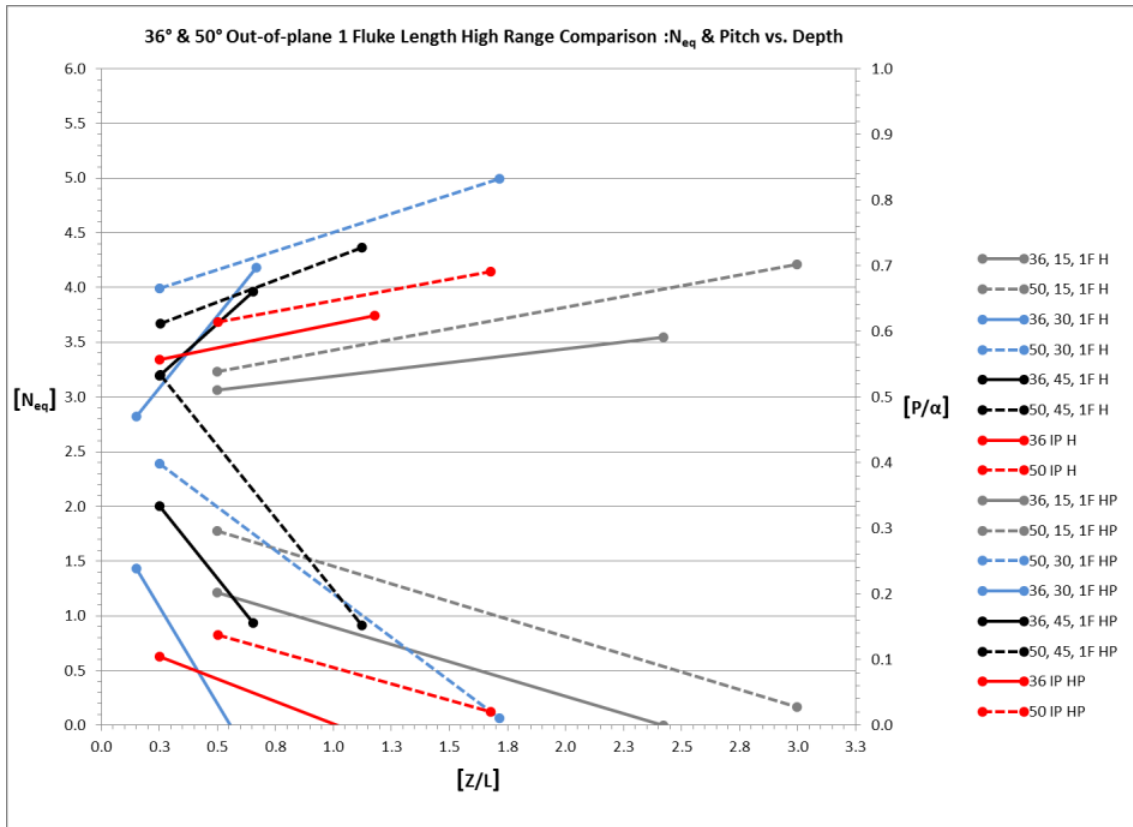


**Fig. 5-18.** 1 Fluke Length Comparison (Case 2)

Fig. 5-19 examines the three fluke length initial pull in distance. The 50° fluke angle exhibits the same proportionality as found in the one fluke length comparison in that as the out-of-plane pull angles increases the rate of change of holding capacity increases as well. However, the 36° fluke angle shows a decrease in holding capacity at out-of-plane pulling angles exceeding 15°. For the 36° fluke angle cases of 30°, and 45° shows that the pitch angle is very near horizontal and as such has reached the maximum depth of embedment. This is not the case for the 50° fluke angle 30°, and 45° out-of-plane pull angle cases.

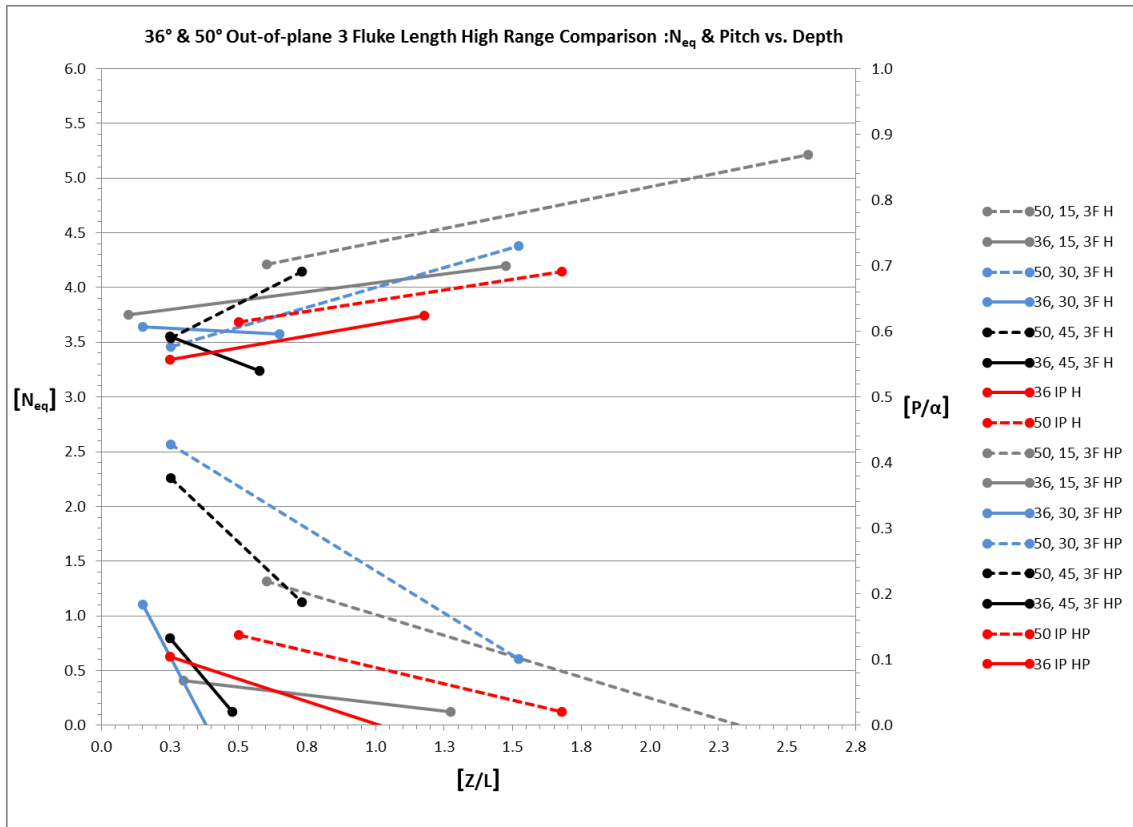


**Fig. 5-19.** 3 Fluke Length Comparison (Case 2)

#### 5.4.2 Fluke Angle Comparison

The data obtained from Fig. 5-18 and Fig. 5-19 provide a comparison for the effect of fluke angles on a case-by-case basis. The maximum embedment depth and holding capacity per out-of-plane pull angle for the 50° and 36° fluke angles is contained in Table 5-2, which displays the difference and the average between the fluke angle settings. The data indicate that the 50° fluke angle embeds on average 0.68 fluke lengths deeper than the 36° for the one fluke length initial embedment cases, and 0.73 fluke lengths deeper for the three fluke lengths initial pull in case.

Examining the holding capacity for the 50° fluke angle setting indicates an average of 0.58 units more of holding capacity than the 36° fluke angle, for the one fluke length initial pull in distance. A greater average increase of 0.97 units is shown when

comparing the 50° fluke angle setting to the 36° for the three fluke length initial pull in tests.

**Table 5-2.** Embedment Depth and Holding Capacity (Case 2)

Embedment Depth [Z/L]							
1 Fluke Length				3 Fluke Lengths			
Out-of-plane Angle	Fluke Angle		$\Delta$	Out-of-plane Angle	Fluke Angle		$\Delta$
	50°	36°			50°	36°	
15°	3	2.4	0.6	15°	2.6	1.5	1.1
30°	1.8	0.75	1.05	30°	1.55	0.65	0.9
45°	1.15	0.75	0.4	45°	0.8	0.6	0.2
<b>Average= 0.6833</b>				<b>Average= 0.7333</b>			
$N_{eq}$							
15°	4.1	3.55	0.55	15°	5.2	4.1	1.1
30°	5	4.2	0.8	30°	4.4	3.6	0.8
45°	4.3	3.9	0.4	45°	4.2	3.2	1
<b>Average= 0.5833</b>				<b>Average= 0.9667</b>			

#### 5.4.3 Analysis of Extrapolated Data

Extrapolation of the data sets that did not reach the horizontal position is performed by solving for the depth required for the non-dimensional pitch value equal to zero. This depth is referred to as the ultimate embedment depth and the exact values used for extrapolation may be referenced in the appendix. The new extrapolated data sets were used to develop Fig. 5-20, representing the change of ultimate holding capacity with respect to the out-of-plane towing angle, and Fig. 5-21, representing the ultimate embedment depth as a function of the out-of-plane towing angle.

The best-fit lines represent power functions and are tabulated in Table 5-3, with the equations for the lines of the measured values determined from Fig. 5-17 for



comparison. Included with the equations is the measure of the goodness of fit,  $R^2$ . The  $R^2$  increased from the measured values by using the extrapolated data sets.

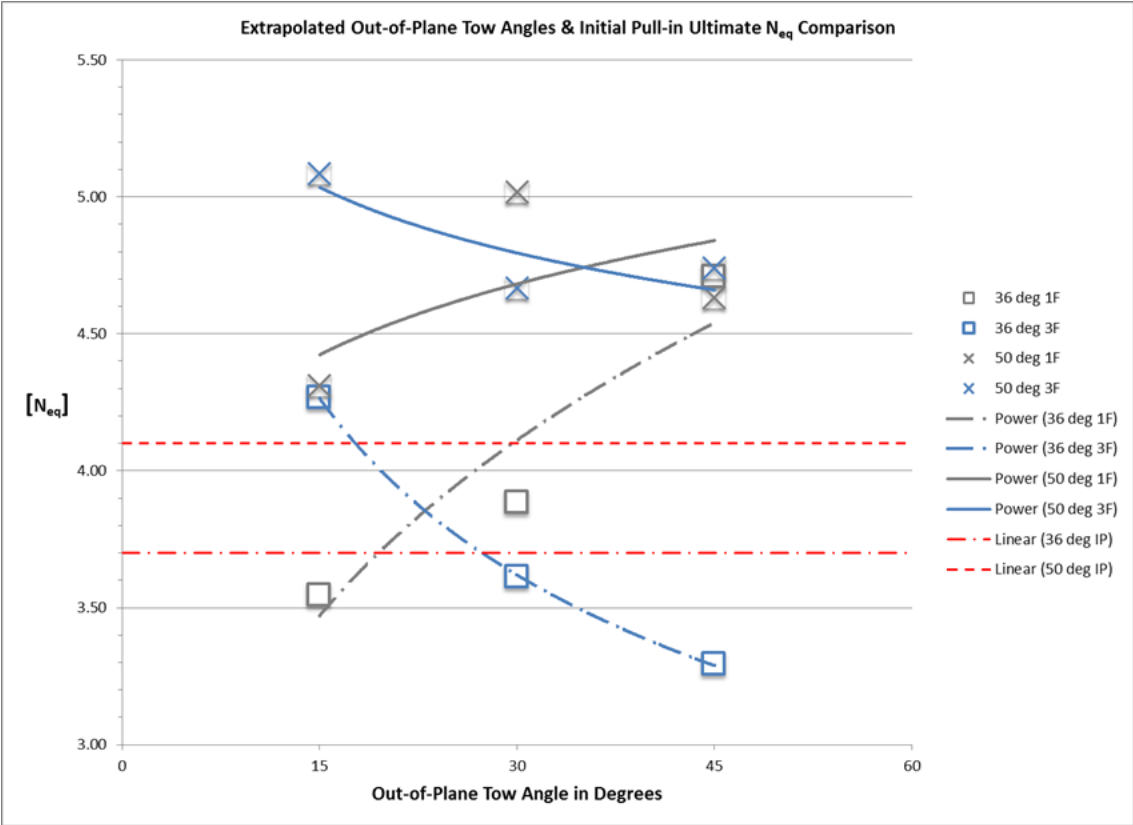
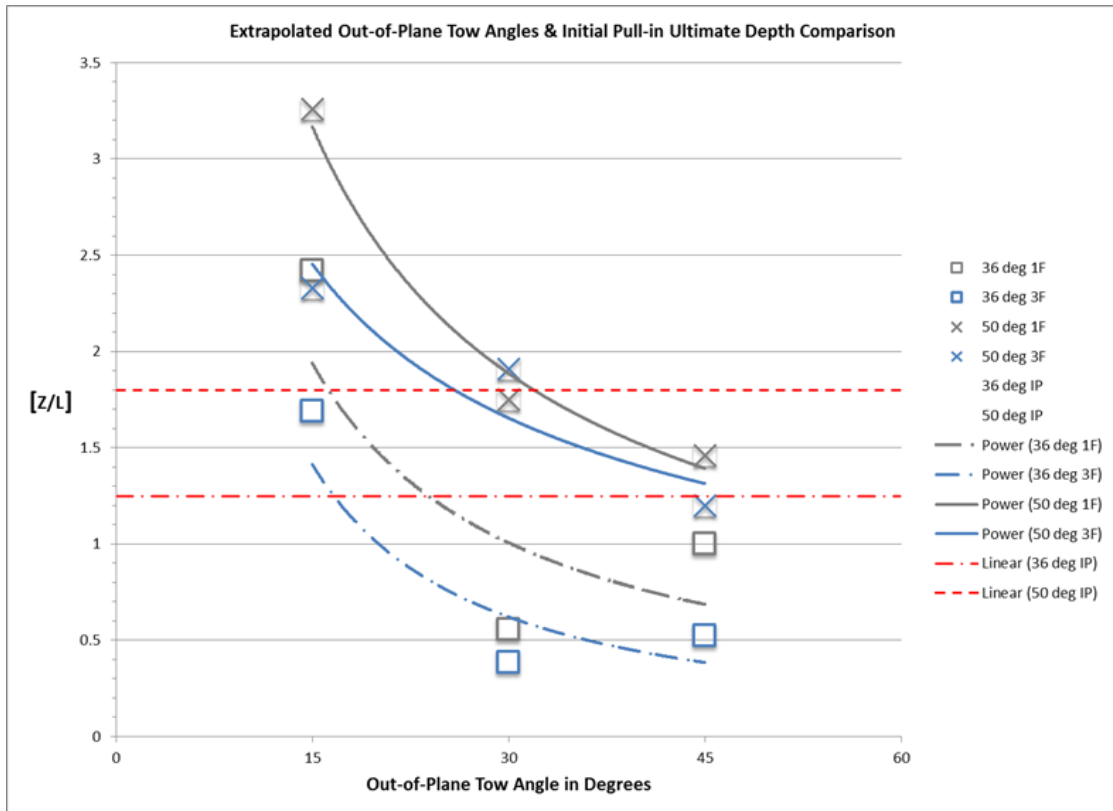


Fig. 5-20. Extrapolated Out-of-Plane Ultimate  $N_{eq}$



**Fig. 5-21.** Extrapolated Ultimate Embedment Depth

The high measure of the goodness of fit indicates that the proposed equations represent the physical system quite well. All test cases indicate a reduction in ultimate embedment depth; however, if the anchors are shallowly embedded there is an increase of holding capacity with an increase in out-of-plane towing angle. The deeper the anchor is embedded initially, as with the three fluke length test cases; there exists both a reduction of holding capacity and reduction of ultimate embedment depth.

**Table 5-3.** Equations of Fit (Case 2)

Description	Fluke angle°	Measured $N_{eq}$	Extrapolated	
			U- $N_{eq}$	U-Z
1 F	36	$y = 1.9095x^{0.1816}$ $R^2 = 0.8143$	$y = 1.792x^{0.2442}$ $R^2 = 0.8799$	$y = 25.104x^{-0.946}$ $R^2 = 0.5022$
3 F	36	$y = 5.7164x^{-0.141}$ $R^2 = 0.9713$	$y = 8.0941x^{-0.237}$ $R^2 = 0.9998$	$y = 34.979x^{-1.185}$ $R^2 = 0.7058$
1 F	50	$y = 2.033x^{0.1838}$ $R^2 = 0.6223$	$y = 3.5435x^{0.0819}$ $R^2 = 0.3597$	$y = 24.031x^{-0.748}$ $R^2 = 0.9757$
3 F	50	$y = 5.103x^{-0.083}$ $R^2 = 0.473$	$y = 6.0931x^{-0.07}$ $R^2 = 0.7295$	$y = 11.442x^{-0.569}$ $R^2 = 0.8631$

#### 5.4.4 Roll Comparison

Inspection of the roll data further supports the observation that the 50° fluke angle is more susceptible to roll due to out-of-plane pull angles than the 36° fluke angle setting as shown in Fig. 5-22 through Fig. 5-25. The 50° fluke angle setting for each case exhibits a greater magnitude of roll in comparison to the 36°. Moreover, as the out-of-plane towing angle increases the rate of change of the roll with respect to the depth increases proportionally.

It is difficult to compare the overall magnitude of the roll angles with respect to the out-of-plane pull angles due to the difference in total towing distance. Inferring from the visual trends of the plots suggest that for a given pull distance the magnitude of roll increases with increasing out-of-plane pull angle, and that the shallower the anchor is embedded the greater the magnitude of roll will occur when pulled out-of-plane. This observation is supported by the case one out-of-plane pull data that shows magnitudes of roll nearly twice that shown for the one fluke length pull in cases.

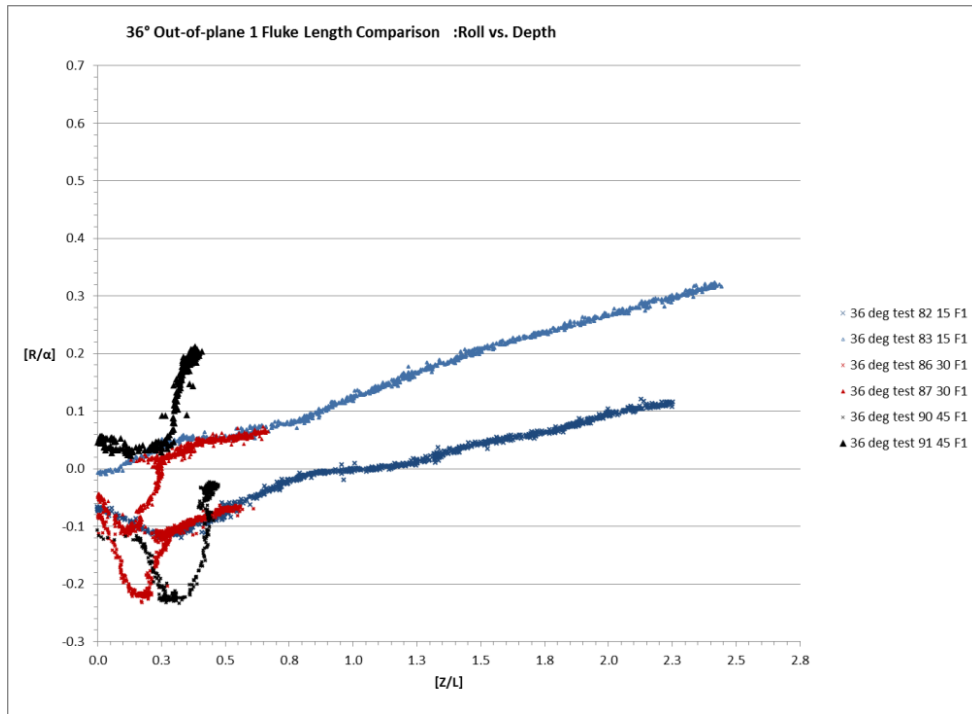


Fig. 5-22. 36° 1 Fluke Length Roll Comparison (Case 2)



Fig. 5-23. 50° 1 Fluke Length Roll Comparison (Case 2)

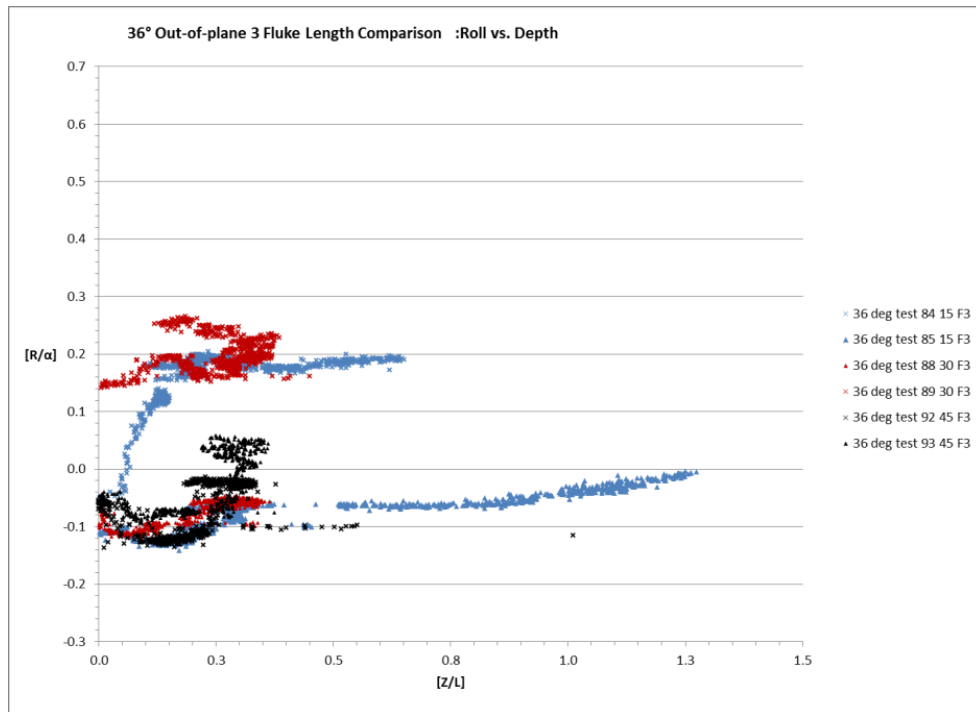


Fig. 5-24. 36° 3 Fluke Length Roll Comparison (Case 2)

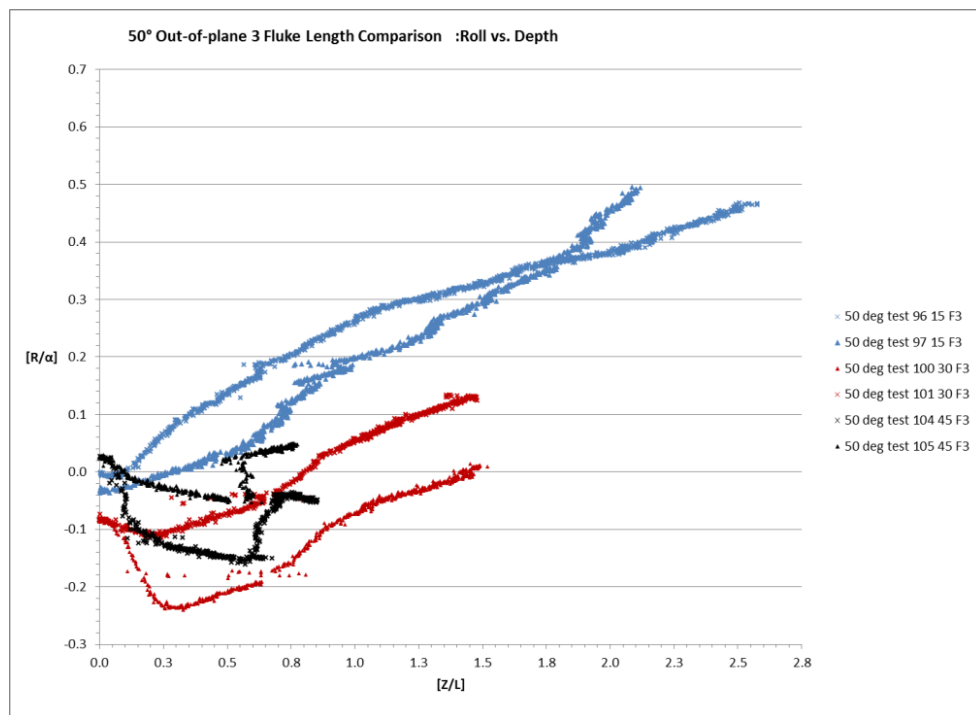


Fig. 5-25. 50° 3 Fluke Length Roll Comparison (Case 2)

The data in Fig. 5-24 does not show as clearly the trends exhibited from the one fluke length pull in comparison. There exists a fair amount of scatter in this plot that may be attributed to the data cable connecting to the inclinometer being damaged at this point during the testing. A fracture in the connector terminal was discovered that allowed water to short out the electrical contacts and contaminating the data.

### **5.5 Out-of-Plane Continuous Degree Change (Case 3)**

Only four cases were examined in this data set. The difficult nature of setting up this case and the fact that only two runs could be performed before mixing of the tank was necessary, prevented additional data from being collected. These cases are unique in that the angle of the main towline remained constant after the anchor embedded to its ultimate depth, unlike the previous cases where as the anchor line moved closer to the towline pulley the angle would increase.

Fig. 5-26 represents the composite charts developed from the four cases tested. There is no clear difference between the one fluke length initial pull versus the three fluke length initial pull in with respect to the holding capacity visual inspection of the holding capacity suggests a relatively straight line of a constant holding capacity of 4.25. The dip in the values between 0.3 and 0.5 fluke lengths of depth are caused by the momentary pause of the dredge carriage as it shifted between moving in the *y*-direction to the *x*-direction.

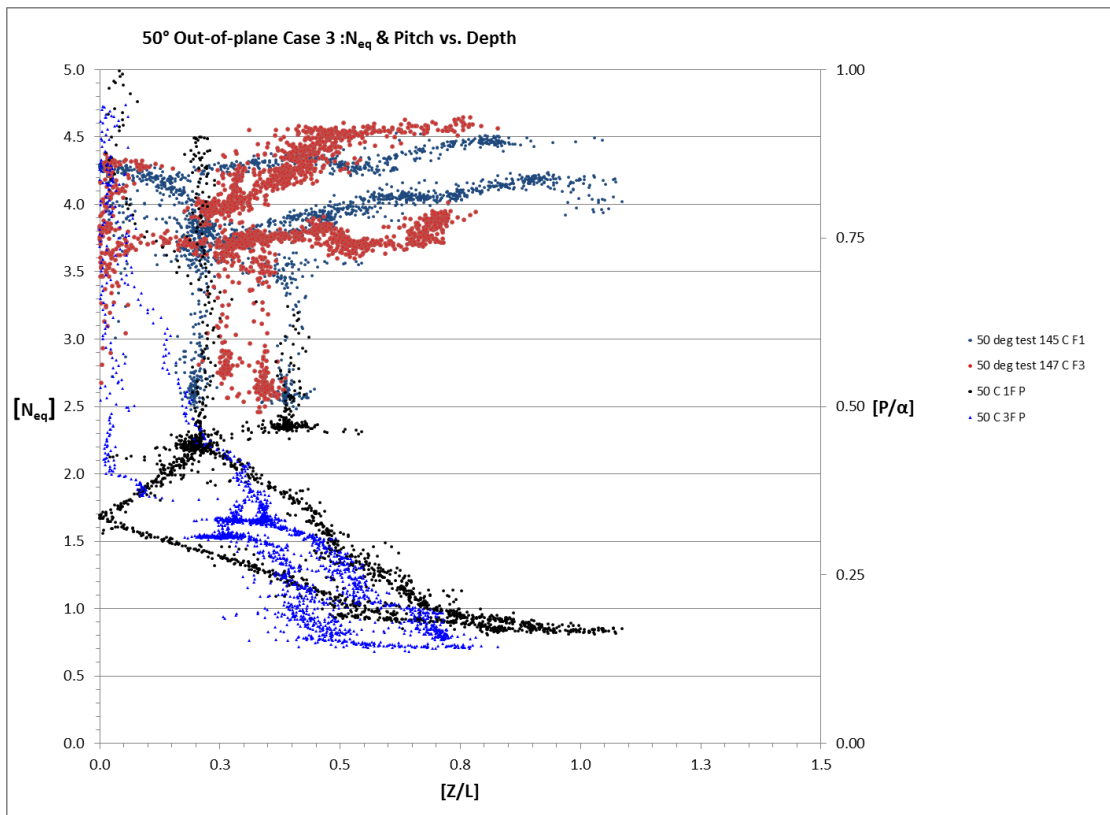


**Fig. 5-26.** Out-of-Plane  $N_{eq}$  and Pitch vs. Depth (Case 3)

The holding capacity for these cases was approximately 9% greater than the 50° fluke angle case as tested during in-plane experiments. The non-dimensional pitch during these tests never reached the horizontal position that suggests the anchor was not at a complete state of equilibrium. This may be attributed to the very short length of towline that was used to perform this experiment. Visual observations during the testing indicated that the anchor line was nearly straight as opposed to a reverse catenary curve exhibited during the in-plane testing and out-of-plane Cases 1 and 2.

Trends regarding the roll versus depth of the four cases showed that during the initial embedment very little roll existed, and increase dramatically as the carriage changed its motion to the  $x$ -direction, as illustrated in Fig. 5-27. The magnitude of the roll was approximately 0.2 for all cases except test number 148, which showed nearly

0.35 for the magnitude of change. There is no apparent pattern relating the change in roll between the initial fluke length pull in distance.

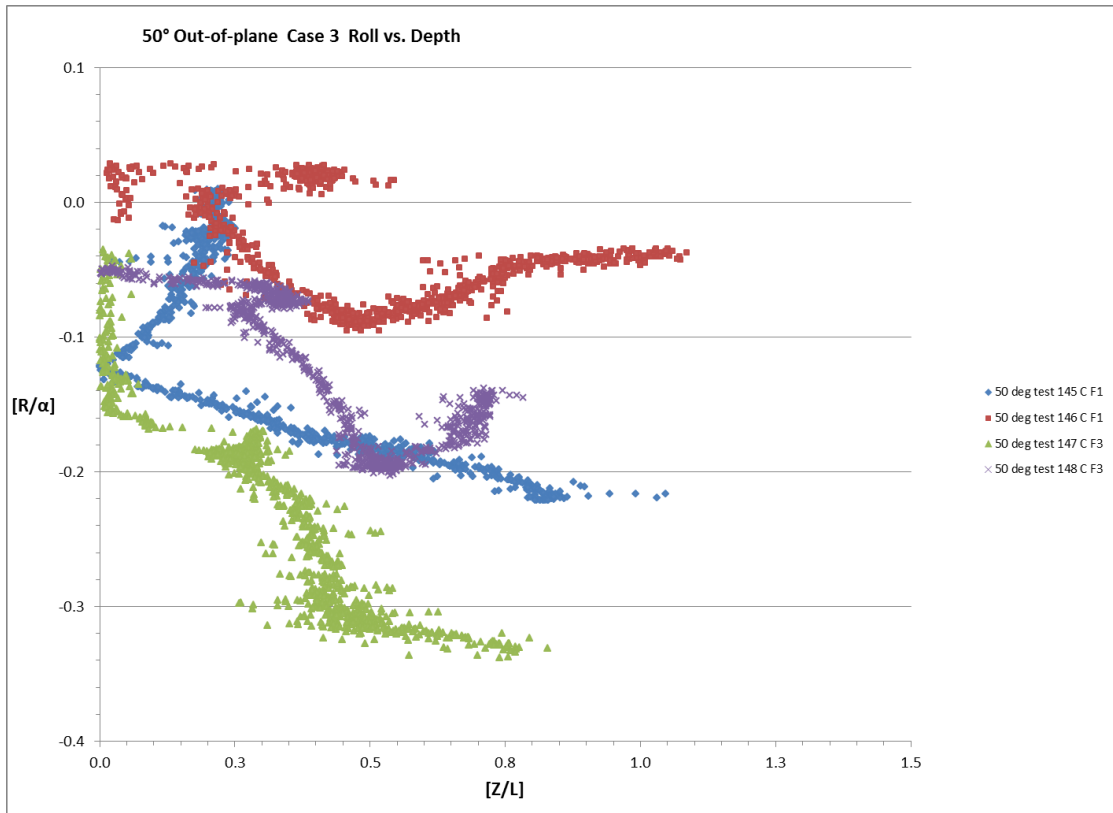


**Fig. 5-27.** Roll Comparison (Case 3)

The y-trajectory paths as shown in Fig. 5-28 indicate that the chaser line accurately followed the anchors path providing reliable data for calculating the trajectory.



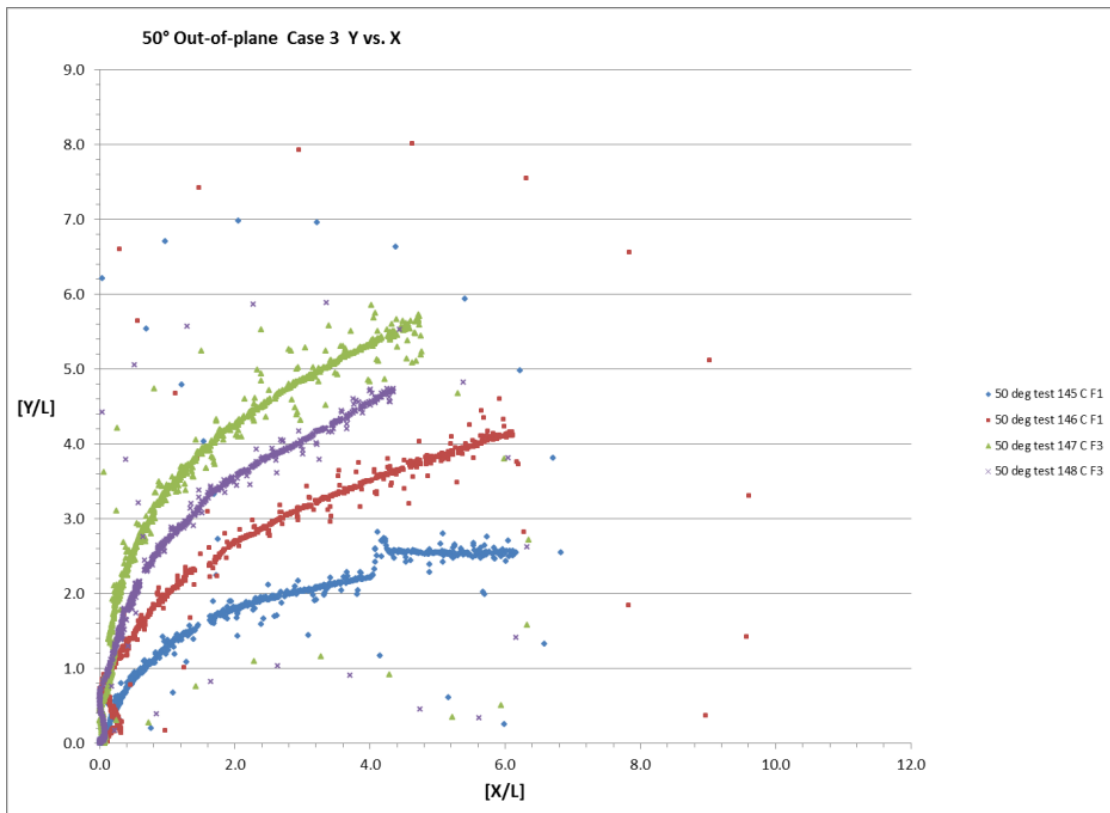


**Fig. 5-28.** Y-Trajectory (Case 3)

The four paths as shown above in Fig. 5-28 resemble the expected path as shown in the previous Fig. 4-5. The scatter present in the data occurred for most of the sensors used during this phase of testing. The scatter may be attributed to noise caused by the high-voltage electric motors powering the dredge carriage. In order for these test to be performed the data cables had to be routed down the carriage ladder and were in much closer proximity to the electric motors than for any other testing case.

## 5.6 Breakout Tests Results

The data provided by the breakout tests was used predominantly for the purpose of analytical models. The exact relationship and comparison of the data sets are not examined in detail in this thesis. However, sample data sets are illustrated below for

knowledge of the results. The repeatability of the data sets indicate that the specially constructed devices performed well for their intended function of isolating the loads in the normal, transverse, and rotational motions of the anchor. Complete data sets may be found in Aubeny et al. (2011). Fig. 5-29 represents a sample of the normal breakout tests and indicates that the anchor has a maximum possible holding capacity of 10. This is nearly twice the value of the measured holding capacity found in any given towing test performed.

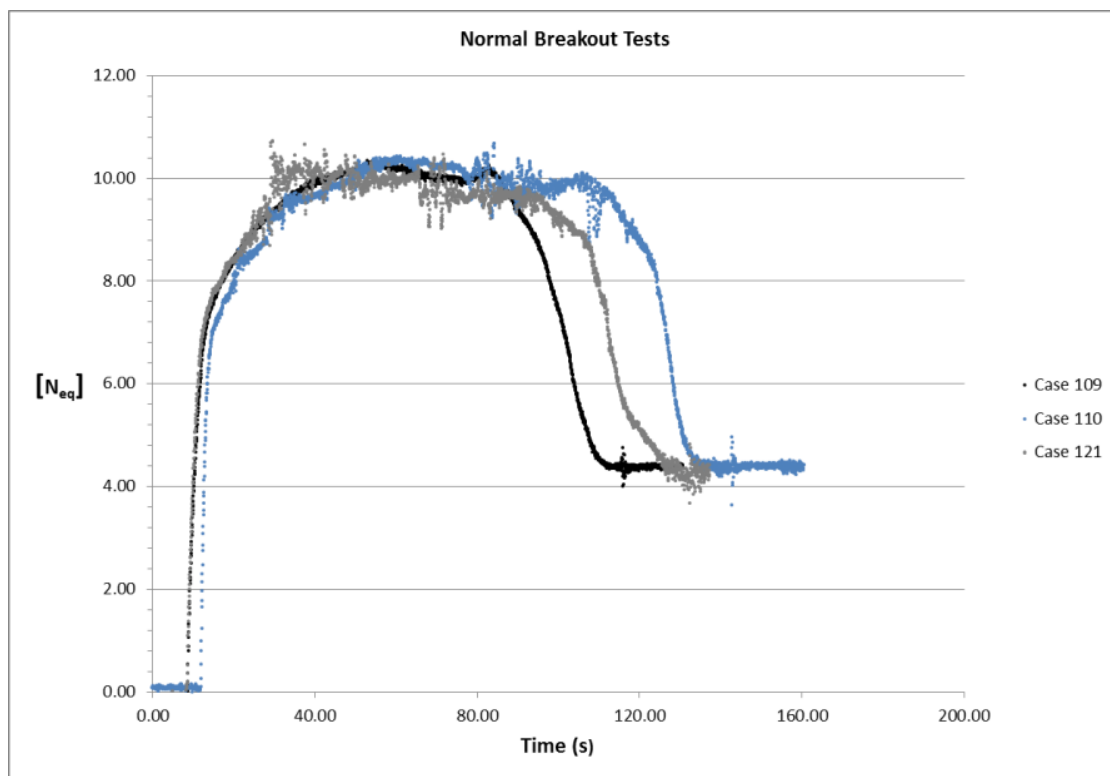


**Fig. 5-29.** Normal Breakout Tests

Examples of forward transverse breakout tests are shown in Fig. 5-30. Two correction factors were applied to the raw data in these tests, a moment arm soil resistance factor and a center of pressure factor. The moment arm soil resistance factor was based on the 3.81 cm (1.5 in) width square steel bar. This effectively removed the

presence of the support bar from the data, allowing the resistance due to the anchor only to be expressed.

The center of pressure term moved the moment upwards from the fluke base to a distance of half the space between the fluke plate and the shank pad eye. This term was unique to the respective fluke angle setting and is listed as follows as distance above the fluke base:  $22^\circ + 5.23$  cm (2.06 in),  $36^\circ + 8.07$  cm (3.18 in), and  $50^\circ + 11.27$  cm (4.44 in). This term transforms the forward transverse resistance of the anchor from the fluke base to the midpoint between the base and the shank pad eye. The moment arm amplification ratio of 6.526 is then applied to transform the moment applied to the load cell into the lateral force caused by the anchor. For the  $36^\circ$  fluke angle case presented here, the forward transverse anchor resistance is approximately 150 (N). An illustration of the moment correction factors is presented in Fig. 5-31.

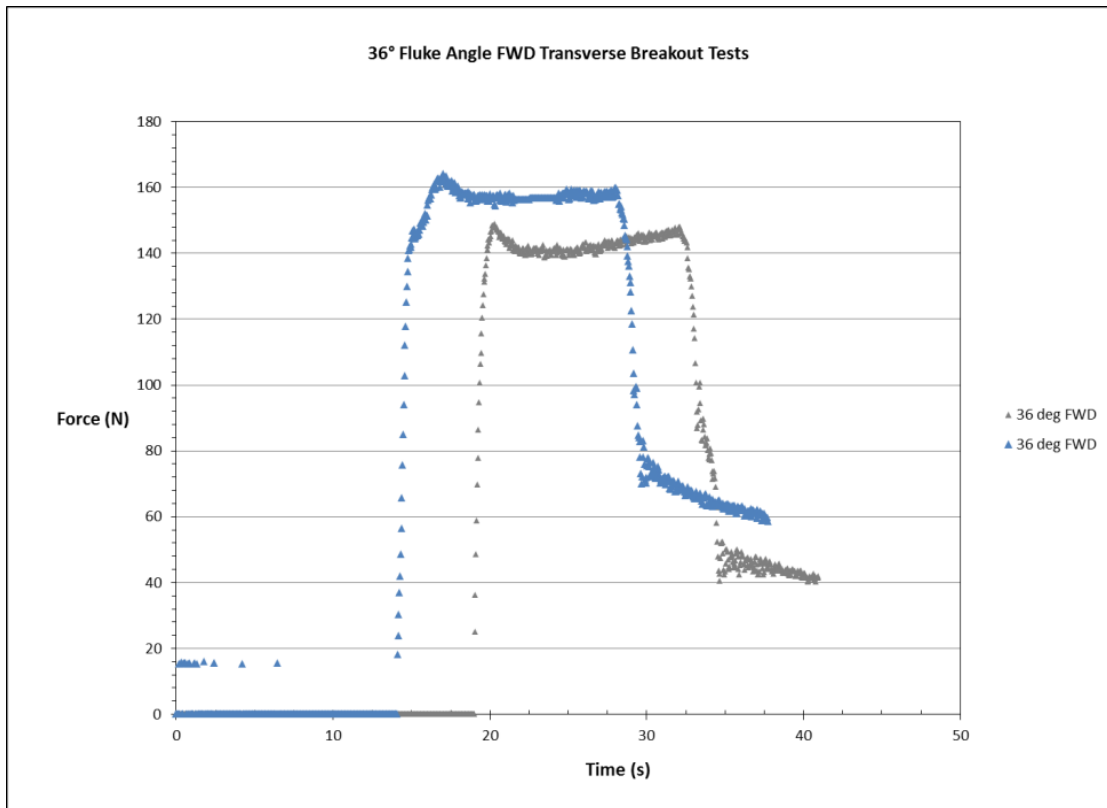


**Fig. 5-30.**  $36^\circ$  Fluke Angle FWR Transverse Breakout Tests

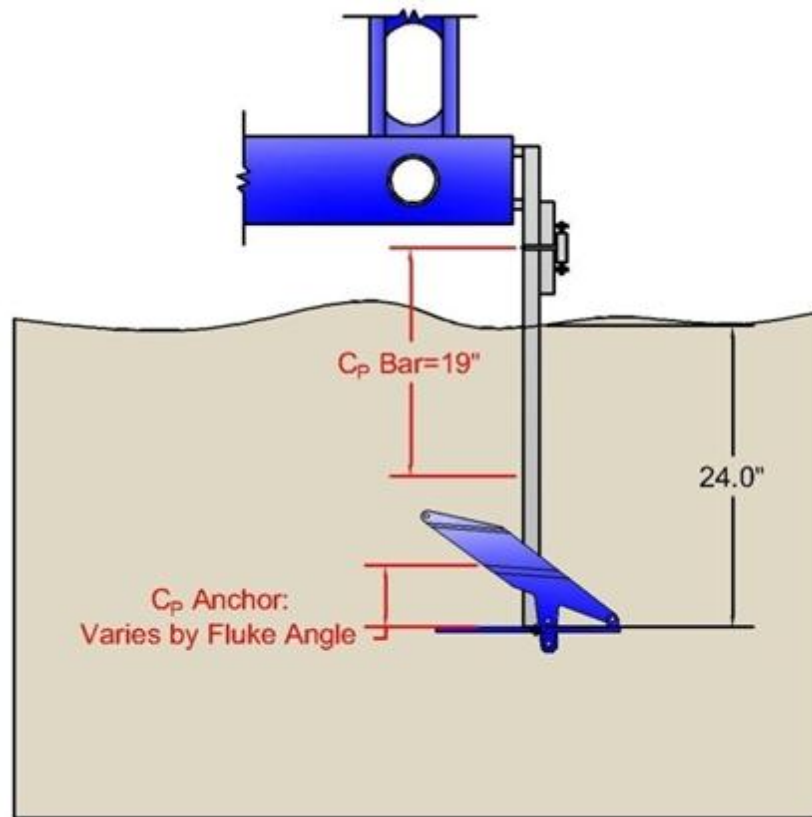


**Fig. 5-31.** Transverse Breakout Tests Center of Pressure and Moment Arm

### 5.7 Pressure Depth and Carriage Force

The pressure depth data was not used for calculations of trajectory or depth. The data obtained from the sensor showed a high degree of scatter as shown in Fig. 5-32 and Fig. 5-33. The pressure depth shown is not transformed from the fluke plate base to the anchor shackle point, therefore it reads on average 0.25 fluke lengths deeper than the chaser line calculated trajectory. Fig. 5-32 represents the data from a case two out-of-plane experiment where after the initial pull in distance there is a large time lapse needed to reset the position of the anchor line gear for continuing the pull. This data is shown in its raw form because it illustrates how the pressure transducer was measuring a dynamic pressure from the soil resistance in addition to the hydrostatic pressure.

Examining the range of data between 20 seconds and 140 seconds shows a static point. The anchor is not moving within this duration. There exists both prior to and directly after this duration a spike in the pressure reading that supports the observation that the pressure transducer is reading an additional dynamic pressure above the hydrostatic component; therefore the pressure depth data cannot be directly compared or transformed to the shackle trajectory data without extensive calculations to determine the dynamic component.

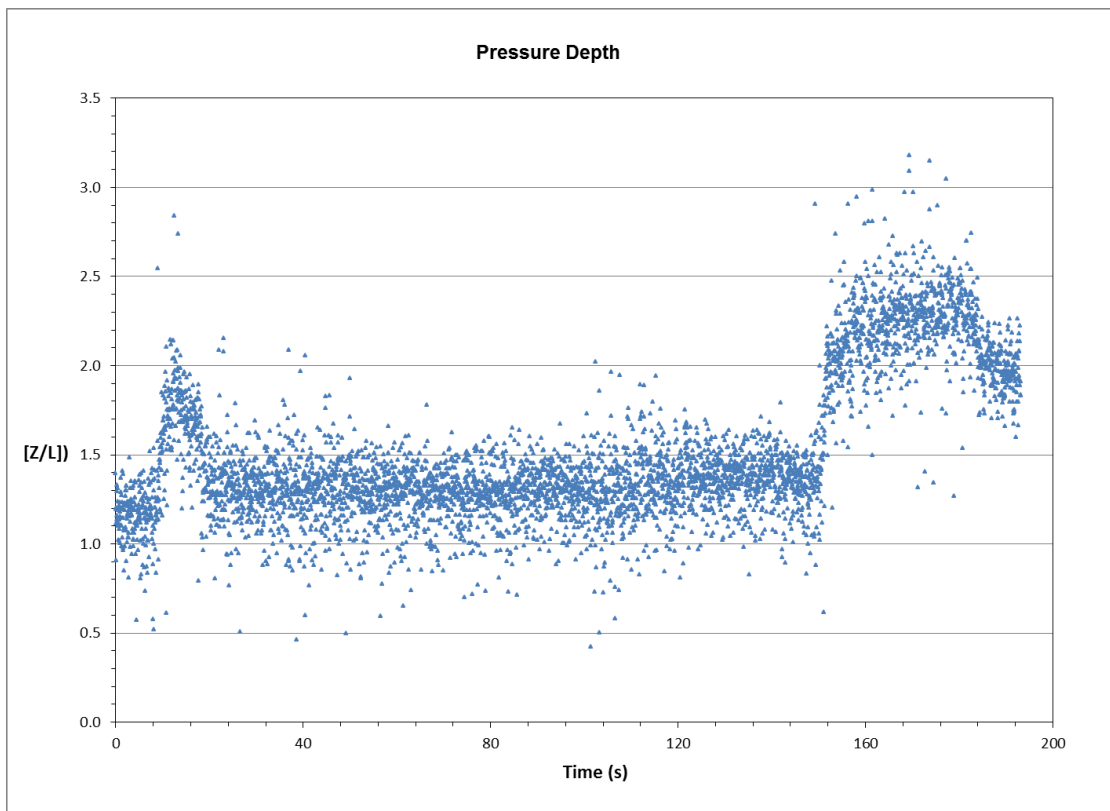


**Fig. 5-32.** Pressure Depth Data (Case 2)

Fig. 5-33 is a representative sample of pressure depth data taken from in-plane tests. Here the data show a smooth curve over the duration of the experiment. The anchor is continually moving in this case and there is no evidence of a spike or sharp

drop in the measured pressure depth. This is used for comparison to Fig. 5-32 where the pressure indeed dropped dramatically after the anchor stopped moving.

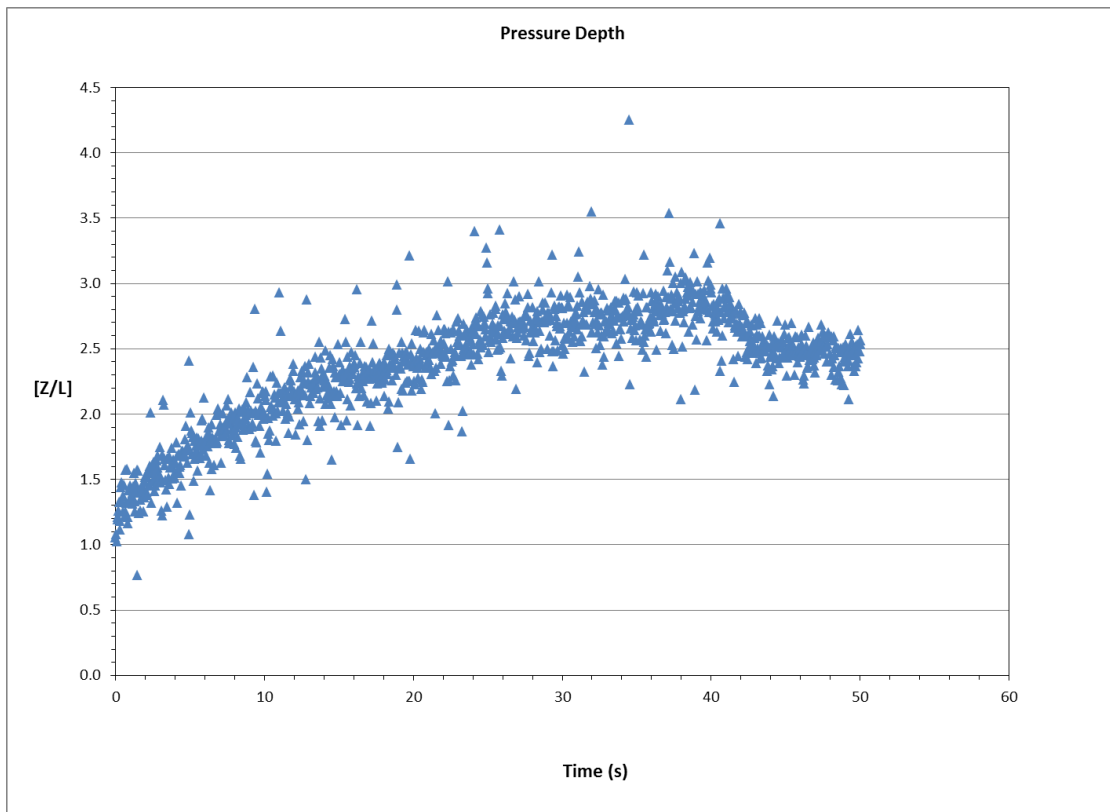


**Fig. 5-33.** Pressure Depth Data for In-Plane Example

The carriage force transducer showed significant noise in the measurements for every test. This may be attributed to the observed vibration that occurred in the long unsupported span of cable located between the top support structure pulley and the connection point to the tow carriage. The source of the vibration is thought to be linked to the buildup of hardened dry sediment on the upper support pulley groove. This sediment accumulation was removed periodically during the testing schedule. The lower pulley was washed free of sediment after each testing day and did not exhibit the accumulation as found with the upper pulley. Comparison with the force measured at the

anchor shackle reveals a reasonable agreement between the two measurements as shown in Fig. 5-34.

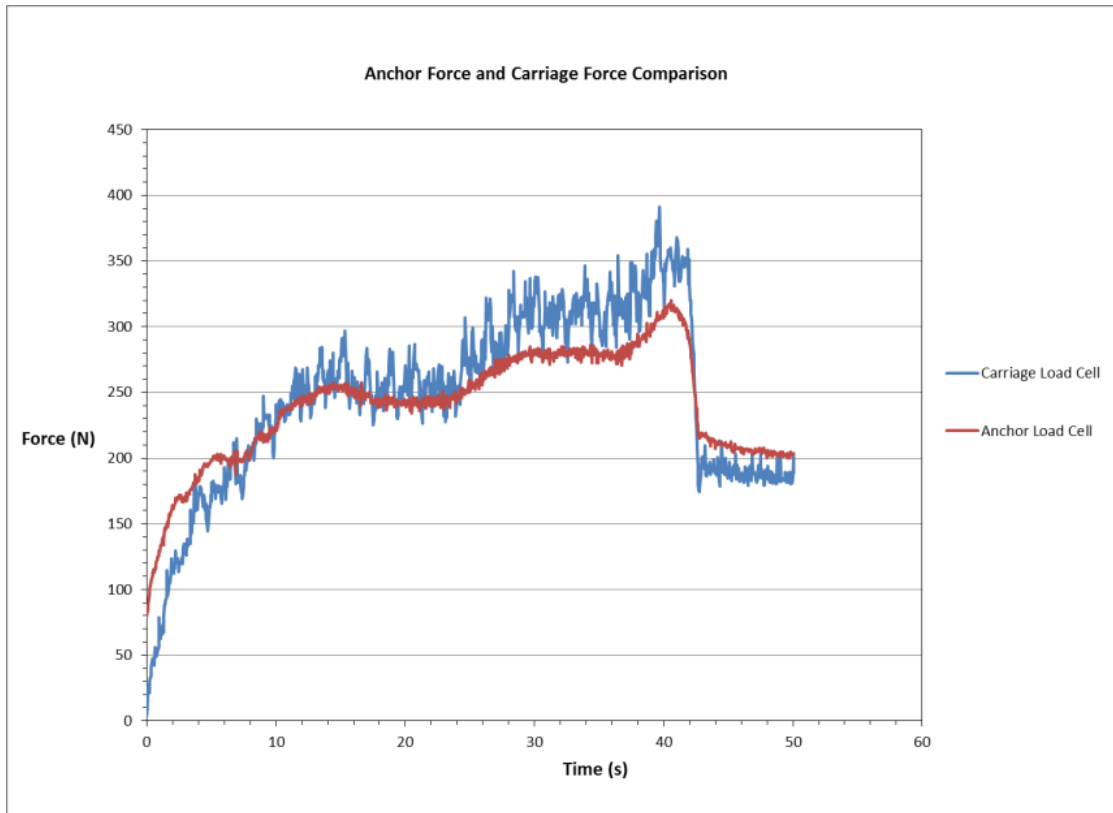


**Fig. 5-34.** Anchor and Carriage Load Cell Example

## 6. CONCLUSIONS AND RECOMMENDATIONS

### 6.1 Conclusions

#### 6.1.1 Overview and In-Plane

Overall, the 1:10 scale drag embedment anchor experiments performed at the Haynes Coastal Engineering Laboratory at Texas A&M University in 2010 developed the methodology and instrumentation critical for the examination of the behavior of drag embedment anchors subjected to both in-plane and out-of-plane loading. The representative sample of deep-water Gulf of Mexico soft clay was created using a bentonite/ sand mixture with an average un-drained shear strength of 0.764 kPa (16 psf). The extensive testing revealed that the initial towline angle with respect to the mud line produced only minor variations of the ultimate holding capacity and depth. There is a slight reduction of approximately 0.2 units of holding capacity for the 10° tests, and only 0.08 units of reduction when comparing the 5° to the 20° tests. The ultimate embedment depths and holding capacity for the 5° initial tow angles is used as a baseline for comparison against the out-of-plane test cases. For the 50° fluke angle the ultimate embedment depth was approximately 1.7 fluke lengths and 1.25 fluke lengths for the 36° fluke angle. The ultimate holding capacity associated with these values of depth is measured to be 4.1 for the 50° fluke angle and 3.7 for the 36°. The effect of the fluke angle setting was examined across all test parameters and indicates that the 50° fluke angle embeds an average of 0.7 fluke lengths deeper and has a holding capacity of 0.73 units greater than the 36° fluke angle. Analysis of the rate affect indicates that with the 46% increase in towing velocity there is an average 3% increase of holding capacity.

Inspection of the in-plane roll versus depth data indicates that the 50° fluke angle setting is more susceptible to rolling than 36°. The 50° fluke angle had an average magnitude of roll of 0.7 units in comparison to the 0.2 units of roll for the 36°. Evidence of rolling existed for each test case and suggests that either human error regarding the



initial placement of the anchor on the surface of the mud, or the swivel connecting the main towline to the chain did not perform as intended.

### *6.1.2 Out-of-Plane (Case 1)*

The surface out-of-plane tests reveal an average of 5.1% reduction in holding capacity as the out-of-plane pull angle increases from 45° to 90°. The average difference due to the fluke angle setting shows that the 50° embedded 0.95 fluke lengths deeper with an average 0.95 higher holding capacity than the 36° fluke angle. This is 35% greater than the overall average and may be attributed to the 50° fluke angle's greater sensitivity to roll. The surface out-of-plane tests induced a uniform pattern of roll with respect to depth. The 90° out-of-plane angle induced a greater magnitude of roll than the 45° tests and shows for both fluke angle settings, a clear tendency towards recovery as the roll reduced with a depth. The 50° fluke angle had a lower rate of recovery. Examination of the 45° out-of-plane angle tests show that the 36° fluke angle exhibited a tendency to recover in three out of the four test cases. The 50° fluke angle showed recovery in only one of the four test cases.

### *6.1.3 Out-of-Plane (Case 2)*

The results obtained from the case 2 out-of-plane loading, where the anchor was embedded either one or three fluke lengths and then towed at out-of-plane angles of either 15°, 30° or 45° indicates there exists a strong relationship with the initial embedment depth to the out-of-plane angle. This pattern is shared between fluke angle settings. For all one fluke length initial pull-in distance tests, the ultimate holding capacity increases while the ultimate embedment depth decreases as the out-of-plane towing angle increases from 15° to 45°. The three fluke length initial pull-in distance tests indicate a contrasting trend, in that as the out-of-plane tow angle increases, both the ultimate holding capacity and ultimate embedment depth decrease. Curves were generated using extrapolated data sets with a high degree of fit relating the ultimate

embedment depth and holding capacity with respect to the fluke angle setting and out-of-plane tow angle as a function of initial embedment distance as listed in Table 6-1. The angle  $\vartheta$  is the out-of-plane tow angle in degrees, and  $N_U$  and  $Z_U$  are the respective non-dimensional ultimate holding capacity and embedment depth.

**Table 6-1.** Equations of  $N_u$  and  $Z_u$  for Out-of-Plane Loading

	<b><u>36° Fluke Angle</u></b>	<b><u>50° Fluke Angle</u></b>
<i>1 Fluke Length</i>	$N_{U\theta} = 1.79 \theta^{0.24}$ $Z_{U\theta} = 25.1 \theta^{-0.95}$	$N_{U\theta} = 3.54 \theta^{0.08}$ $Z_{U\theta} = 24.0 \theta^{-0.75}$
<i>3 Fluke Length</i>	$N_{U\theta} = 8.1 \theta^{-0.24}$ $Z_{U\theta} = 35 \theta^{-1.19}$	$N_{U\theta} = 6.1 \theta^{-0.07}$ $Z_{U\theta} = 11.4 \theta^{-0.57}$

The magnitude of roll for Case 2 experiments increased proportionally with the increase of out-of-plane angle. No clear relationship between roll and the initial pull-in distance was developed.

#### 6.1.4 Out-of-Plane (Case 3)

The data obtained from Case 3 out-of-plane tests, where the anchor was towed in using the dredge carriage ladder produced results that differed greatly in both holding capacity trend lines and rate of change of pitch with depth when compared to the other test cases. The ultimate holding capacity exhibited only minor changes after the transitional phase of embedment and showed the relatively constant holding capacity value equal to 4.25. In these cases, the anchor pitch angle never reached the horizontal position; this may be

attributed to the shorter main towline used to perform these tests. The towline appeared nearly straight as opposed to the reverse catenary shape observed during the other tests. No discernible pattern was developed from the roll data and requires further investigation.

#### *6.1.5 Breakout Tests*

Breakout test data reveals that the specially constructed devices performed as intended, and accurately produced results for the anchor's resistance in pure normal, transverse, and rotational motion.

### **6.2 Recommendations and Future Work**

Further investigation is recommended in order to refine the results on the behavior of drag embedment anchors subjected to out-of-plane loading. A close analysis and incorporation of the fluke angle setting, initial depth, rate effects, anchor line diameter, anchor weight and scale effects should be performed in order to fully encompass the variables that may affect the ultimate embedment depth and holding capacity. The accuracy of the curves developed from these experiments would benefit from additional testing of the aforementioned parameters.

It is recommended for future endeavors to examine these parameters in detail. The testing schedule should include multiple experiments using different diameter anchor chain and a 1:20 anchor model ratio to examine scale effects. With appropriate funding allowance, every effort should be made to incorporate the smallest size sensors and associated data cables capable of measuring the anchor's parameters. The mass of the anchor tension load cell and pressure depth transducer and projected area of the data cables may have altered the trajectory and holding capacity. Furthermore, a three-axis gyroscope should replace the two-axis inclinometer.

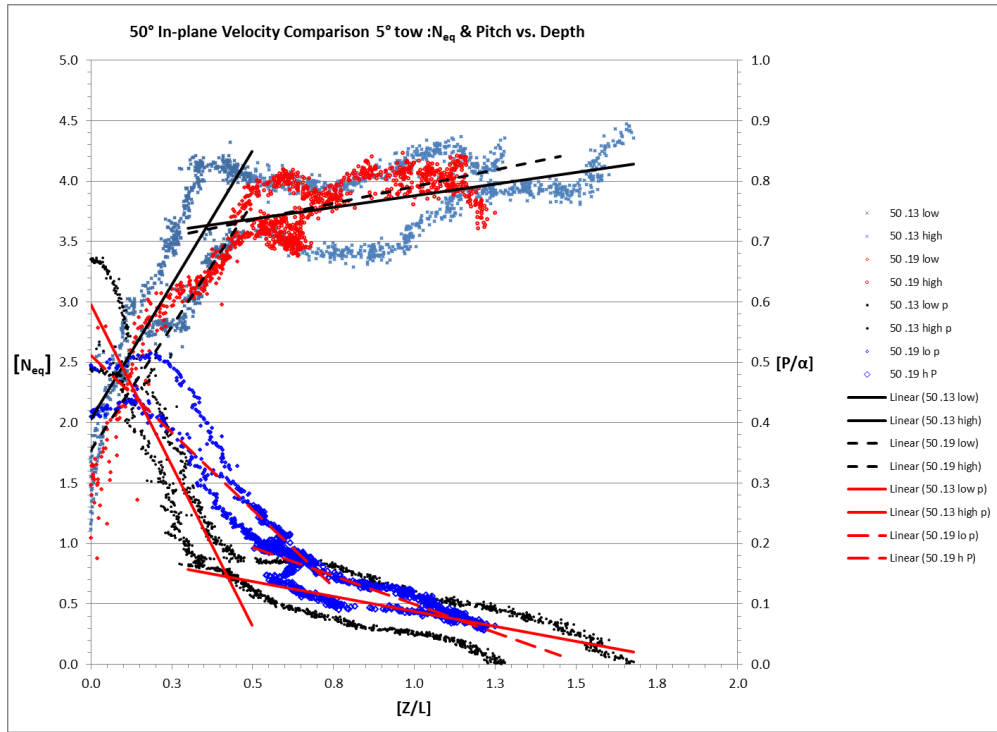
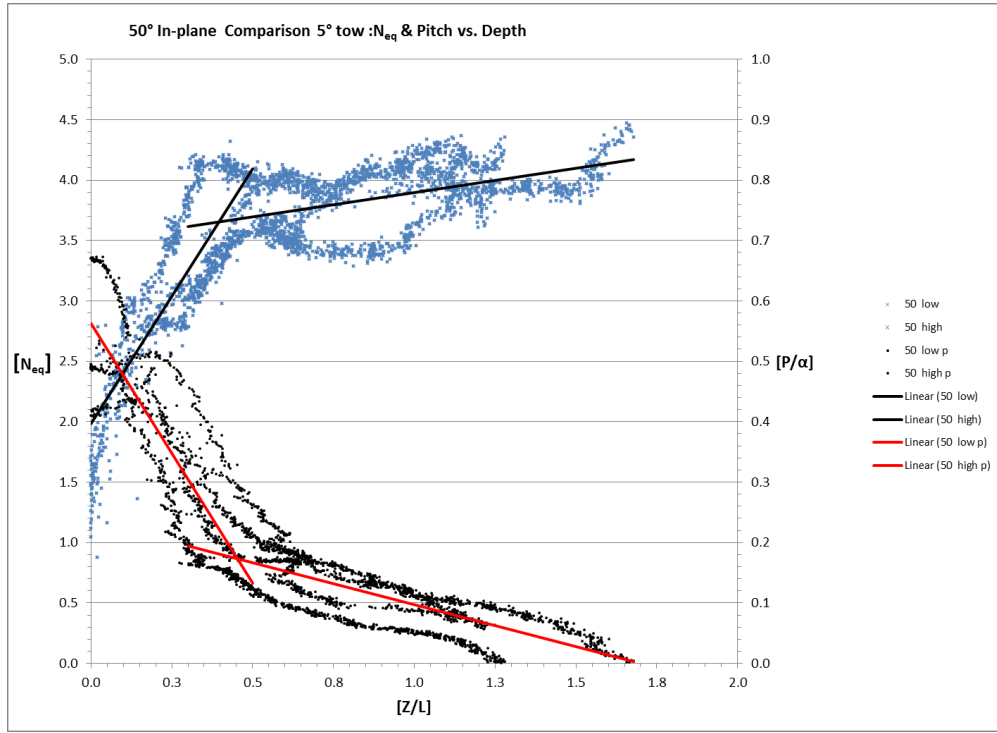
Regarding the in-plane roll that occurred during every test, a sealed swivel with proper bearings would help to reduce the roll imparted by the main towline. This towline was eventually replaced halfway through the testing schedule due to the formation of kinks and loops. Finally, even though every effort was made to ensure repeatability and accuracy of the experiments performed we did overlook one aspect. The exact placement of the anchor within the sediment basin was not accurately logged. This prevented the identification of the tests that were towed through the lane of higher un-drained shear strength sediment located at the northwestern most position of the basin.

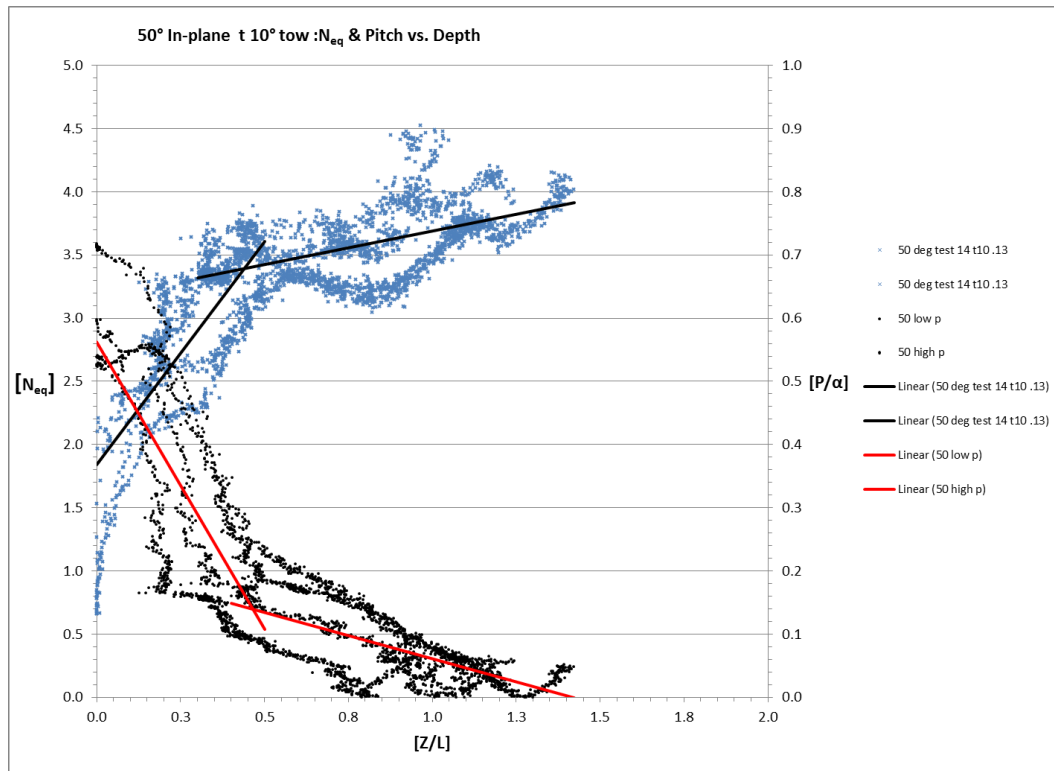
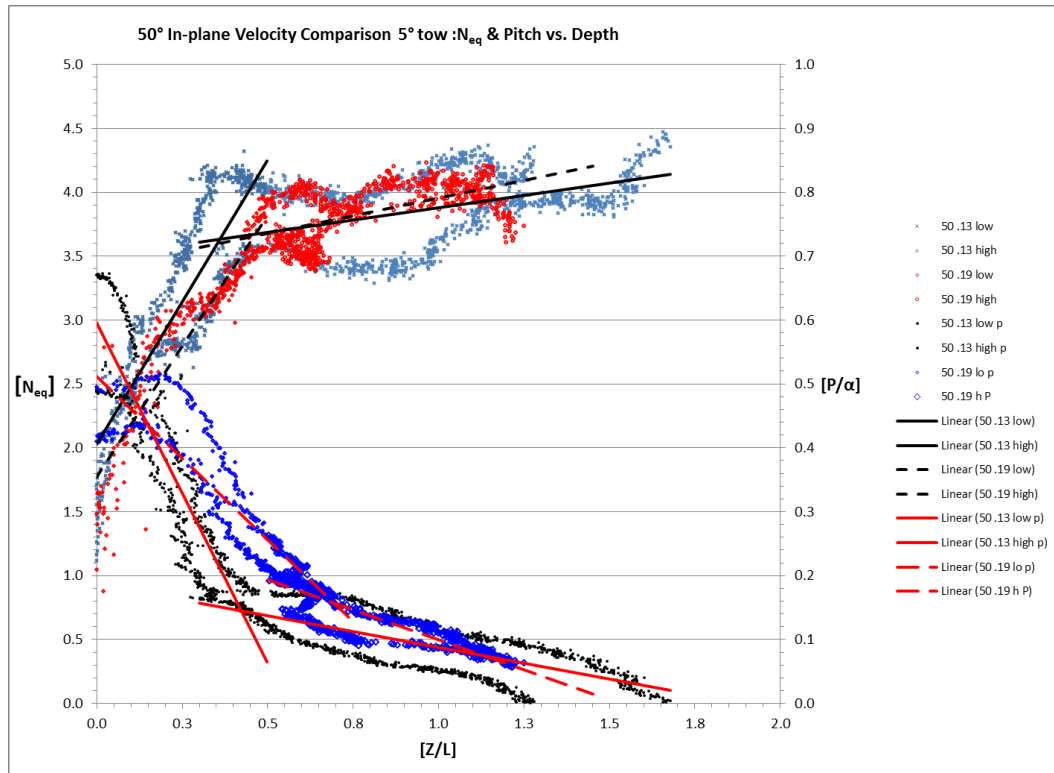
## REFERENCES

- American Petroleum Institute (2005). *Design and analysis of stationkeeping systems for floating structures: API Recommended Practice 2SK*. 3rd Edition. API Publishing Services, Washington, D.C.
- ASM (2010). "Automation, sensors and measurements products." *ASM*, accessed October 2009, [www.asm-sensor.com](http://www.asm-sensor.com).
- Aubeny, C.P., Gilbert, R., Randall, R.E., Zimmerman, E., McCarthy, K., et al. (2011). "The performance of drag embedment anchors (DEA)." Minerals Management Service, Washington D.C., RP-645.
- Aubeny, C.P., and Chi, C. (2010A). "Trajectory prediction for drag embedment anchors under out of plane loading." *Proc., Int. Symp. on Frontiers in Offshore Geotechnics, IS-FOG10*, Balkema, Perth, Australia, 699-703.
- Aubeny, C. P., and Chi, C. (2010B). "Mechanics of drag embedment anchor in a soft seabed," *J. of Geotech. and Geoenviron. Eng.*, 136(1), 57-68.
- Aubeny, C. P., and Shi, H. (2007). "Effect of rate-dependent soil strength on cylinders penetrating into soft clay," *IEEE J. of Oceanic Engr.*, 32(1), 1-8.
- Carchedi, D.R., Nacci, V.A., Pekin, O., and Morgan, R.J., (1984). "An experimental study of drag anchors and implications for OTEC." *Proc., 16th Annual Offshore Technology Conf.*, Houston, TX, Paper No. OTC 4768.
- Dahlberg, R. (1998) "Design procedures for deepwater anchors in clay," *Proc., 30th Offshore Technology Conf.*, Houston, TX, Paper No. OTC 8837.
- Dunnavant, T.W., and Kwan, C.T.T., (1993). "Centrifuge modeling and parametric analyses of drag anchor behavior." *Proc., 25th Annual Offshore Technology Conf.*, Houston, TX, Paper No. OTC 7202.
- Det Norske Veritas A.S. (2007). "Pipeline damage assessment from hurricanes Katrina and Rita in the Gulf of Mexico." Minerals Management Service, Washington D.C., RP-448-14183.
- Naval Civil Engineering Laboratory (NCEL),(1987). "Drag embedment anchors for navy moorings." Techdata Sheet 83-08R, Port Hueneme, CA.

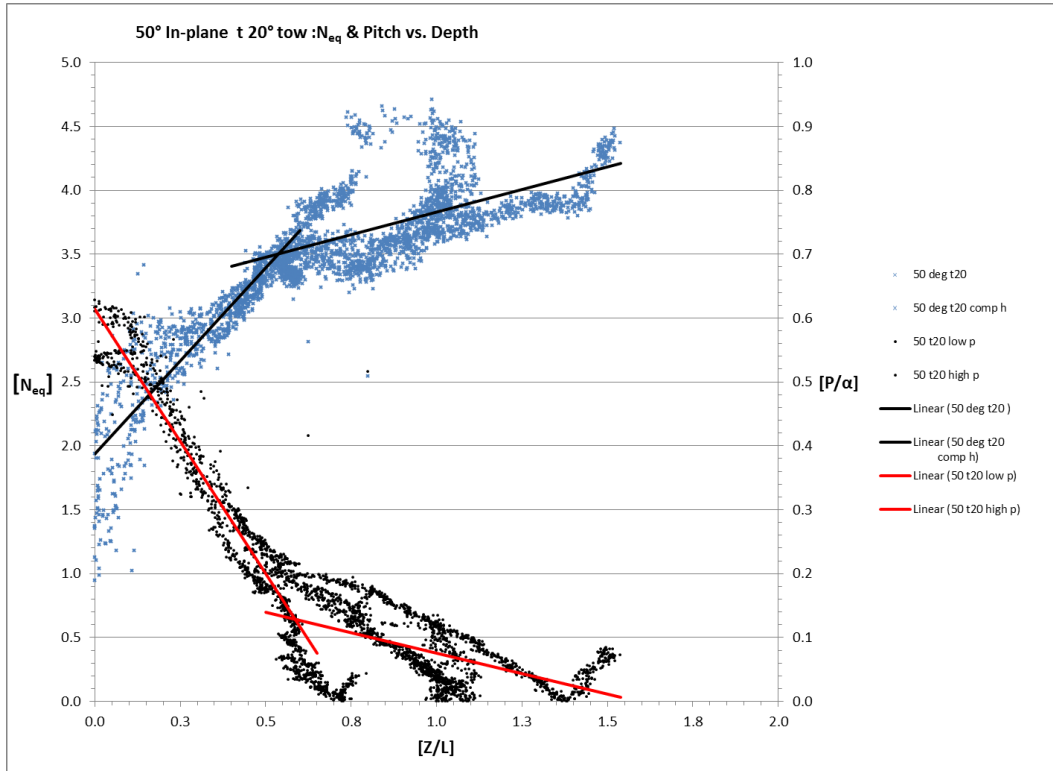
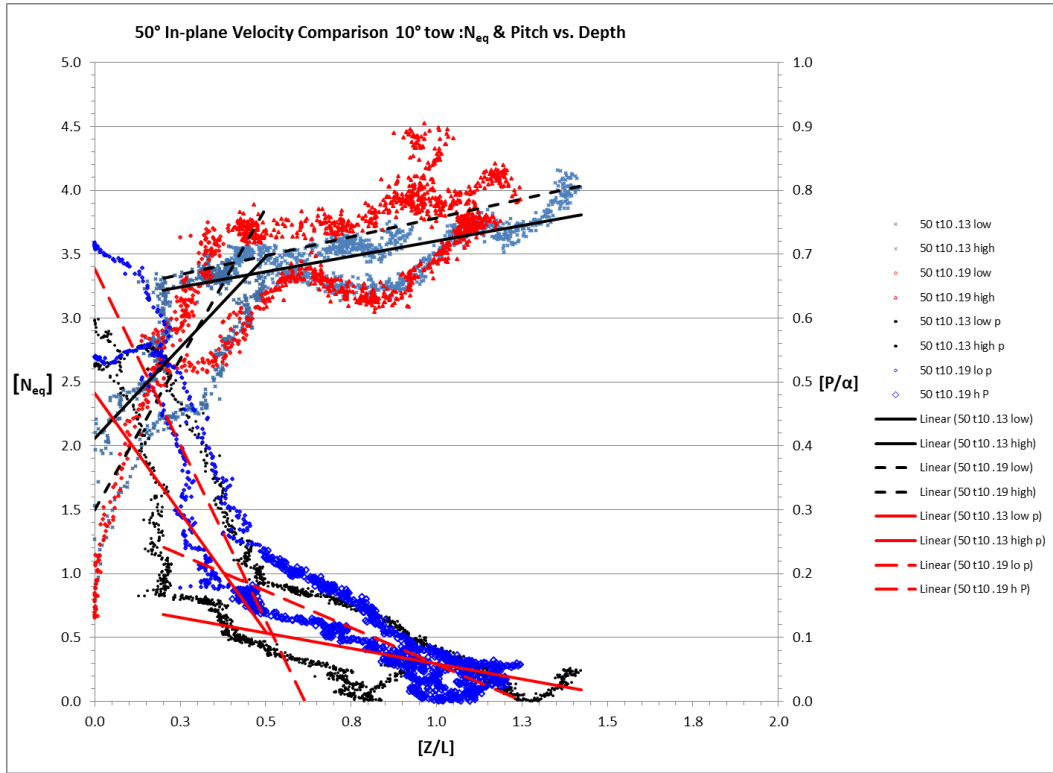
- Neubecker, S. R., and Randolph, M. F. (1995). "Profile and frictional capacity of embedded anchor chain," *J. of Geotechnical Engineering Division*, ASCE, 121, 11, 787-803.
- Neubecker, S.R. and Randolph, M.F. (1996) "The performance of embedded anchor chains systems and consequences for anchor design," *Proc. 28th Offshore Technology Conf.*, Houston, TX, Paper No. OTC 7712.
- O'Neill, M.P., Bransby, M.F. and Randolph, M.F. (2003) "Drag anchor fluke-soil interaction in clays," *Can. Geotech. J.*, 40: 78-94.
- Omega Engineering Inc. (2010). "Pressure, strain and force products." *Omega Engineering Inc.*, accessed October 2009, [www.omega.com](http://www.omega.com).
- Omega Marine Services International. (1990). Joint Industry Project: Gulf of Mexico Large Scale Anchor Tests – Test Report, Omega Marine Services International, Houston.
- Stellar Technology Inc. (2010). "Pressure sensor products." *Stellar Technology Inc*, accessed October 2009, [www.stellartech.com](http://www.stellartech.com).
- Stewart, W.P., (1992). "Drag embedment anchor performance prediction in soft clay." *Proc., 24th Annual Offshore Technology Conf.*, Houston, TX, Paper No. OTC 6970.
- Stewart, D.P., and Randolph, M.F. (1994). "T-bar penetration testing in soft clay." *ASCE J. of Geotechnical Eng.*, 120(12), 2230-2235
- Vryhof Anchors BV (2010). *Anchor manual 2010*. Capelle a/d Yessel; The Netherlands.
- Vryhof Anchors BV (2005). *Anchor manual 2005*. Capelle a/d Yessel; The Netherlands.
- Young, D. R. (2009). "Forces on laboratory model dredge cutterhead." M.S. Thesis, Department of Ocean Engineering, Texas A&M University, College Station, TX.

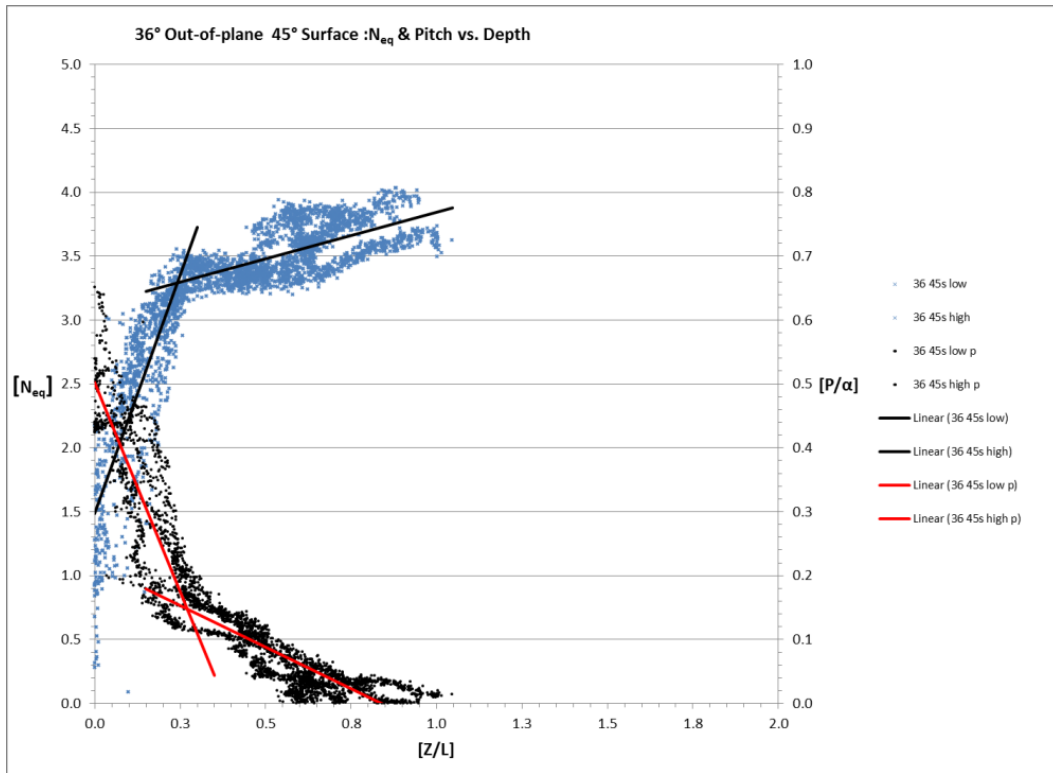
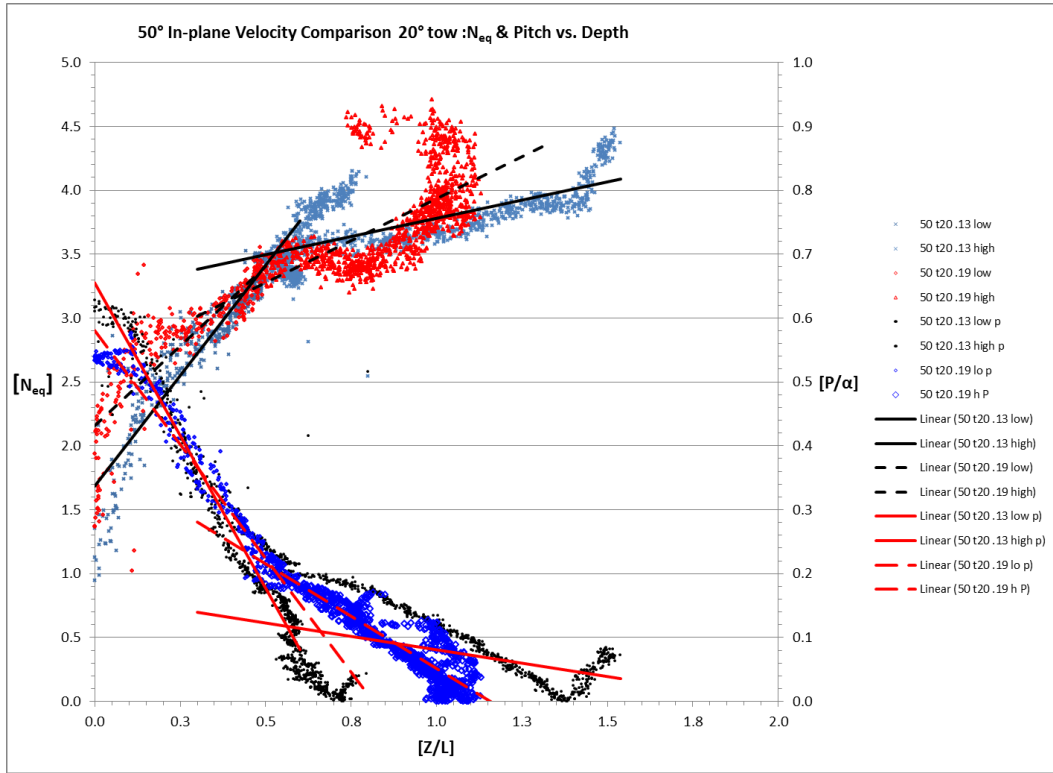
## APPENDIX A

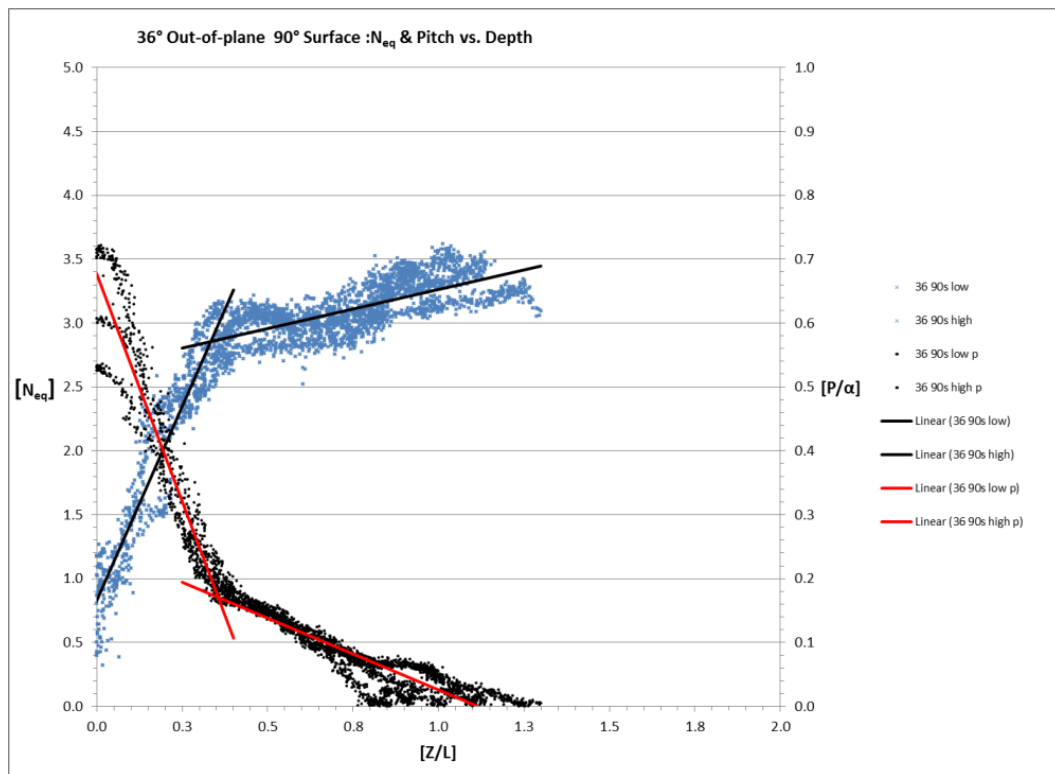
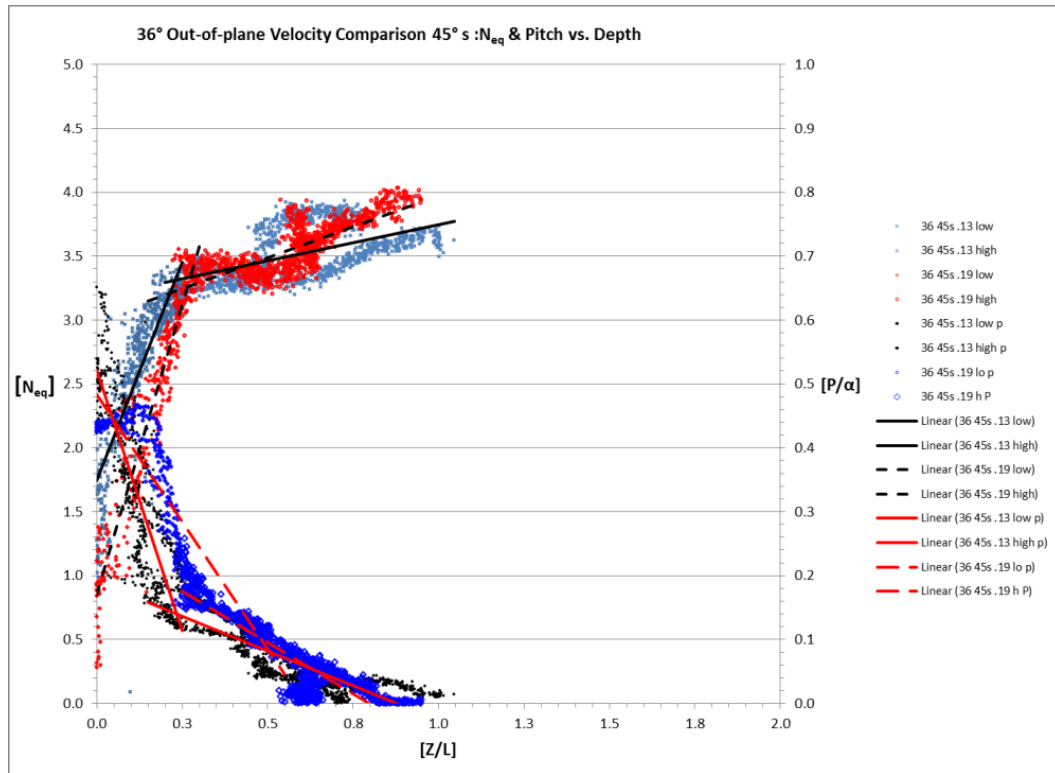


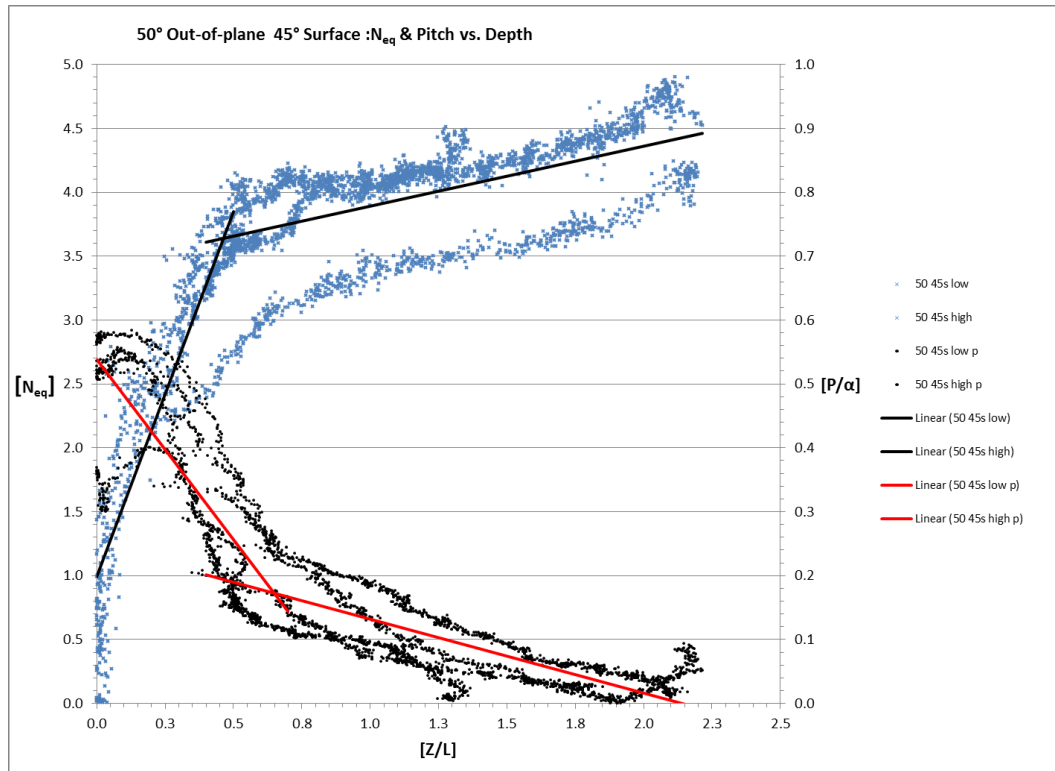
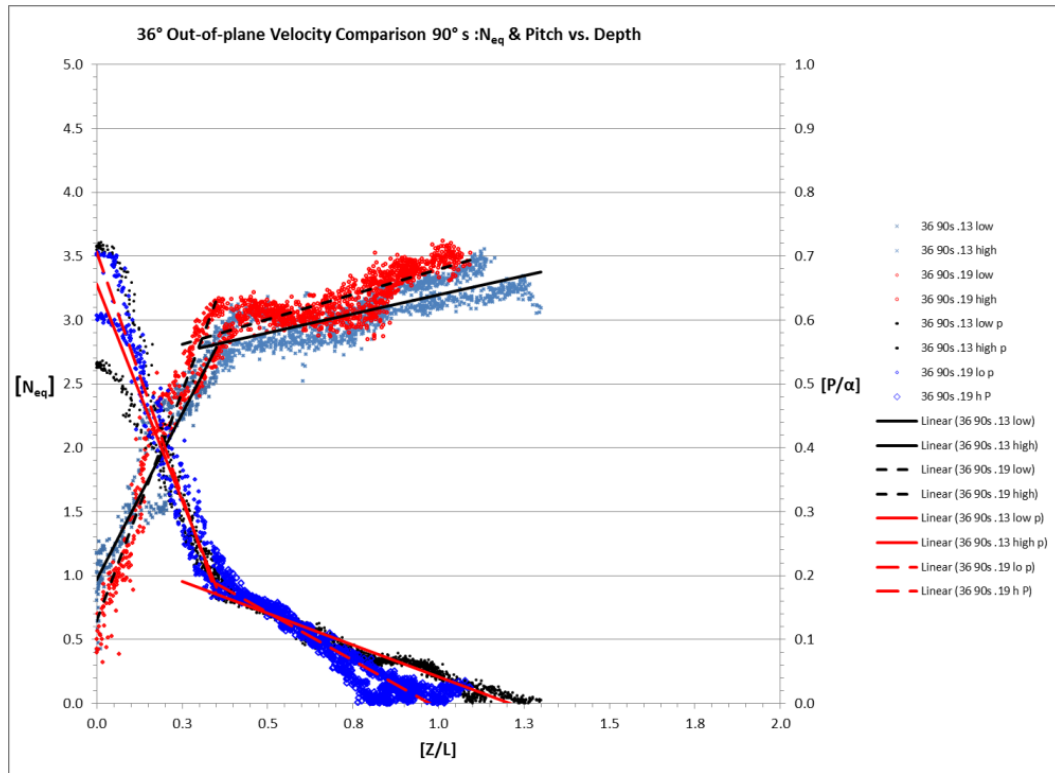


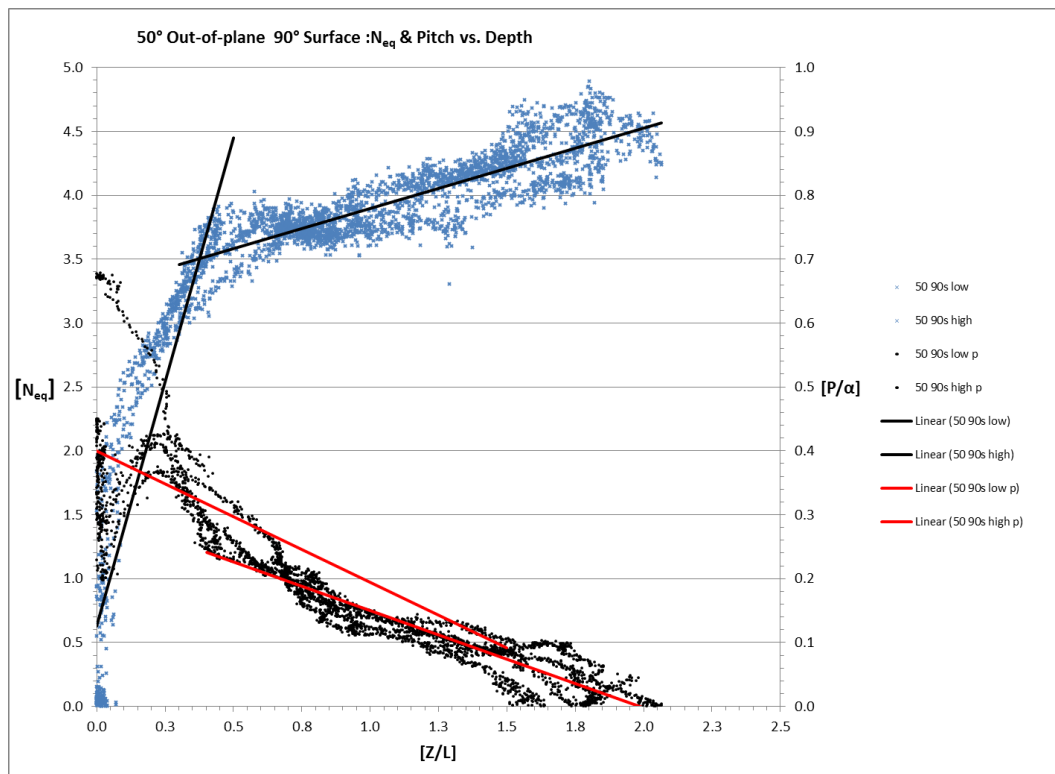
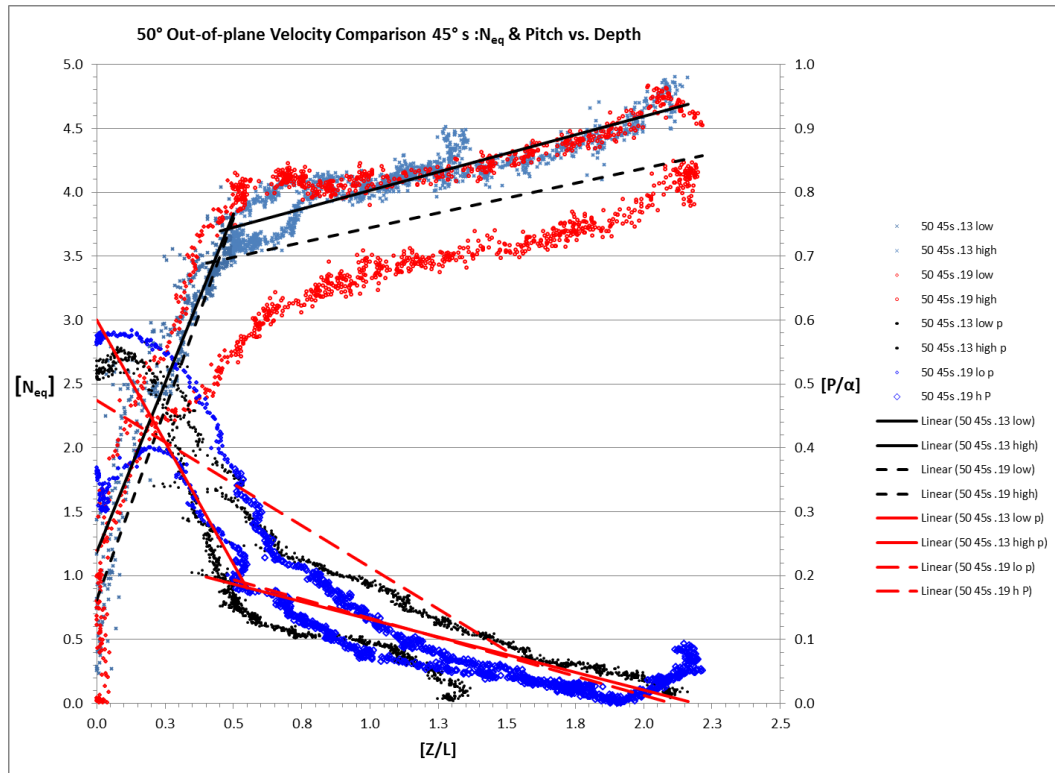


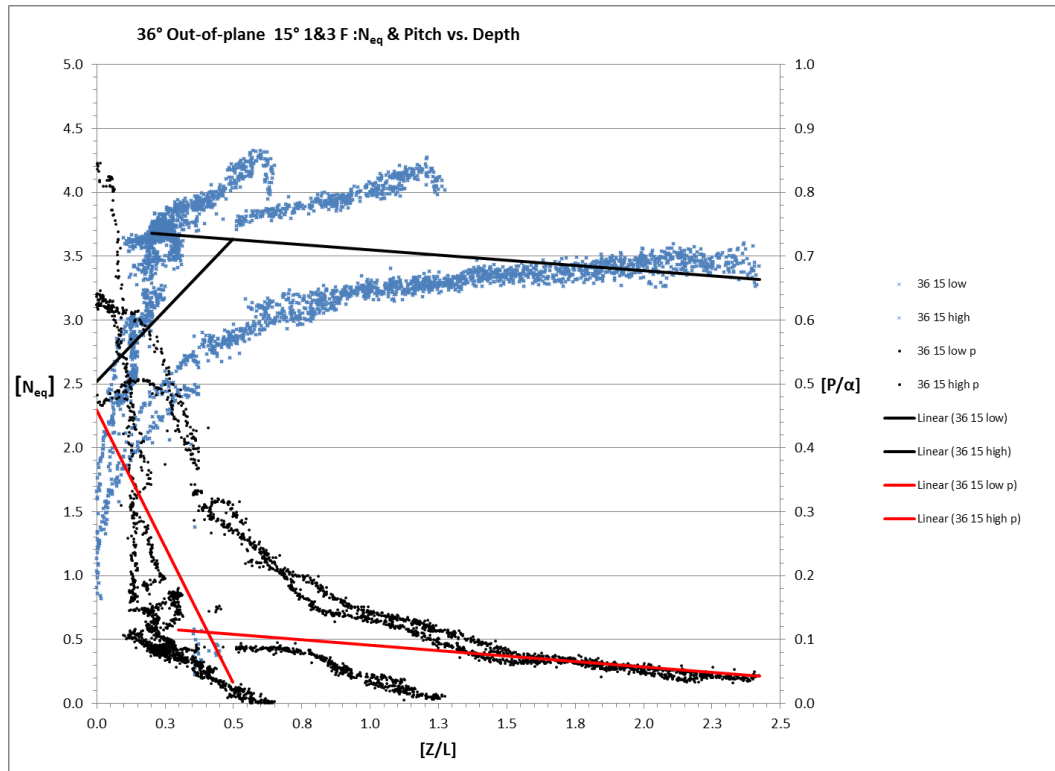
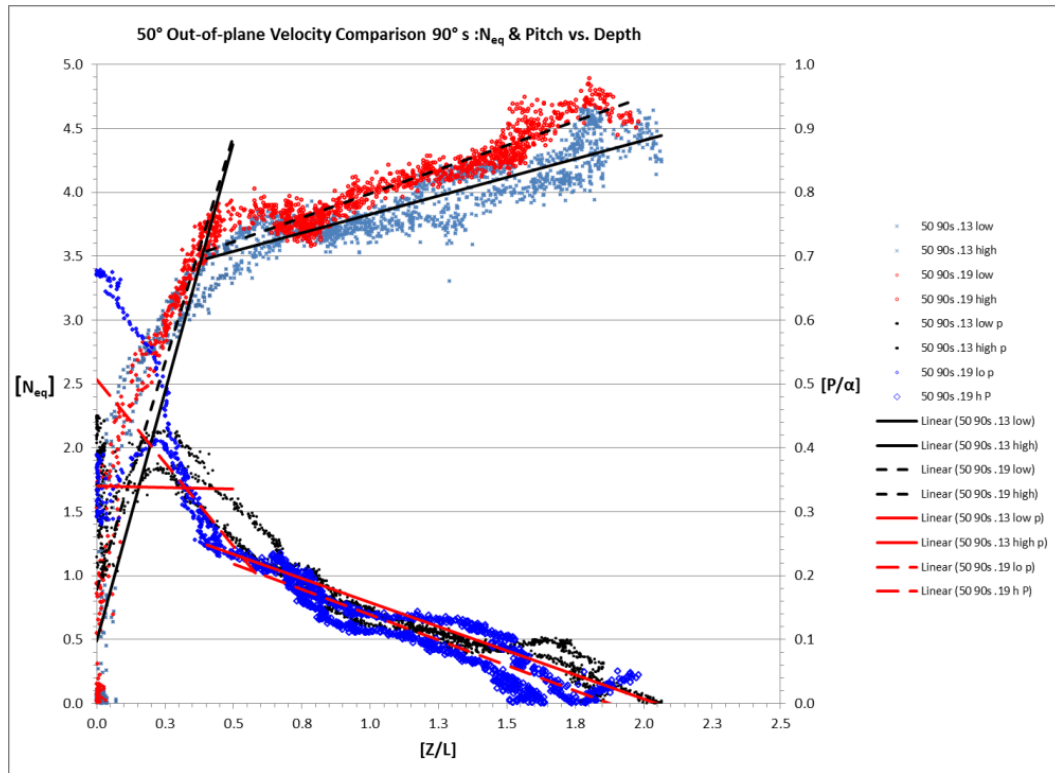


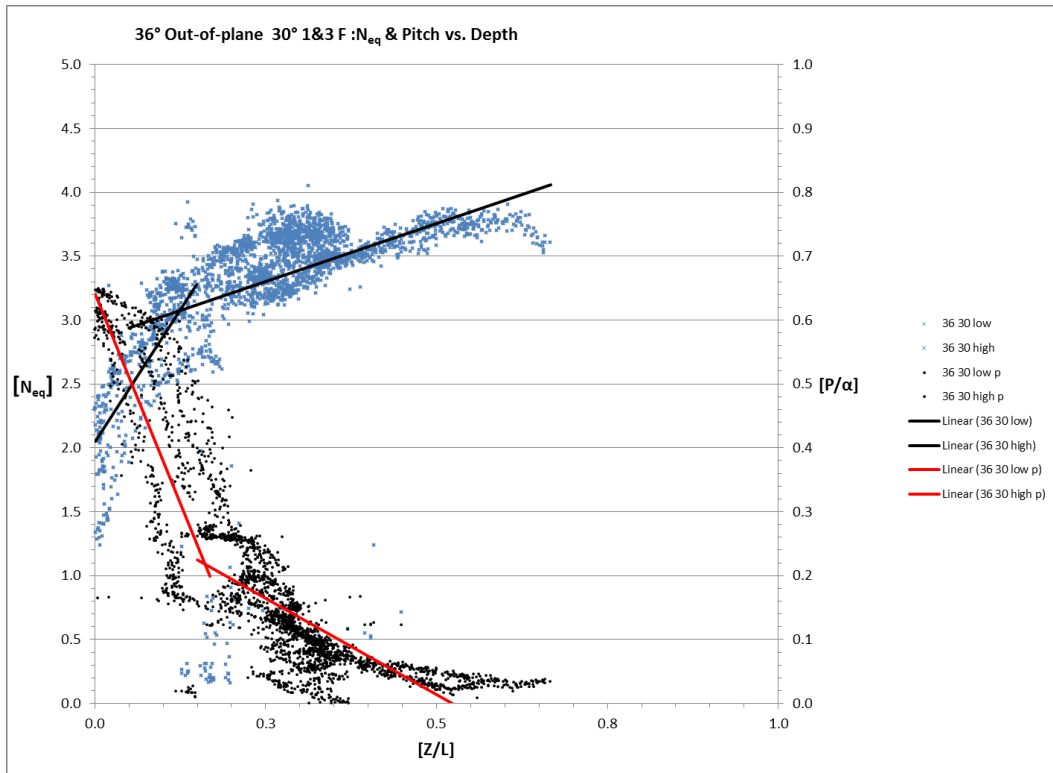
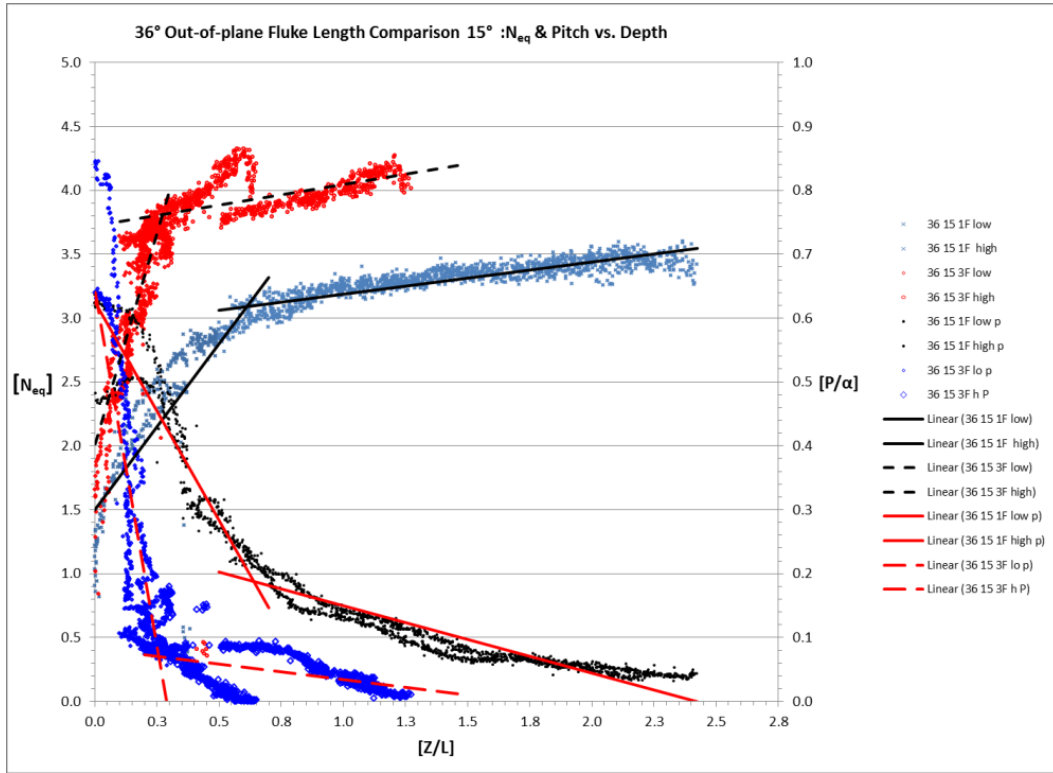


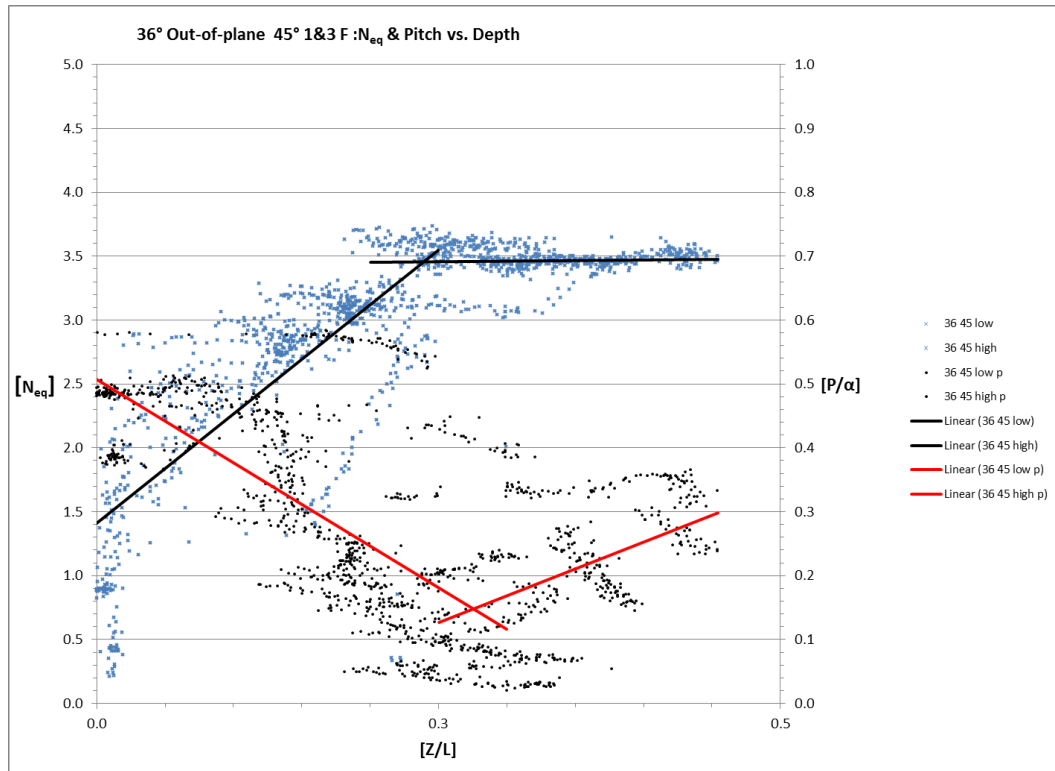
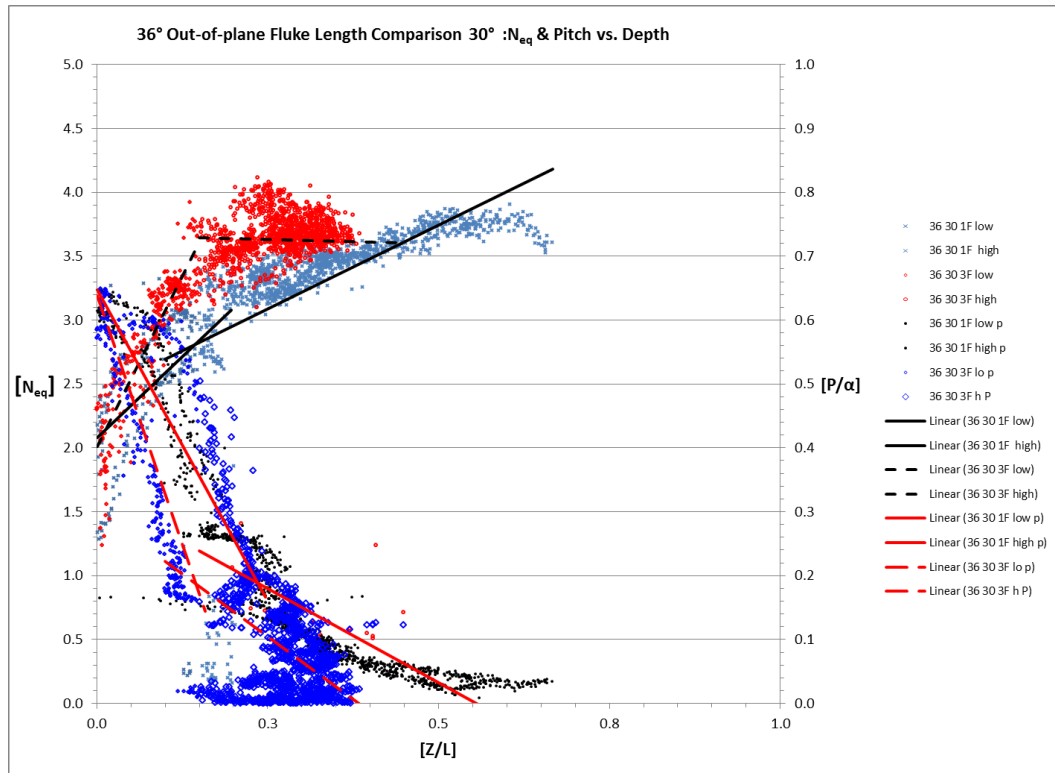




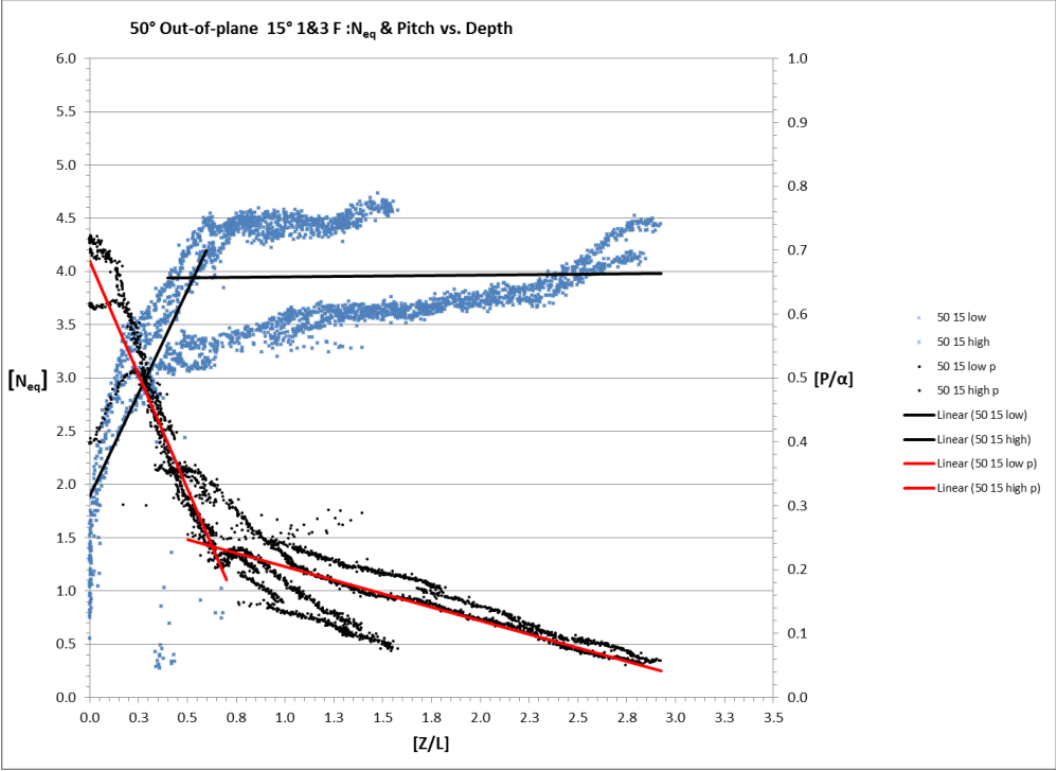
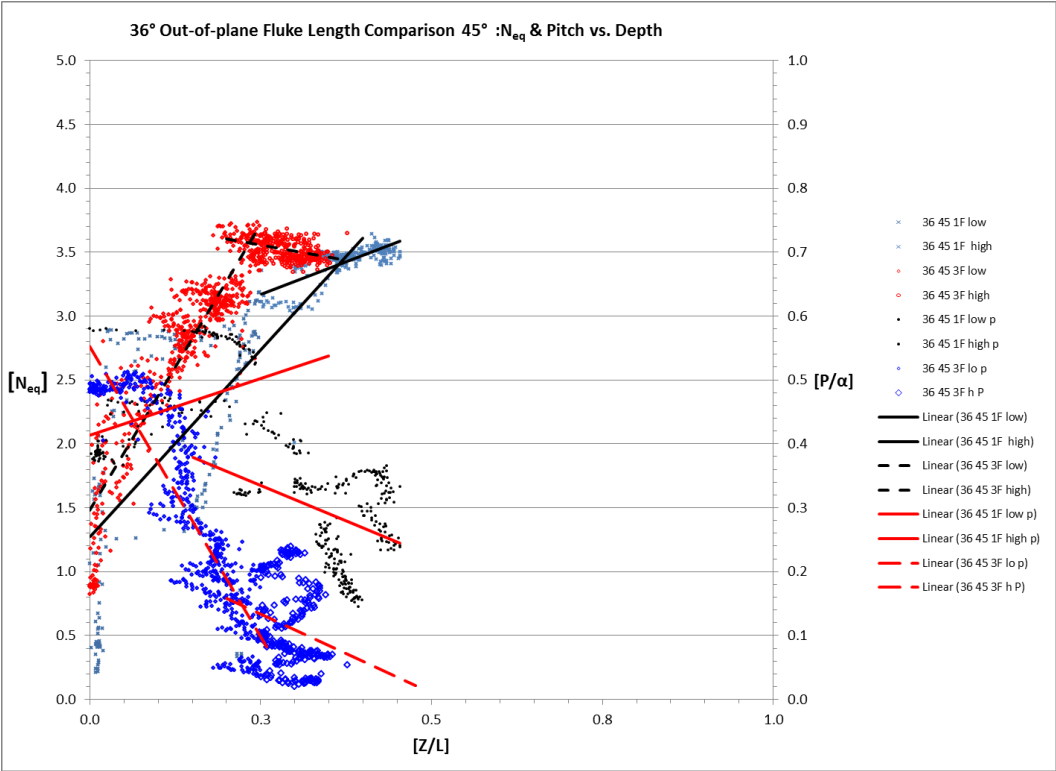


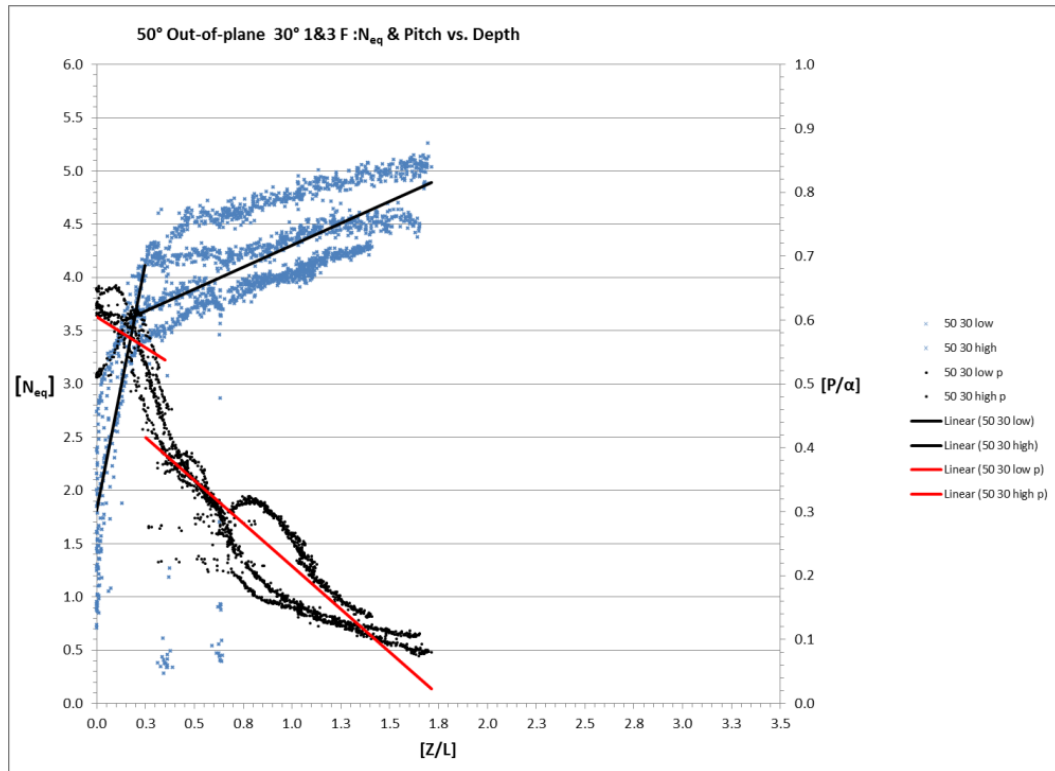
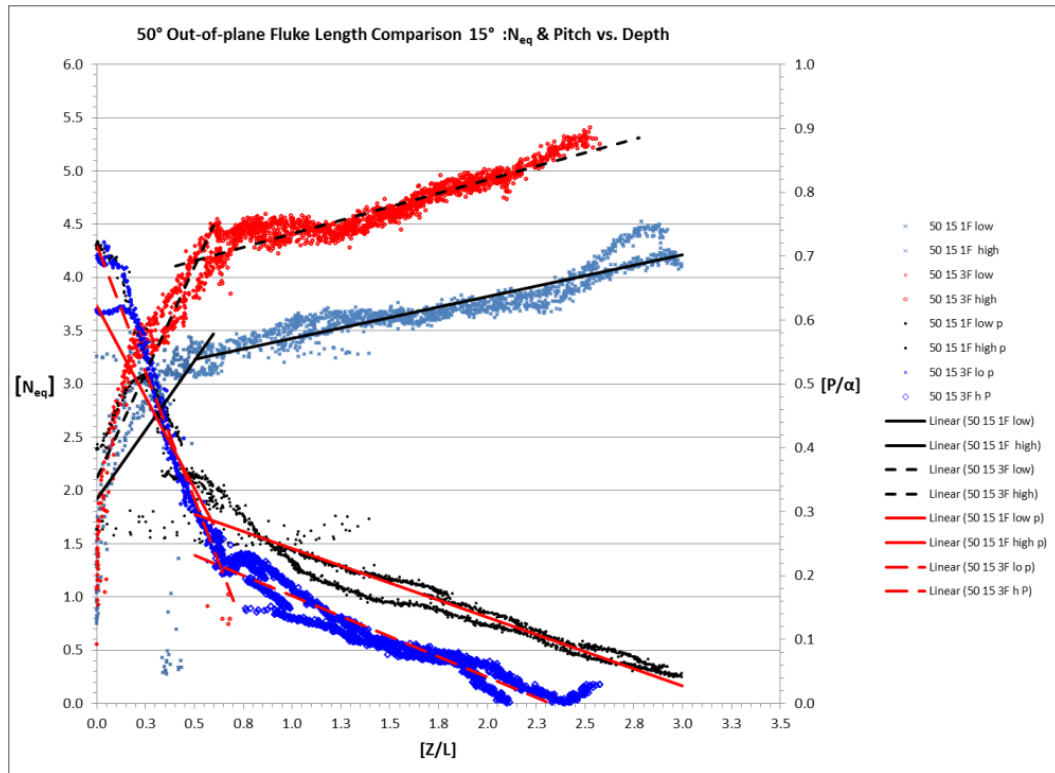


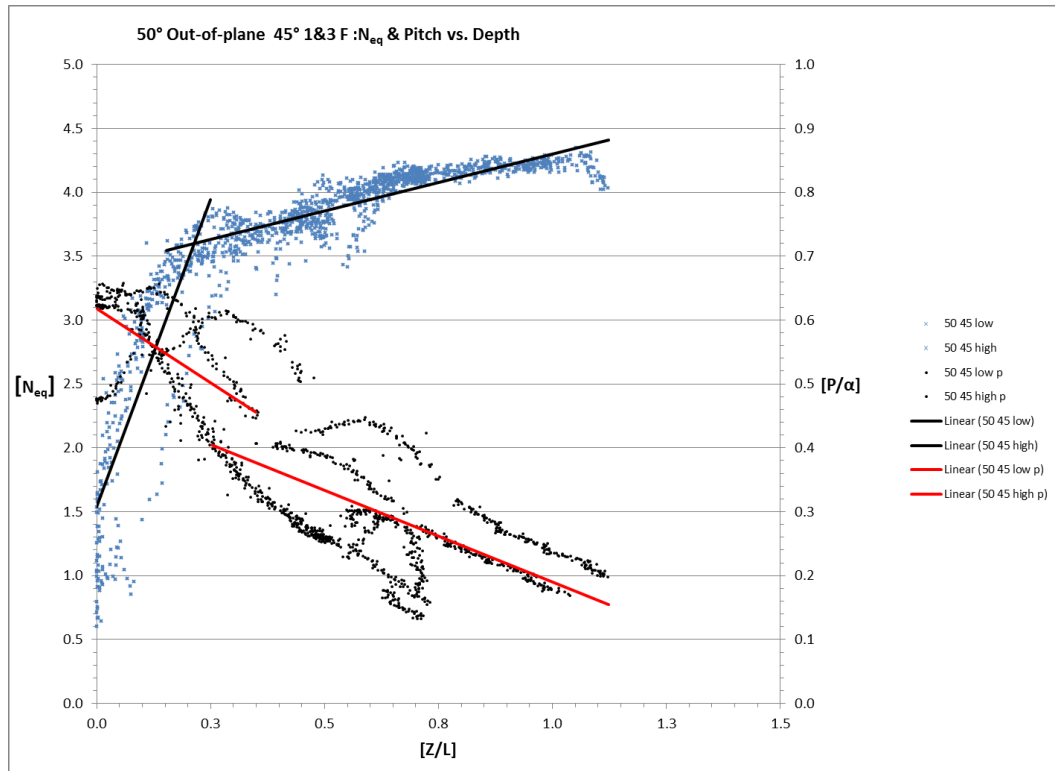
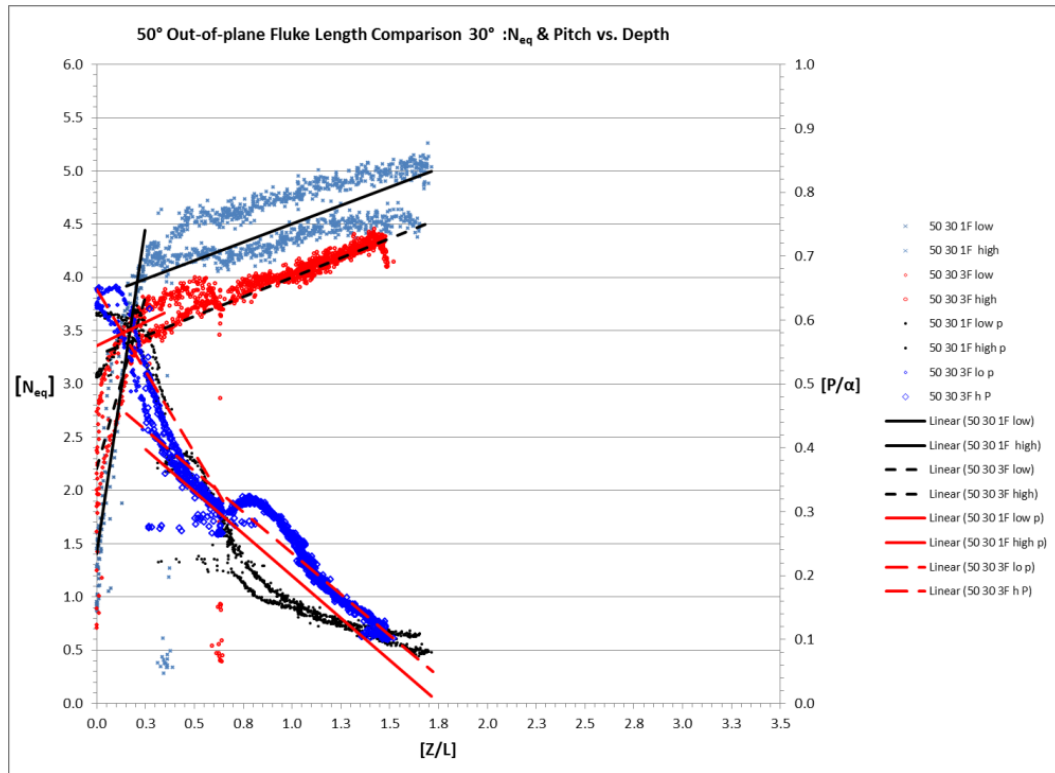


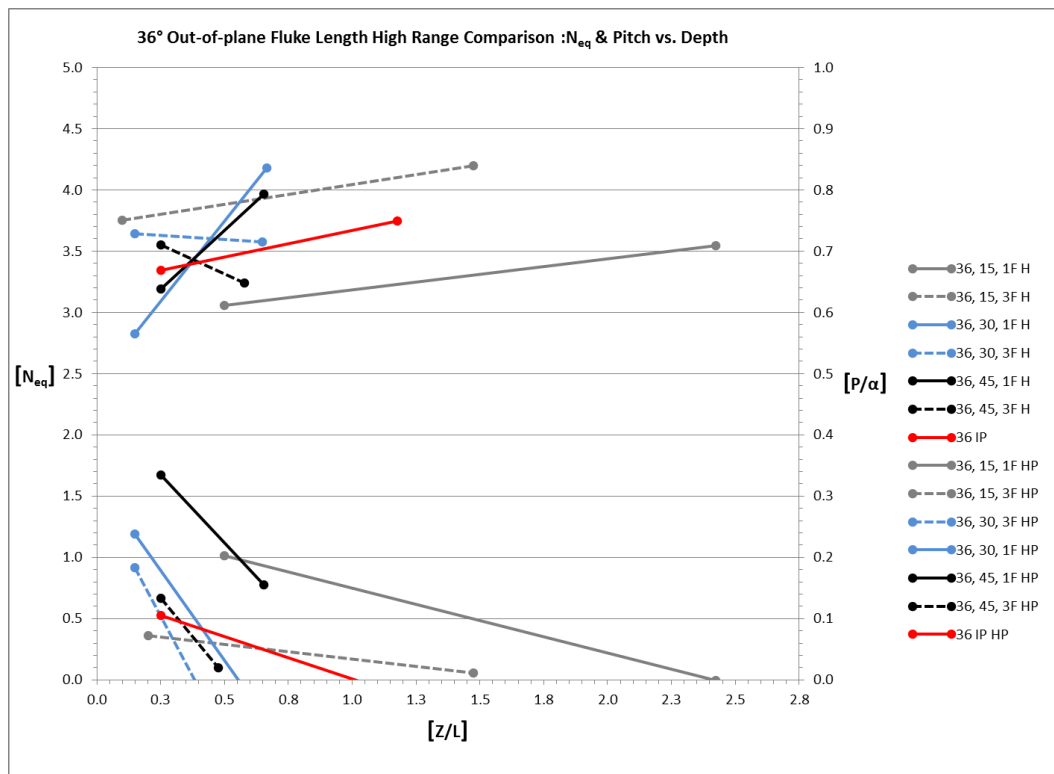
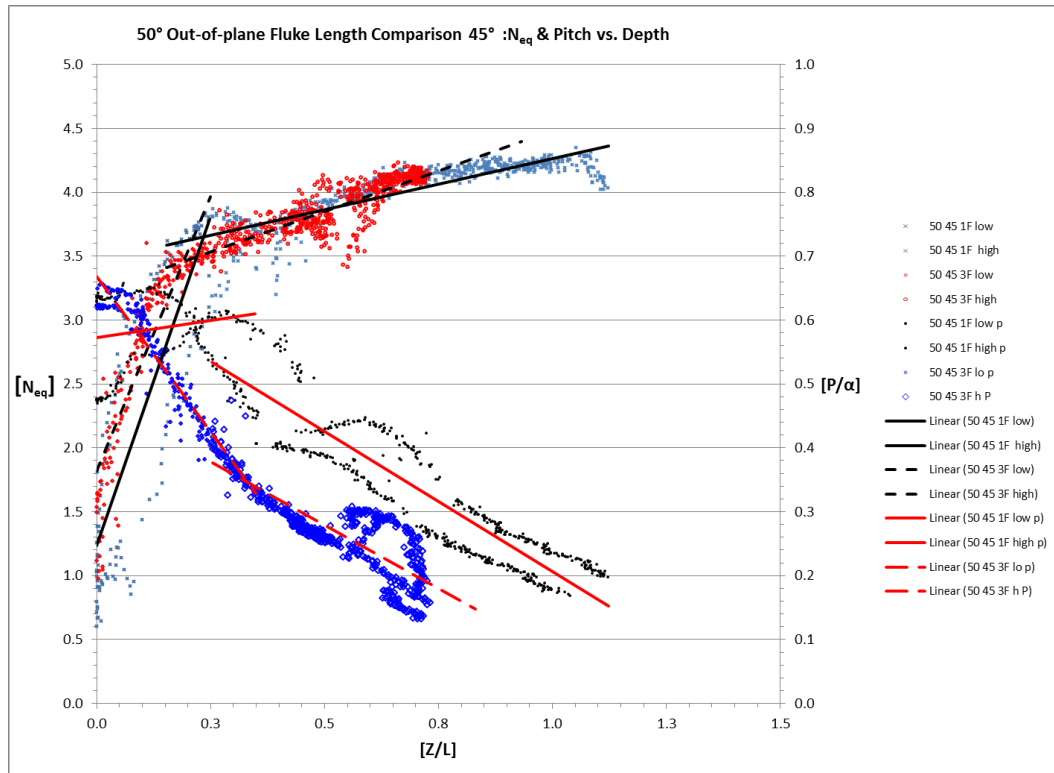


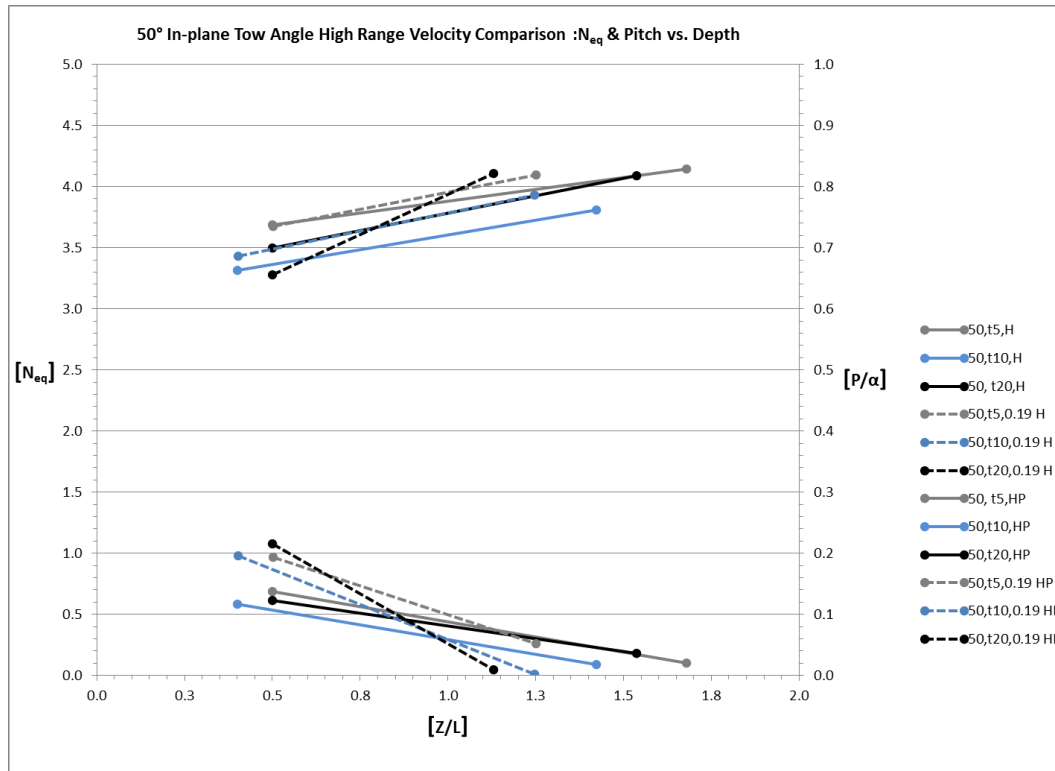
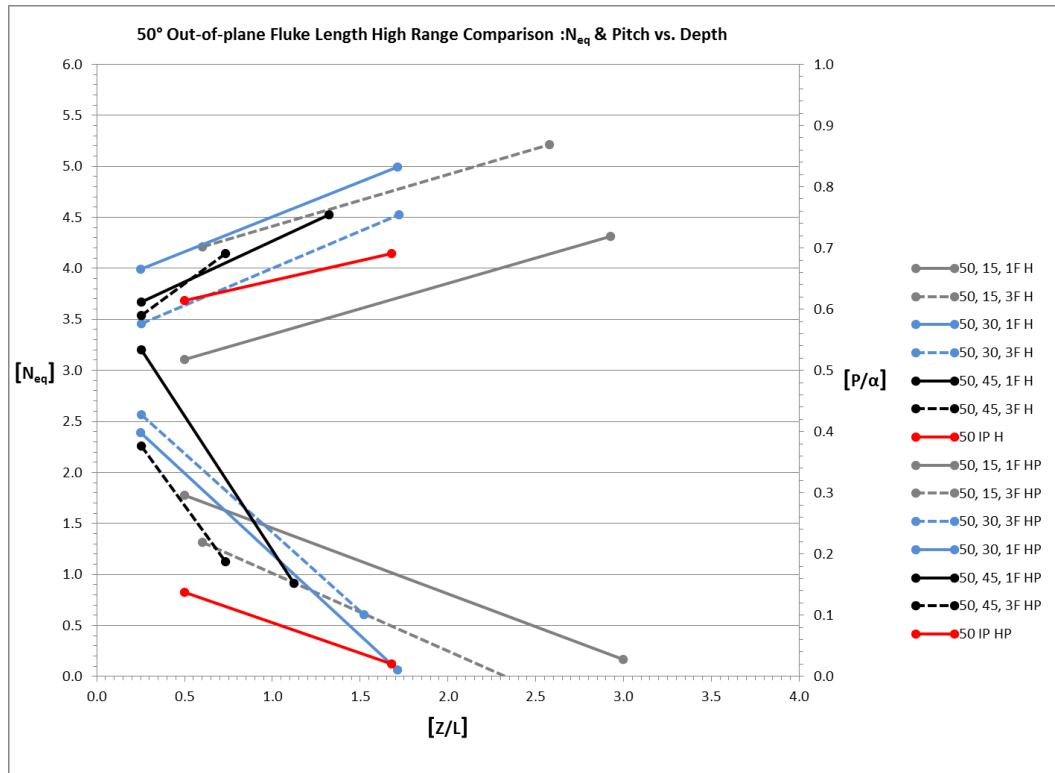












## Extrapolated Data Set

Description	Fluke angle°	Tow angle°	Velocity (m/s)	U-N <sub>eq</sub>	Stage 2 N	U-Z	Stage 2 Pitch
1 F	36	15	0.13	3.55	$y = 0.2536x + 2.933$ $R^2 = 0.7713$	2.417	$y = -0.1055x + 0.255$ $R^2 = 0.8516$
3 F	36	15	0.13	4.27	$y = 0.3232x + 3.7218$ $R^2 = 0.0667$	1.69	$y = -0.0488x + 0.0825$ $R^2 = 0.1748$
1 F	36	30	0.13	3.88	$y = 2.625x + 2.4292$ $R^2 = 0.3065$	0.554	$y = -0.5893x + 0.3268$ $R^2 = 0.7355$
3 F	36	30	0.13	3.61	$y = -0.1283x + 3.6615$ $R^2 = 0.0003$	0.3825	$y = -0.789x + 0.3018$ $R^2 = 0.2062$
1 F	36	45	0.13	4.71	$y = 2.0504x + 2.6568$ $R^2 = 0.4111$	1	$y = -0.4464x + 0.4468$ $R^2 = 0.0846$
3 F	36	45	0.13	3.29	$y = -0.9607x + 3.7943$ $R^2 = 0.1216$	0.522	$y = -0.4904x + 0.256$ $R^2 = 0.0422$
1 F	50	15	0.13	4.31	$y = 0.3909x + 3.0386$ $R^2 = 0.854$	3.257	$y = -0.1073x + 0.3495$ $R^2 = 0.9302$
3 F	50	15	0.13	5.09	$y = 0.5072x + 3.9054$ $R^2 = 0.6265$	2.327	$y = -0.1272x + 0.2961$ $R^2 = 0.9254$
1 F	50	30	0.13	5.02	$y = 0.6865x + 3.8166$ $R^2 = 0.2315$	1.75	$y = -0.2644x + 0.4643$ $R^2 = 0.8071$
3 F	50	30	0.13	4.67	$y = 0.7291x + 3.2736$ $R^2 = 0.3055$	1.91	$y = -0.2573x + 0.4929$ $R^2 = 0.9206$
1 F	50	45	0.13	4.63	$y = 0.8002x + 3.4646$ $R^2 = 0.7194$	1.46	$y = -0.4394x + 0.6455$ $R^2 = 0.8398$
3 F	50	45	0.13	4.74	$y = 1.2697x + 3.2169$ $R^2 = 0.7007$	1.2	$y = -0.3953x + 0.4762$ $R^2 = 0.6973$

## Composite Chart Trendline Equations

Description	Fluke angle	Tow angle	Velocity	Stage 1 N	Stage 2 N	Stage 1 Pitch	Stage 2 Pitch
36 deg comp	36	5	all	$y = 8.1206x + 1.2539$ $R^2 = 0.6689$	$y = 0.4626x + 3.2591$ $R^2 = 0.2305$	$y = -1.4189x + 0.5166$ $R^2 = 0.5095$	$y = -0.1557x + 0.1579$ $R^2 = 0.6851$
36 velocity	36	5	0.13	$y = 6.098x + 1.5189$ $R^2 = 0.5695$	$y = 0.4336x + 3.2358$ $R^2 = 0.18$	$y = -1.5861x + 0.5417$ $R^2 = 0.4736$	$y = -0.1376x + 0.1394$ $R^2 = 0.6588$
36 velocity	36	5	0.19	$y = 9.4283x + 1.0873$ $R^2 = 0.7451$	$y = 0.5575x + 3.2651$ $R^2 = 0.4911$	$y = -1.3003x + 0.4978$ $R^2 = 0.5631$	$y = -0.1829x + 0.185$ $R^2 = 0.7891$
50 deg comp	50	5	all	$y = 4.2316x + 1.9828$ $R^2 = 0.7242$	$y = 0.4196x + 3.4845$ $R^2 = 0.2336$	$y = -0.5724x + 0.5144$ $R^2 = 0.3172$	$y = -0.1395x + 0.2365$ $R^2 = 0.5928$
50 velocity	50	5	0.13	$y = 4.4557x + 2.0261$ $R^2 = 0.7369$	$y = 0.3884x + 3.4904$ $R^2 = 0.1844$	$y = -1.0655x + 0.5954$ $R^2 = 0.8447$	$y = -0.0987x + 0.1864$ $R^2 = 0.4375$
50 velocity	50	5	0.19	$y = 4.0994x + 1.7741$ $R^2 = 0.8783$	$y = 0.5576x + 3.3977$ $R^2 = 0.3298$	$y = -0.5101x + 0.5114$ $R^2 = 0.6637$	$y = 0.5576x + 3.3977$ $R^2 = 0.3298$
50 deg comp	50	10	all	$y = 3.534x + 1.8421$ $R^2 = 0.5383$	$y = 0.5265x + 3.1632$ $R^2 = 0.2259$	$y = -0.9084x + 0.5619$ $R^2 = 0.5134$	$y = -0.1467x + 0.2073$ $R^2 = 0.4317$
50 velocity	50	10	0.13	$y = 2.8521x + 2.0561$ $R^2 = 0.4663$	$y = 0.4811x + 3.1246$ $R^2 = 0.4295$	$y = -0.747x + 0.4831$ $R^2 = 0.4425$	$y = -0.0968x + 0.156$ $R^2 = 0.2698$
50 velocity	50	10	0.19	$y = 4.7316x + 1.4948$ $R^2 = 0.6673$	$y = 0.5908x + 3.1922$ $R^2 = 0.1685$	$y = -1.1001x + 0.6771$ $R^2 = 0.7183$	$y = -0.2296x + 0.288$ $R^2 = 0.7376$
50 deg comp	50	20	all	$y = 2.9122x + 1.9355$ $R^2 = 0.7435$	$y = 0.7103x + 3.1185$ $R^2 = 0.3508$	$y = -0.8307x + 0.615$ $R^2 = 0.9171$	$y = -0.1284x + 0.2037$ $R^2 = 0.2914$
50 velocity	50	20	0.13	$y = 3.4717x + 1.6811$ $R^2 = 0.8457$	$y = 0.5694x + 3.2117$ $R^2 = 0.4903$	$y = -0.9555x + 0.6548$ $R^2 = 0.9309$	$y = -0.0836x + 0.1647$ $R^2 = 0.1705$
50 velocity	50	20	0.19	$y = 2.5059x + 2.1544$ $R^2 = 0.7167$	$y = 1.3151x + 2.62$ $R^2 = 0.3614$	$y = -0.7115x + 0.5806$ $R^2 = 0.9459$	$y = -0.327x + 0.3789$ $R^2 = 0.851$
36 deg comp	36	45s	all	$y = 7.4654x + 1.4866$ $R^2 = 0.6606$	$y = 0.7293x + 3.1132$ $R^2 = 0.417$	$y = -1.3105x + 0.5024$ $R^2 = 0.591$	$y = -0.2607x + 0.2188$ $R^2 = 0.7374$
36 velocity	36	45s	0.13	$y = 6.8555x + 1.7415$ $R^2 = 0.7419$	$y = 0.5666x + 3.1821$ $R^2 = 0.2858$	$y = -1.6377x + 0.5227$ $R^2 = 0.7271$	$y = -0.2175x + 0.1909$ $R^2 = 0.7196$
36 velocity	36	45s	0.19	$y = 9.1124x + 0.8468$ $R^2 = 0.8675$	$y = 0.9685x + 3.0039$ $R^2 = 0.6436$	$y = -0.7996x + 0.4843$ $R^2 = 0.6036$	$y = -0.3214x + 0.2564$ $R^2 = 0.8028$
36 deg comp	36	90s	all	$y = 6.0858x + 0.8276$ $R^2 = 0.8804$	$y = 0.6147x + 2.6494$ $R^2 = 0.5157$	$y = -1.4292x + 0.6774$ $R^2 = 0.8881$	$y = -0.224x + 0.25$ $R^2 = 0.8446$
36 velocity	36	90s	0.13	$y = 5.2217x + 0.9654$ $R^2 = 0.8755$	$y = 0.5956x + 2.5994$ $R^2 = 0.6245$	$y = -1.3604x + 0.6563$ $R^2 = 0.8597$	$y = -0.199x + 0.2401$ $R^2 = 0.9528$
36 velocity	36	90s	0.19	$y = 7.1687x + 0.6428$ $R^2 = 0.9229$	$y = 0.7796x + 2.6161$ $R^2 = 0.6521$	$y = -1.5259x + 0.7062$ $R^2 = 0.9318$	$y = -0.2998x + 0.292$ $R^2 = 0.8856$

## Composite Chart Trendline Equations Cont.

Description	Fluke angle	Tow angle	Velocity	Stage 1 N	Stage 2 N	Stage 1 Pitch	Stage 2 Pitch
50 deg comp	50	45s	all	$y = 5.7146x + 0.9888$ $R^2 = 0.823$	$y = 0.4692x + 3.4219$ $R^2 = 0.3446$	$y = -0.5635x + 0.5391$ $R^2 = 0.5314$	$y = -0.1156x + 0.2475$ $R^2 = 0.5944$
50 velocity	50	45s	0.13	$y = 5.2962x + 1.1849$ $R^2 = 0.8547$	$y = 0.58x + 3.4374$ $R^2 = 0.8324$	$y = -0.7636x + 0.6002$ $R^2 = 0.7893$	$y = -0.1102x + 0.2415$ $R^2 = 0.5089$
50 velocity	50	45s	0.19	$y = 5.9701x + 0.8088$ $R^2 = 0.7708$	$y = 0.4616x + 3.2627$ $R^2 = 0.2738$	$y = -0.2613x + 0.474$ $R^2 = 0.156$	$y = -0.1205x + 0.2535$ $R^2 = 0.6715$
50 deg comp	50	90s	all	$y = 7.6524x + 0.6261$ $R^2 = 0.8313$	$y = 0.628x + 3.2659$ $R^2 = 0.7296$	$y = -0.206x + 0.4003$ $R^2 = 0.1084$	$y = -0.1524x + 0.3027$ $R^2 = 0.8631$
50 velocity	50	90s	0.13	$y = 7.8098x + 0.4848$ $R^2 = 0.7972$	$y = 0.5806x + 3.245$ $R^2 = 0.7762$	$y = -0.0093x + 0.3404$ $R^2 = 0.0006$	$y = -0.151x + 0.3091$ $R^2 = 0.8946$
50 velocity	50	90s	0.19	$y = 7.1135x + 0.8882$ $R^2 = 0.8778$	$y = 0.7551x + 3.2347$ $R^2 = 0.8956$	$y = -0.5228x + 0.5066$ $R^2 = 0.3952$	$y = -0.1588x + 0.2981$ $R^2 = 0.8647$
36 deg comp	36	15	all	$y = 2.2279x + 2.5188$ $R^2 = 0.0966$	$y = -0.1602x + 3.7085$ $R^2 = 0.053$	$y = -0.8548x + 0.4599$ $R^2 = 0.1886$	$y = -0.0335x + 0.1245$ $R^2 = 0.1058$
1 F	36	15	0.13	$y = 2.5991x + 1.4989$ $R^2 = 0.3305$	$y = 0.2536x + 2.933$ $R^2 = 0.7713$	$y = -0.6861x + 0.626$ $R^2 = 0.7982$	$y = -0.1055x + 0.255$ $R^2 = 0.8516$
3 F	36	15	0.13	$y = 6.596x + 2.0062$ $R^2 = 0.7134$	$y = 0.3232x + 3.7218$ $R^2 = 0.0667$	$y = -2.2183x + 0.6444$ $R^2 = 0.638$	$y = -0.0488x + 0.0825$ $R^2 = 0.1748$
36 deg comp	36	30	all	$y = 8.2854x + 2.0434$ $R^2 = 0.3779$	$y = 1.8132x + 2.8492$ $R^2 = 0.1255$	$y = -2.6208x + 0.6418$ $R^2 = 0.457$	$y = -0.6016x + 0.3145$ $R^2 = 0.5406$
1 F	36	30	0.13	$y = 5.107x + 2.0734$ $R^2 = 0.1426$	$y = 2.625x + 2.4292$ $R^2 = 0.3065$	$y = -1.9534x + 0.6494$ $R^2 = 0.5102$	$y = -0.5893x + 0.3268$ $R^2 = 0.7355$
3 F	36	30	0.13	$y = 10.72x + 2.0018$ $R^2 = 0.8015$	$y = -0.1283x + 3.6615$ $R^2 = 0.0003$	$y = -3.1191x + 0.6395$ $R^2 = 0.5255$	$y = -0.789x + 0.3018$ $R^2 = 0.2062$
36 deg comp	36	45	all	$y = 8.5499x + 1.408$ $R^2 = 0.6087$	$y = 0.096x + 3.4322$ $R^2 = 0.0016$	$y = -1.3048x + 0.5073$ $R^2 = 0.431$	$y = 0.8386x - 0.083$ $R^2 = 0.174$
1 F	36	45	0.13	$y = 5.8582x + 1.2715$ $R^2 = 0.2893$	$y = 2.0504x + 2.6568$ $R^2 = 0.4111$	$y = 0.3563x + 0.4132$ $R^2 = 0.1317$	$y = -0.4464x + 0.4468$ $R^2 = 0.0846$
3 F	36	45	0.13	$y = 8.958x + 1.4795$ $R^2 = 0.8316$	$y = -0.9607x + 3.7943$ $R^2 = 0.1216$	$y = -1.8168x + 0.5522$ $R^2 = 0.8043$	$y = -0.4904x + 0.256$ $R^2 = 0.0422$
50 deg comp	50	15	all	$y = 3.8526x + 1.888$ $R^2 = 0.5272$	$y = 0.0149x + 3.9342$ $R^2 = 0.0005$	$y = -0.7149x + 0.6834$ $R^2 = 0.7983$	$y = -0.0846x + 0.2896$ $R^2 = 0.6586$
1 F	50	15	0.13	$y = 2.596x + 1.9142$ $R^2 = 0.245$	$y = 0.3909x + 3.0386$ $R^2 = 0.854$	$y = -0.5706x + 0.6226$ $R^2 = 0.4575$	$y = -0.1073x + 0.3495$ $R^2 = 0.9302$
3 F	50	15	0.13	$y = 3.9539x + 2.1176$ $R^2 = 0.7779$	$y = 0.5072x + 3.9054$ $R^2 = 0.6265$	$y = -0.795x + 0.7166$ $R^2 = 0.9385$	$y = -0.1272x + 0.2961$ $R^2 = 0.9254$
50 deg comp	50	30	all	$y = 9.2649x + 1.8098$ $R^2 = 0.714$	$y = 0.8256x + 3.4751$ $R^2 = 0.2483$	$y = -0.1931x + 0.6047$ $R^2 = 0.1142$	$y = -0.2687x + 0.4835$ $R^2 = 0.8178$
1 F	50	30	0.13	$y = 12.294x + 1.4022$ $R^2 = 0.8611$	$y = 0.6865x + 3.8166$ $R^2 = 0.2315$	$y = 0.148x + 0.5599$ $R^2 = 0.1087$	$y = -0.2644x + 0.4643$ $R^2 = 0.8071$
3 F	50	30	0.13	$y = 6.4407x + 2.2041$ $R^2 = 0.6182$	$y = 0.7291x + 3.2736$ $R^2 = 0.3055$	$y = -0.5102x + 0.6481$ $R^2 = 0.6087$	$y = -0.2573x + 0.4929$ $R^2 = 0.9206$
50 deg comp	50	45	all	$y = 9.6454x + 1.5345$ $R^2 = 0.6933$	$y = 0.8885x + 3.4101$ $R^2 = 0.7106$	$y = -0.4631x + 0.6178$ $R^2 = 0.2582$	$y = -0.287x + 0.4773$ $R^2 = 0.3981$
1 F	50	45	0.13	$y = 10.312x + 1.2342$ $R^2 = 0.6671$	$y = 0.8002x + 3.4646$ $R^2 = 0.7194$	$y = 0.1097x + 0.5719$ $R^2 = 0.0242$	$y = -0.4394x + 0.6455$ $R^2 = 0.8398$
3 F	50	45	0.13	$y = 8.6244x + 1.8151$ $R^2 = 0.8085$	$y = 1.2697x + 3.2169$ $R^2 = 0.7007$	$y = -0.972x + 0.6682$ $R^2 = 0.8699$	$y = -0.3953x + 0.4762$ $R^2 = 0.6973$



## VITA

Name: Aaron C. Drake

Address: Ocean Engineering Program  
Zachry Department of Civil Engineering  
3136 TAMU  
Texas A&M University  
College Station, TX 77843-3136

Email Address: [acdaustin@hotmail.com](mailto:acdaustin@hotmail.com)

Education: B.S., Ocean Engineering, Texas A&M University, 2009  
M.S., Ocean Engineering, Texas A&M University, 2011